Series Hybrid Electric Aircraft

Comparing the Well-to-Propeller Efficiency With a Conventional Propeller Aircraft

R.H. Lenssen

Technical University Delft

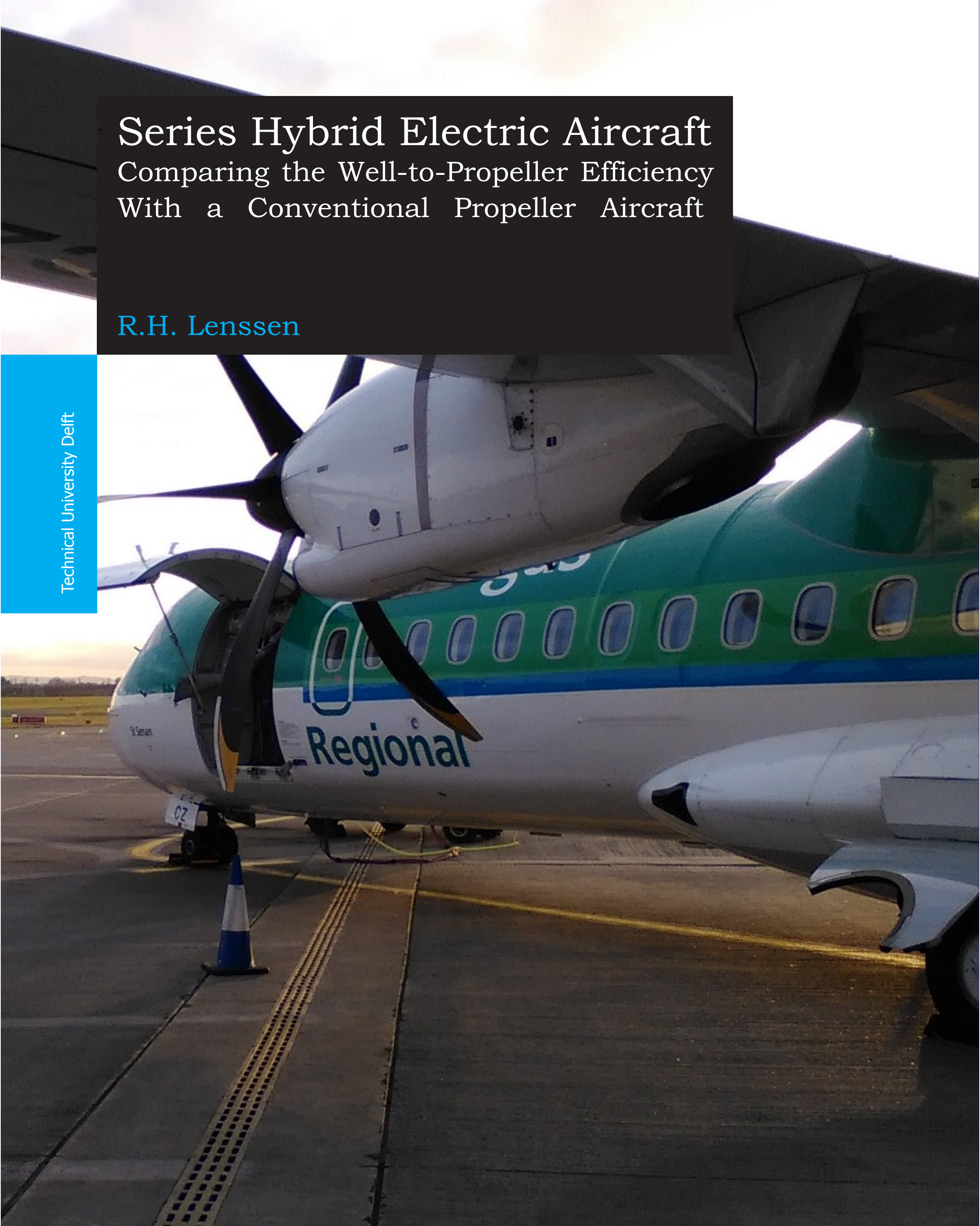

TU Delft Delft University of Technology

Challenge the future

Series Hybrid Electric Aircraft

Comparing the Well-to-Propeller Efficiency With a Conventional Propeller Aircraft

by

R.H. Lenssen

in partial fulfillment of the requirements for the degree of

Master of Science
in Aerospace Engineering

at the Delft University of Technology,
to be defended publicly on Thursday August 4, 2016 at 13:30 AM.

Supervisor:	Ir. J. A. Melkert	TU Delft
Thesis committee:	Prof. dr. ir. L. L. M. Veldhuis	TU Delft
	Ir. P. C. Roling	TU Delft

July 24, 2016

Thesis Number: 081#16#MT#FPP

Acknowledgements

I would like to make use of this opportunity to express my gratitude towards my supervisor, ir. Joris Melkert, for his guidance and support during this master thesis. I especially liked the open discussions on technical subjects and the clear efficient communication that allowed me to finish my thesis in time.

Furthermore, I would like to thank ir. Henk Polinder for his valuable time and insights in future electronics. I would also like to thank the members of my committee, ir. Paul Roling and prof.dr.ir. Leo Veldhuis for their time and effort in assessing this research project.

Finally I would like to thank my family and friends, both for their support and the good memories. During my stay in Delft, you all were a source of energy.

Rick Lenssen
Delft, August 4th 2016

Summary

THE aviation industry is responsible for 12% of the total transportation impact of CO_2 while awareness, for decreasing the total carbon footprint, is rising. Both the aerospace and the automotive industry are facing an increasing pressure from society to make the transportation sector more sustainable. Within the automotive industry slowly an increase in electric vehicles can be noticed (<1%). Also in the aerospace industry a rise in electrification can be seen, with small aircraft as the E-Star and E-Fan (two seaters) as commercial examples. Electrification of the transportation sector could further result in a decrease in noise and an increase in lifespan of parts as vibrations are decreased.

This master's thesis is written in conjunction with the chair Flight Performance and Propulsion at the faculty of Aerospace Engineering at the Delft University of Technology. The main purpose is to gain more insight in modelling an (hybrid) electric aircraft and the potential improvements with respect to well-to-propeller efficiency (usefull energy over total energy ratio). This is achieved by first creating a baseline conventional propeller aircraft model (ATR72) and then a hybrid electric version of the same aircraft. The variations between the sub-models and validation data are calculated in order to have a feeling for the accuracy of each individual model. Furthermore, both the theoretical and current practical state of technologies are used in the overall model. Finally, a sensitivity analysis is performed to find the driving parameters in the outcome of the model.

The analysis of the series hybrid electric aircraft showed first of all that the expected advantages of the concept are 'small to non-existent'. The electric energy used to charge the batteries should first of all come from a renewable source of energy to make the concept feasible. Secondly, the theoretical limits of technology should be approached in order for the well-to-propeller efficiency to exceed that of the conventional ATR72 aircraft (with a maximum of 2%). It is seen that the model converges to an all electric version of the ATR72 if the battery energy density is increased to 2,802 [Wh/kg], this would correspond to the theoretical limit of Lithium Sulphur battery-technology. Furthermore, for an increase in voltage the battery efficiency decreases while all other components will improve in efficiency. The optimum is found in increasing the voltage up to the practical limit of 25 [kV].

Electric propulsion creates new design possibilities as distributed propulsion and variable shaft-speed. Within this thesis it is however shown that the 'benefits' of distributed propulsion do not outweigh the downsides (increase in weight and decrease in efficiency of all components). Furthermore electric motors allow for temporary torque overloading, by decreasing the rotational speed and increasing the torque, the overall result is an increase in efficiency, which could for example be usefull during the climb or take-off phase.

Concluding, the concept of series hybrid electric aircraft is at this moment in time rendered infeasible. The potential within a 35 year time-frame is doubtfull as especially battery technology should improve with at least 400 [%]. In order to accelerate the transition to hybrid electric or all electric aircraft, the main areas of research should be: battery technology and the integration of alternating current and superconducting materials in rotating machine parts.

CONTENTS

The list of figures and the list of tables are (from a sustainability point of view) intentionally left out of this report as discussed with supervisor J.A. Melkert.

List of Notations

Greek Symbols

α	Angle of attack	*deg*
δ	Increment	-
η	Efficiency	-
γ	Glide slope	*deg*
μ_{TF}	Tyre friction coefficient	*N/kg*
μ_0	Magnetic permeability of free space constant	*H/m*
ω	Rotational Velocity	*rad/s*
Ω	Rotational Speed	*RPM*
ϕ	Angle power factor	*deg*
ρ	Density	kg/m^3
σ	Relative density	-
σ	Resistivity	$\Omega \cdot mm^2/m$
τ	Torque	*Nm*
θ	DC to AC factor	*deg*

ROMAN SYMBOLS

a	Speed of sound	*m/s*
A	Aspect ratio, Area, Constant	*- or* m^2 *or -*
b	Wing span	*m/s*
B	Magnetic Field or number of blades	*T or -*
c	Chord	*m/s*
C	Coefficient	-
C_D	Drag Coefficient	-
C_L	Lift Coefficient	-
C_T	Thrust Coefficient	-
D	Drag or Diameter	*N or m*
$d_{cog-engine}$	Distance COG Engine to COG aircraft	*m*
dt	Time-step	*s*
e	Oswald-factor	-
E	Glide ratio	-
e	Oswald Factor	-
E	Energy	*J*
F	Force	*N*
f	Frequency (Switching)	*Hz*
F_g	Residual Thrust	*N*
FF	Fuel Flow	*kg/s*
g	Gravitational Constant	m/s^2
H	Altitude	*m*
h	Height	*m*
I	Current	*A*
J	Advance Ratio	-
k	Coefficient or Constant	-
l	length	*m*
L	Lift	*N*
m	Mass	*kg*
m	Constant	-
M, M_∞	Free stream Mach number	-
n	Constant	-
N	Number of windings in the coils	-
P_a	Power Available	*W*
q	Dynamic pressure	*Pa*
R	Range	*km*
s	distance	*m*
t	Time	*s*
T	Thrust / Temp	*N or K*
U	Voltage	*V*
V	Velocity	*m/s*
W	Weight	*N*

Subscripts

$()_0$	Start point in time
$()_a$	Available
$()_{Approach}$	Approach phase
$()_{avg}$	Average
$()_{CR}$	Cruise Phase
$()_{CLB}$	Climb phase
$()_{cond}$	Conducting / Conductor
$()_D$	Drag
$()_{data}$	Fit to data
$()_{DES}$	Descent phase
$()_e$	Eddy Current
$()_{elec}$	Electric
$()_{end}$	Last point in time
$()_f$	Form
$()_h$	Hysteresis
$()_{in}$	Input
$()_L$	Lift
$()_{Land}$	Landing phase
$()_{LOF}$	Lift-off
$()_{mech}$	Mechanical
$()_{model}$	Fit to model
$()_{Motor}$	Motor
$()_{out}$	Output
$()_{par}$	Parallel
$()_{prop}$	Propeller
$()_R$	Rotation
$()_{req}$	Required
$()_S$	Stall point
$()_{scr}$	Screen Height
$()_{ser}$	Series
$()_{sw}$	Switching
$()_{TF}$	Tyre Friction
$()_{TO}$	Take-off phase
$()_\infty$	Free stream conditions

Aerodynamic Subscripts

$()_0$	Zero Lift Drag Coefficient
$()_{FL}$	Flaps
$()_{LG}$	Landing Gear
$()_W$	Wing
$()_F$	Fuselage
$()_N$	Nacelles
$()_H$	Horizontal Tail
$()_V$	Vertical Tail
$()_i$	Induced Drag Coefficient

Abbreviations

$\eta_{TTP,t}$ Total Tank-to-Propeller Efficiency 46

η_{TTP} Tank-to-Propeller Efficiency 46, 62, 63, 79

η_{WTP} Well-to-Propeller Efficiency 46, 50, 62, 63, 77, 79, 80, 91

η_{WTT} Well-to-Tank Efficiency 46, 62, 79, 91

AC Alternating Current 16, 18, 50, 53, 56

ADT Actuator Disc Theory 21, 23, 24, 42, 45, 50

AEA All Electric Aircraft 10, 76

AEO All Engines Operative 34, 41, 42, 70, 79

APU Auxiliary Power Unit 56, 60, 61

AR Advance Ratio 23, 73

BEM Blade Element Method 21, 23, 24, 45, 99

BJT Bipolar Junction Transistor 50, 51

BJTs Bipolar Junction Transistors 16

BPR Bypass Ratio 21

BSOC Battery State of Charge 13

BSOH Battery State of Health 13

CAS Calibrated Airspeed 38

CC Combustion Chamber 89

CEMF Counter Electromotive Force 17

CG Centre of Gravity 70, 71

DC Direct Current 16, 50, 53, 56, 58, 59, 79

DOC Direct Operating Costs 19

DUT Delft University of Technology 3, 88

FAR Federal Aviation Regulations 35

HEA Hybrid Electric Aircraft 7, 9, 47, 49, 50, 55, 61, 62, 64, 65, 71, 75, 79, 80, 81

HLDs High Lift Devices 36

HPC High Pressure Compressor 87, 89

HPT High Pressure Turbine 87, 89

HTS High Temperature Superconducting 79

IGBT Insulated-gate bipolar transistor 50, 51, 52, 58

IGBTs Insulated-gate bipolar transistors 16

LHV Lower Heating Value 89

Li-Ion Lithium Ion 10, 12, 13, 63

Li-O_2 Lithium Oxygen 12

Li-S_8 Lithium Sulpher 12

LPC Low Pressure Compressor 87, 89

LPT Low Pressure Turbine 87, 89

MAC Mean Aerodynamic Chord 71

MFR Mass Flow Rate 87

MOSFET Metal-Oxide-Semiconductor Field-Effect Transistor 50, 51

MOSFETs Metal-Oxide-Semiconductor Field-Effect Transistors 16

MTOW Maximum Take-off Weight 19, 31, 36

OEI One Engine Inoperative 34, 41, 55, 70, 71, 72, 79, 80

PCU Propeller Control Unit 24, 50

PEC Propeller Electronic Controller 24, 50

PHEA Parallel Hybrid Electric Aircraft 33

PM Permanent Magnet 16, 26, 27, 50, 58

PR Pressure Ratio 89

SFC Specific Fuel Consumption 87

SHEA Series Hybrid Electric Aircraft 4, 6, 11, 33, 49, 77, 79, 80, 91

TAS true airspeed 40

UAVs Unmanned Aerial Vehicles 3

I

Project Initiation & Literature Study

1 INTRODUCTION

THIS chapter explains the structure of this Master of Science thesis report with the subject: "Well-to-propeller efficiency differences between a conventional and a series hybrid electric aircraft". It is written in conjunction with the chair Flight Performance and Propulsion at the faculty of Aerospace Engineering at the Delft University of Technology (DUT). And should be read in combination with the preliminary literature study on the electrification of both the automotive and the aerospace industry, [1]. The motivation for this project is the keen interest of the writer in both the areas of electronics and aerospace engineering and the combination of both these topics in a single platform.

The topic is also chosen because the subjects of Series Hybrid Electric Aircraft (SHEA) and hybrid electric flight have yet to be touched in depth by the scientific community. Hybridisation of vehicles is however covered in the automotive industry ([2],[3],[4]) and some related work can be found in the area of Unmanned Aerial Vehicles (UAVs), ([5],[6],[7]). A previous thesis work has been carried out by Boagaert [8] on the topic of Parallel Hybrid Electric Aircraft (PHEA). However the topic of SHEA is only touched top-level and mostly in combination with All Electric Aircraft ([9],[10],[11]). The writer could not find any evidence of a study on the modelling of the different parts used within a full electric or hybrid electric aircraft. More in-depth explanations of the concepts mentioned in this paragraph are covered in section 2.1.

First, the research objectives including the main goal and the relevance of this thesis are discussed in respectively section 1.1 and section 1.2. Then the methodology used and the chapter buildup are covered in section 1.3. The outline of this report is displayed in section 1.4.

1.1. RESEARCH OBJECTIVES

Within this section the research question and sub-objectives are discussed. They will function as the dot on the horizon throughout this final thesis report. As described in the preliminary literature study executed by R.H Lenssen [1], the main research question is:

- **How does the well-to-propeller efficiency change between a conventional aircraft and a Series Hybrid Electric Aircraft (SHEA)?**

Here the word 'well' indicates the source of the energy used for the primary functionality of the engines/aircraft (producing thrust). From well to propeller, indicates a ratio of energies: usefull energy / total energy.

In order to give focus to this research, a specific type of aircraft is selected as main subject, this is further elaborated in section 4.1. First, the conventional version of this aircraft, the ATR72 is modelled, then the hybrid electric version of the aircraft is modelled. Finally the well-to-propeller efficiency of both these models is calculated and conclusions can be drawn with respect to the main research question. In order to structure this process the following sub-questions are formulated:

- What is the well-to-propeller efficiency of a conventional ATR72 aircraft?
    1. What fare the power requirements throughout the mission profile?
    2. How much power is available from a traditional ATR72 turboprop engine?
- What is the well-to-propeller efficiency of a SHEA version of the ATR72 aircraft on the same mission?
    1. What models can be used for the electric system of a SHEA version of the ATR72?
    2. What is the accuracy of these models?
    3. What is the size and performance of the electric system in the electric version of the ATR72?
- In what category should potential benefits of hybrid electrification of a medium sized aircraft (70 passengers) be studied?
    1. What are the potential benefits of switching to a SHEA?
    2. What are the key drivers in the well-to-propeller efficiency in this research? And how sensitive are these key drivers?

1.2. RELEVANCE OF THE RESEARCH

Within this section, the relevance of the project is highlighted. There are multiple reasons why the research conducted in this final master thesis is highly relevant. First of all the potential decrease in pollution, both from a noise and a carbon emission point of view are worthwhile researching. Furthermore, it is wise to invest the limited resources available within the scientific community in those subjects that could have the largest impact. This research contributes in identifying these high impact subjects and their potential benefits.

As already explained within the literature study [1], the topic of hybrid electric aircraft is relatively novel and therefore not researched in depth yet. This thesis tries to give insight in the validity of, and setting up of several theoretical models by comparing them with validation data available (where required from other industries). By showing opportunities in the field of electrification of aircraft, further research can be better aimed at those topic that are of interest and that require the most progress.

1.3. METHODOLOGY

Within section 1.1 the goal and main research questions are shown. In this section the method is shown that is used to come to an answer to these questions. As explained in the previous section, two models are created within this thesis in combination with a sensitivity analysis. In order to find an answer to why and how much the well-to-wheel efficiency of a series-hybrid-electric aircraft (SHEA) varies with a regular comparable propeller aircraft, a baseline model needs to be used. The tool or model that will mimic the behaviour of both the aircraft designs will likely never be able to give an exact output that is representable of reality. Therefore a baseline aircraft within the CS-25 regulations with propeller propulsion is used as a baseline aircraft [12]. This aircraft is then generated in both its current state and with a substituted electric propulsion system. By comparing relative results instead of absolute results the validity of the overall results will increase.

1.3.1. BASELINE MODELLING

The first model is covered in chapter 4, by modelling the conventional ATR72 aircraft in an Excel and Matlab environment, see Appendix J. The main purpose of this model is to find the power consumption at every moment in time for a typical mission-profile for the ATR72. First the model is introduced, then the validity of the found relations is checked and finally the well-to-propeller efficiency is calculated.

1.3.2. SERIES HYBRID ELECTRIC AIRCRAFT MODELLING

Because no empirical relations exist for SHEA a different approach is chosen in chapter 5. First, all sub-components are modelled and validated, for example the battery, motor and inverter but also the cooling system, propeller and generator. Then the new power consumption and well-to-propeller efficiency are calculated by integrating all these components into a larger model. The program Excel is used in order to validate sub-models and to find optima on component level, Matlab is used to find an overall optimum by varying parameters (e.g. rotational velocity, bus-voltage, battery energy density, etc.). By making the models used for all sub-components incrementally (agile/scrum) more difficult and by going back to a working program at the end of every day, the schedule can be maintained with a working product.

1.3.3. SENSITIVITY ANALYSIS

Finally, in chapter 6, the dependency of the model on certain assumptions is tested by using the Matlab environment. Furthermore the influence of advancements in technology (increase in [Wh/kg] or [W/kg], etc.) are investigated. A parametrised model allows for relatively convenient changes.

1.3.4. EXTERNAL PARTNERS

Contact is found with several suppliers of electric motors, inverters and cables. By combining these datasheets it is possible to validate the models used. Despite the effort, it was unfortunately not possible to come into contact with ATR, several data sources are however found that are used for validation purposes.

1.4. REPORT STRUCTURE

In order to create structure, this report is divided into four parts.

- Part I - Project Initiation
- Part II - Modelling
- Part III - Results
- Part IV - Appendices

1.4.1. PART I - PROJECT INITIATION & LITERATURE STUDY

First, a literary background is created on top of the aforementioned literature study in Part I. This is done by presenting a small recap of Hybrid Electric Aircraft (HEA) and the generation, distribution and conversion of electric energy in an airframe in chapter 2. Within the latter chapter also the fundamentals of electronic systems are introduced in order to create a better understanding of the topics introduced in this thesis. Then, in chapter 3, the theoretical models available for turboprop engine design and for electric motor design are presented.

1.4.2. PART II - MODELLING & SUB-RESULTS

As explained in section 1.3, within this thesis first a model is created in Part II of a conventional aircraft and a HEA, this process is explained in chapter 4 and chapter 5. The chapters have a similar structure:

1. Introduction of models
2. Validation of models
3. Calculation of well-to-propeller efficiency
4. Presentation of intermediary results

1.4.3. PART III - RESULTS

The results of the comparison between these two models are presented in Part III, first chapter 6 shows the overall results and performs a sensitivity analysis, finally chapter 7 draws the final conclusions.

1.4.4. PART IV - APPENDICES

In order to limit the overall size of this master thesis report several theoretical models and findings are moved to the appendices, these can be found in Part IV.

2

Electric Aircraft

Within this section, a theoretical background is introduced in order to bridge the gap between the commonly accepted knowledge within the faculty of Aerospace Engineering and the topics in electronics discussed in this master thesis. First, relevant topics from the pre-executed literature-study by Lenssen [1] are covered in section 2.1. Second, the different components required for a HEA are covered by making the distinction in the following subjects:

- Storage of energy (section 2.2)
- Distribution of energy (section 2.3)
- Conversion of energy (section 2.4)

A HEA produces energy by making use of an onboard gas-turbine that drives a generator that produces electricity. This electricity is then distributed within the airframe by means of cables to the inverters (i.e. motor controllers) that drive the motors. These motors convert the electric energy into kinetic energy by means of a propeller. In order to visualise the systems used within a typical HEA Figure 2.1 is created.

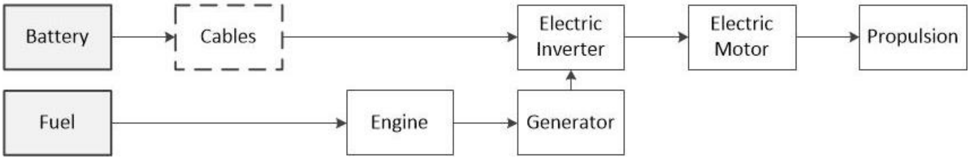

Figure 2.1: The series hybrid electric system visualised in order to create an overview of this chapter, taken from [1]

2.1. OVERVIEW ELECTRIFICATION IN THE INDUSTRY

Within this section the literature review performed by Lenssen [1] is summarised shortly.

Both the aerospace as the automotive industry are facing an increasing pressure from society to make the transportation sector more sustainable [13]. Within the automotive industry slowly an increase in electric vehicles can be noticed (<1 [%]) [14]. Also in the aerospace industry a rise in electrification can be seen, with small aircraft as the E-Star and E-Fan [15],[16] (two seaters) as commercial examples. The aviation industry is responsible for 12 [%] of the total transportation impact of CO_2 [17], while awareness for decreasing the total carbon footprint is rising. Electrification of the transportation sector has several potential benefits [18]:

- Potential decrease of the noise footprint both inside as outside the airframe
- Increase in lifespan of individual parts as vibration is decreased and the amount of moving parts is decreased [18]
- Potential decrease in carbon footprint [19]
- Increased efficiency of the drivetrain [20]

There are multiple institutes, organisations and persons in both the aerospace as the automotive sector that believe that electrification brings a lot of benefits. There are however an equal number of critics, their main concerns are the following:

- The viability of All Electric Aircraft (AEA) are overestimated as exorbitant powers are required (comparable to the power production of windfarms) in order to bring such an aircraft in the air [21],[22]
- Transmission and distribution of electricity within an airframe are highlighted as dangerous (mainly for human health) due to the high magnetic fields generated [23], [24], [25], [26]
- Full system integration, performance and environmental impact are unknown and not described well within literature [27], [28],[29],[30],[31]
- Benefits of superconductivity inside an airframe are not clear ([32], [22], [27]
- Currently no solution exists for the distribution of electricity inside an airframe from a weight perspective [33], [34], [35], [36], [37]
- The cost involved with the introduction of a new type of aircraft are approximately 20-25 billion euros [38],[39],[40]. While the cost involved in the introduction of a new type of electric car are a tenfold lower [41]
- The sustainability of Lithium Ion (Li-Ion) batteries is uncertain [42],[43]
- Certifyability is 'currently' unknown

In order to reach the goals set for reducing climatic change it is important that the concept of electric flight is researched more in depth. In total three types of electric aircraft can be distinguished, in increasing order of amount of electrification:

1. More Electric Aircraft (MEA) - Partly electric (e.g. the control systems). The propulsion system is non-electric.
2. Hybrid Electric Aircraft (HEA) - Power required comes from multiple sources (e.g. electrical and a gasturbine combination)
   (a) Parallel Hybrid Electric Aircraft (PHEA) - The gasturbines provide both a direct thrust force and drive a generator that produces electric energy. The gasturbines are mostly located at the conventional wing location and the generator is integrated inside. Batteries supply additional power when required.
   (b) Series Hybrid Electric Aircraft (SHEA) - The onboard gasturbine is only used for the production of electricity. For example: an onboard gasturbine drives a generator that produces the required electricity. As the turbine can run at a more favourable speed, the efficiency increases with respect to regular gasturbines. The electrical energy is then used by motors that drive the propellers.
3. All Electric Aircraft (AEA) - At this moment in time rendered infeasible for commercial airlines as the power required are too high and mainly the battery energy density is not sufficient. The technique is however used in multiple two-seaters are that are currently commercially available [44],[45]

As the SHEA has not yet been researched in literature this type of aircraft is researched more in depth in this master thesis.

In section 2.2 the storage of electric energy is discussed, state-of-the-art and future technologies are shown briefly and the influence of battery architecture on the performance of a battery is covered.

2

2.2. STORAGE OF ELECTRICITY

Within this chapter a small literature review is given on the three different cell technologies used within this research. Here the definition 'cell' refers to the smallest singular object capable of storing energy inside a battery pack. The model is further explained in section 5.1, more information on battery cell technology and the current state-of-the-art can be found in [1] and in Appendix A. The status in 2015 and the theoretical limits for the cell technologies covered within this section are shown in Figure 2.2 in combination with the energy-density of kerosene. The currently most used technology in the electric automotive and aerospace industry is the NRC18650 Li-Ion cell by Panasonic [46]. A very promising technology is Lithium Sulpher (Li-S_8) and the absolute 'currently' known theoretical limit of cell technology is Lithium Oxygen (Li-O_2). It can be seen in Figure 2.2 that the current practical, future theoretical energy density of batteries and that of kerosene do not 'yet' share a common ground.

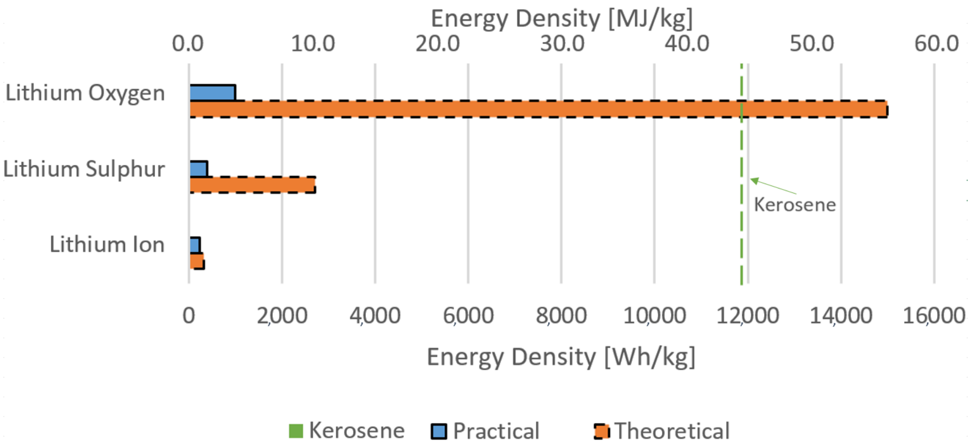

Figure 2.2: Both the current practical ([46],[47],[48]) and the theoretical ([49]) energy density limits are shown in combination with the energy density of kerosene (43 [MJ/kg]).

2.2.1. LITHIUM ION

Current state-of-the-art Li-Ion battery cell energy density, [46], is slightly above 240 [Wh/kg] and improves with approximately 7 to 8 [Wh/year], [1]. The theoretical limit of Li-Ion cells is 320 [Wh/kg], [49]. The downside of using Li-Ion cells is the limited range of discharge; 20 [%] of the energy stored inside the battery pack cannot be used, due to the possibility of decreasing the cell performance.

2.2.2. LITHIUM SULPHUR

The main advantage of using Li-S_8 cells is the decreased weight of the battery pack (theoretical limit of 2700 [Wh/kg]) while maintaining a very large discharge range [47]. The depth of discharge is theoretically 100 [%]. Furthermore the cells can theoretically be stored for an extended period of time, without the need of periodically recharging the cells. Current Li-S_8 technology resides at approximately 400 [Wh/kg] at lab-scale.

2.2.3. LITHIUM OXYGEN

Although no practical applications exist yet for the Li-O_2 technology, it is interesting to see what the impact could be on the models used within this Master Thesis. Li-O_2 has a theoretical limit of 15 [kWh/kg], however here the non-active materials and the additional weight due to the formation of oxygen inside the cell are not taken into account (Li-O_2 cells become more heavy while using them as oxygen accumulates inside the cells). A more practical upper limit would be 1,000 [Wh/kg], [48] as is used within this research.

2.2.4. BATTERY MODEL

In literature, [47], four different types of models for the Battery State of Charge (BSOC) are often discussed: mathematical models, electrochemical models, thermal models and electrical equivalent circuit networks. These models are often combined in order to render more accurate results. Because the exact parameters of the chosen battery technologies are not yet known, a generic mathematical model where $BSOC = f(I, U, E^*)$, is chosen that is further elaborated upon in chapter 5, here the dependency of the BSOC on the ageing effect, the Battery State of Health (BSOH), as well as the effect of temperature are neglected.

2.2.5. BATTERY ARCHITECTURE

The efficiency of charging and discharging is dependent on both the battery architecture as the materials used as shown in the previous sections. The battery weight and the energy density are independent of bus-voltage as the number of cells connected in series and parallel remains constant and thus the overall number of cells remains constant. The electric resistance of the battery is however dependent on the amount of cells connected in series and in parallel as the battery-cells possess an internal resistance, as shown in Figure 2.3. As a result it is more efficient for the battery (if large currents are required) to lower the voltage as far as possible by putting the most cells in parallel. If current is not the leading parameter in battery design then the voltage should be increased in order to lower the I^2R losses and thereby increase the battery efficiency.

The internal resistance of a commonly used (for example by Tesla ([50]) Li-Ion battery cell, the Panasonic NRC18650 is 55 [$m\Omega$], [46]. The lower the current drawn per battery-cell the higher the capacity, if a nominal current of of 2.9 [A] is drawn, a capacity of 95 [%] can be utilised as can be seen in Appendix H. The power losses at this rate of current are shown in Equation 2.1. These result in a charging and discharging efficiency of 95 [%]. The difference in power losses for the two examples shown in Figure 2.3 for the parallel and series example are respectively 0.15 and 1.39 [W].

$$P_{loss,single\ cell} = I^2 \cdot R = 2.9^2 \cdot 55 \cdot 10^{-3} = 0.46\,[W] \tag{2.1}$$

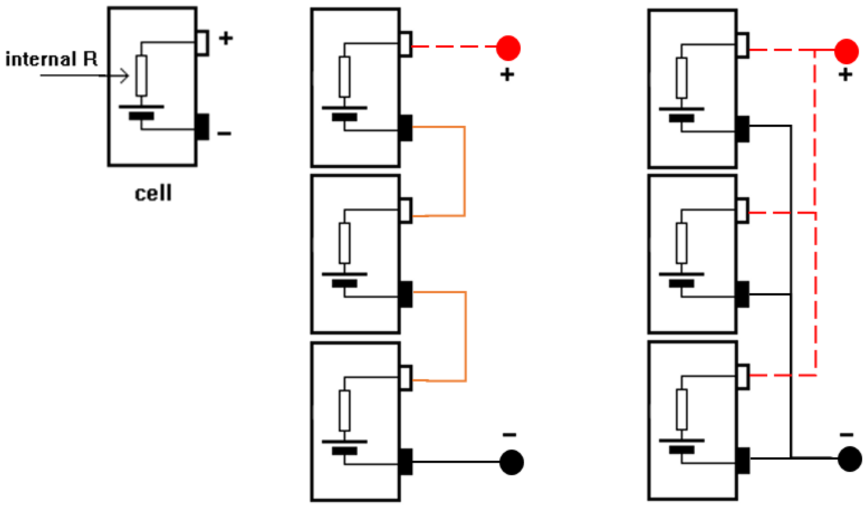

Figure 2.3: From left to right: Single battery cell, three battery cells connected in series and three battery cells connected in parallel configuration.

2.3. TRANSMISSION OF ELECTRIC POWER

From the batteries (see previous section), the energy needs to be transferred to other devices within the airframe. Within this thesis the only viable manner of transporting energy from one geographical location to the next is by means of cables with a solid conductor. Wireless transportation of energy (e.g. induction, etc.) is not considered. In section 5.1 several types of conductor materials are covered, within this section the theoretical background and limitations of energy transportation are covered.

In Figure 2.4 the different parts that makeup a cable are shown. It can be seen that every cable consists out of a main conducting element (conductor). This element is surrounded by a non-conducting material called the shield that is again surrounded by a (mostly plastic type) material that functions as the insulation. On the outer edge of the cable assembly the screen can be found, covered both on the inner and the outer side by a insulating layer of material.

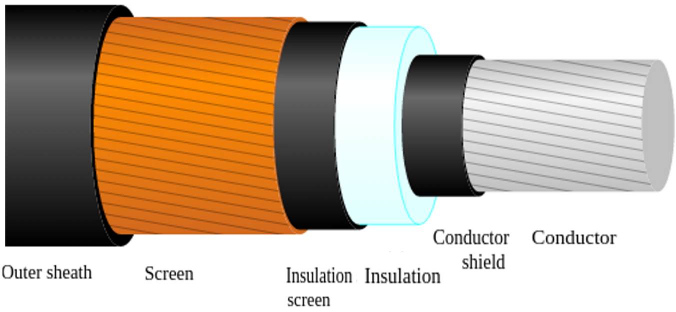

Figure 2.4: Both a multi-stranded and a single conductor cable layout are shown, [51]

The function of the main conductor is to transfer the electricity from geographical location A to B while at the same time having the lowest weight possible and with the lowest amount of electric losses possible. The function of the shielding is to isolate a conducting material from other conducting materials in order to prevent short-circuiting.

As there exists a difference in voltage (potential) between the conductor (live wire) and the surroundings (i.e. the ground-wire) the current will want to flow in that direction. Air is a natural conducting material with a very low conductivity of $2.2 \cdot 10^{-13}$ $[S/m]$ [52]. This conductivity is dependent on density and will increase exponentially with altitude (factor 10 at 10 [km] altitude) as also ionisation of atmosphere increases with altitude. Furthermore the conductivity is higher for pure air, as dust, fog and water-vapor will all lower the conductivity [53].

In order to prevent current from travelling through the air, insulation surrounding the wire is required. As the voltage (and thus potential difference with the ground) is increased, an increasing amount of insulation is required. The screen layer (working as a cage of Faraday) is finally applied in order to reduce 'electrical noise' that might interfere with other devices.

2

2.4. GENERATION OF PROPULSION

Within this section the theory behind the inverter (motor controller) and motor are covered. A more in-depth review of the Permanent Magnet (PM) motor can be found in section 3.2, while the models used in this master thesis to model both these components are covered in section 5.1.

2.4.1. INVERTER (MOTOR CONTROLLER)

The main purpose of the inverter is to control the speed and torque of the electric motor, [54]. It does so by varying the frequency of the Alternating Current (AC) and the working voltage [55], [56]. In practice this varying is achieved by opening and closing switches in a controlled manner very fast (<10,000 [Hz]). In most applications an AC to AC conversion is used, however as soon as a battery is involved in the system (mostly in combination with solar energy) a Direct Current (DC) to AC conversion is required [57]. The inverter then functions both as a DC/AC converter and as a control unit for the motor.

For switching purposes the commonly most used components are (voltage controlled) Metal-Oxide-Semiconductor Field-Effect Transistors (MOSFETs), (current controlled) Bipolar Junction Transistors (BJTs) and the (voltage controlled) Insulated-gate bipolar transistors (IGBTs). The latter component is a cross-product between the MOSFET and the BJT. It is commonly understood that MOSFETs work well below 250 [V] and 50 [W] and for high switching frequencies above 200 [kHz] [58]. Furthermore it is commonly accepted that IGBTs are ideal for high voltage (>1 [kV]) and high power (>5 [kW]) operations at lower frequencies (<20 [kHz]) [58]. As voltage range of interest in this master thesis is in between 1 [kV] and 50 [kV], the IGBT is used to model the motor controller in section 5.1. The influence of switching frequency on the amount of current allowed through the IGBT is shown in Appendix I.

2.4.2. ELECTRIC MOTOR

This section is created in addition to section 3.2 with the purpose of explaining the different concepts involved in the modelling of an electric motor. First, the general concept is explained including some terminology, then, the types of electrical losses are introduced. Overall three types of electric motors can be distinguished:

- **Brushed DC** or Servo Motor (±80 [%] efficient [59]) - A brushed contact is used to connect a DC source to a rotating wireframe that is in a uniform magnetic field. For every half cycle of rotation the direction of flow of current is flipped, causing the resulting force on the wireframe to be in the direction of rotation.

- **Induction Motor** (±90 [%] efficient [60]) - Electricity is inducted in the rotor by magnetic induction from the stator instead of a direct electric connection. Because the magnetic field induced is rotation the stator will also start rotating.

- **Permanent Magnet AC** (±95 [%] efficient [61]) - The stator is similar to the induction motor, however the rotor is no longer made of a passive metal, but permanent magnets are used in order to increase the magnetic field.

Because the latter two are more efficient and required less maintenance than the first type of motor, these are perfectly suited for the transportation industry.

TERMINOLOGY IN ELECTRIC MOTOR DESIGN

- **Phases** - By making use of different 'sets' of coils (called a phase) and by applying current to these phases in a rotating fashion, it is possible to create a rotating magnetic field.
- **Coils** - By winding wires a magnetic field is created, by winding wires around a magnetic material (e.g. an iron bar) the magnetic field is amplified, see Figure 2.5.
- **Star Point** - This is the point where all phases paths converge, the resulting current in the star-point is zero in a well balanced (i.e. similar resistance and conductivity) circuit.
- **back-EMF** - or a Counter Electromotive Force (CEMF) is created as the coils that turn inside a magnetic field induce an EMF. This works against the applied voltage and thus reduces the required current. The CEMF can be used to indirectly measure the speed of the motor as the two are related.

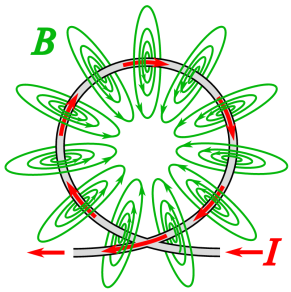

Figure 2.5: Visualisation of the magnetic field created by a circular wire, [62]

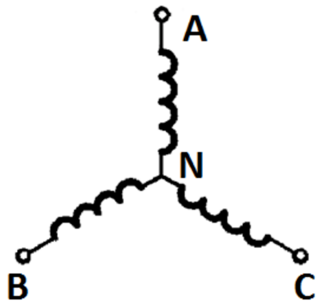

Figure 2.6: Visualisation of the starpoint of three phases in a motor, [63]

TYPES OF LOSSES

The efficiency of electric devices is partially determined by the amount of electronic losses involved. In this section the most dominant losses are described (i.e. Ohmic, iron, hysteresis, Eddy's and skin effect losses). They occur in all parts described in this master thesis(e.g. in cables (conductors), inverters, motors, etcetera).

- **Ohmic Losses** - Arises from the flow of current and a resistance to this flow by a conductor. $P_{Loss_{Ohmic}} = I^2 \cdot R$
- **Iron Losses** - Power loss created by hysteresis and Eddy currents in the iron that is used inside the coils
- **Hysteresis** - The effect of magnetising and demagnetising a material and the losses involved in the process. $P_{Loss_{Hysteresis}} = K_h \cdot f \cdot B_m^{1.6}$

- **Eddy Currents** - Are created by the varying magnetic field in a motor inside the lamination. They are mainly reduced by making use of stacked iron sheets, that are isolated from each other or by a core in the coils made of powder. $P_{Loss_{Eddy}} = K_e \cdot f^2 \cdot K_f^2 \cdot B_m^2$
- **Skin Effect** - As an AC flows through a wire, the current-density tends to be higher near the skin of the wire, hence the name skin-effect. This effect can be reduced by for example making use of Litz-wire (multiple smaller strands of wire confined in a single conductor) instead of a single solid conductor [64].

3

ENGINE SIZING METHODS FOR COMMERCIAL AIRCRAFT

THE main characteristic of hybrid electric aircraft is the onboard generation of electricity. The use of electricity from other energy sources (e.g. batteries) should result in less stringent design boundaries on the gasturbine engine in order for the hybrid electric aircraft concept to be feasible.

Within this chapter, aircraft engine sizing methods are researched in order to find the leading design boundaries in the designs of the turboprop engine. It is not possible to size the engine as a separate entity, therefore it is required to investigate aircraft sizing tools. Commonly used aircraft sizing methods are Nicolai, Loftin [65], Roskam [66], Raymer and Torenbeek. All these sizing methods are based on empirical relations based on minimisation of Maximum Take-off Weight (MTOW) or Direct Operating Costs (DOC). Within this thesis empirical models will be used in co-junction with theoretical models to estimate the performance of sub-systems. The combined performance of these subcomponents will give an indication of the overall performance of the aircraft. Within this thesis the overall power consumption will be minimised, this is a combination of both weight and efficiency optimisation.

For every sizing method it is important to use a well-defined set of top-level requirements as it is impossible to start designing without knowing the end-goal. One of these top-level requirements is the flight mission, for commercial aircraft that fall within the CS-25 regulations a standardised flight segment can be assumed as shown in Figure 3.1.

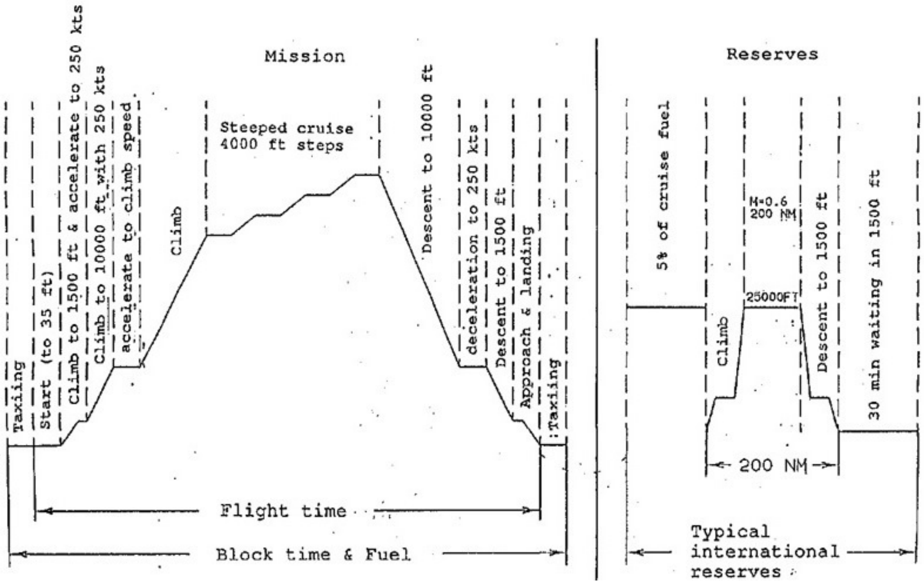

Figure 3.1: Typical mission profile for a commercial aircraft. Both the main mission as a potential additional mission (reserve) are shown, [66].

In the above figure different segments can be distinguished, the fuel weight of the aircraft will decrease over these segments and are commonly denoted as fuel fractions. In the design process of an engine, it is important to know the power requirements (and thus the fuel fraction and time) per flight segment and the total flight time and fuel consumption (block time & fuel). From this information it is possible to find out what the most stringent design boundaries are with respect to turboprop (section 3.1) aircraft. section 3.2 will investigate what the more relaxed boundary conditions could be for hybrid electric aircraft.

3.1. SIZING TURBOPROP AIRCRAFT ENGINES

When the Bypass Ratio (BPR) of the engine is increased beyond a factor 10 it becomes wise to use a propeller instead of a fan. The increase in weight and wetted area that would otherwise be involved would be very detrimental to the overall design [67]. A turboshaft engine using a propeller for thrust generation is called a turboprop engine and it can have a BPR up to 50 - 100.

The power available during cruise (P_a) from a turboshaft engine is a function of both altitude (H by the variable σ) and free-stream Mach number (M_∞) as is shown in Equation 3.1. The parameters A, m and n used within this relation are based on empirical data and dependent on the type of engine that is used [68]. The parameter σ is equal to $\frac{\rho(H)}{\rho_0}$.

$$P_a = P_{TO} \cdot A \cdot M^m \cdot \sigma^n \tag{3.1}$$

Because the final results of this Thesis research depend heavily on the chosen parameters, a sub-research is performed within this section. Several theories suggest the use of different parameters; Schaufele [69], Bruning [70], Russel [71], Loftin [65] and McCormick & Barnes [72]. Actual flight data [73] is compared against the aforementioned models in Figure 3.2 on the next page. As can be seen in Table 3.1 the 'general' model described by Loftin [65] has a good resemblance with the actual flight data and has an R^2 value of 0.999. The values for A, m and n are respectively 1.089, 0.091 and 0.924 [-].

Table 3.1: The different models accompanied by their respective average R^2 value gives a good overview of the best model to use for the estimation of the cruise power. The average R^2 values are derived from Figure 3.2.

Model Name	**Source**	**Average R^2 Value**
Loftin	[65]	0.9995
Schaufele	[69]	0.9986
Bruning	[70]	0.9978
McCormick & Barnes	[72]	0.9561
Russel	[71]	0.9508

The model by Loftin has a very high accuracy over a wide range of velocities and altitudes. Although the model by McCormick & Barnes is optimised for an PW-120 engine, which is very similar to the engine used in the ATR72, the R^2 value is relatively low. This is due to the fact that the model is only optimised for the cruise speed and altitude; if the model deviates from these parameter the results vary heavily. If the model is only used at the cruise speed an R^2 value of 0.9998 is reached. A similar feature holds for the model by Russel, where an R^2 value of 0.997 is reached when only the lowest speed is taken into account. Because the model by Russel is actually calculated for a jet engine and this type of engine is more sensitive to changes in flight velocity, the parameter m is set to insensitive.

In section 5.2 the chosen model is further discussed and combined with a propeller model that is also dependent on altitude, thereby making the overall model more dependent on height.

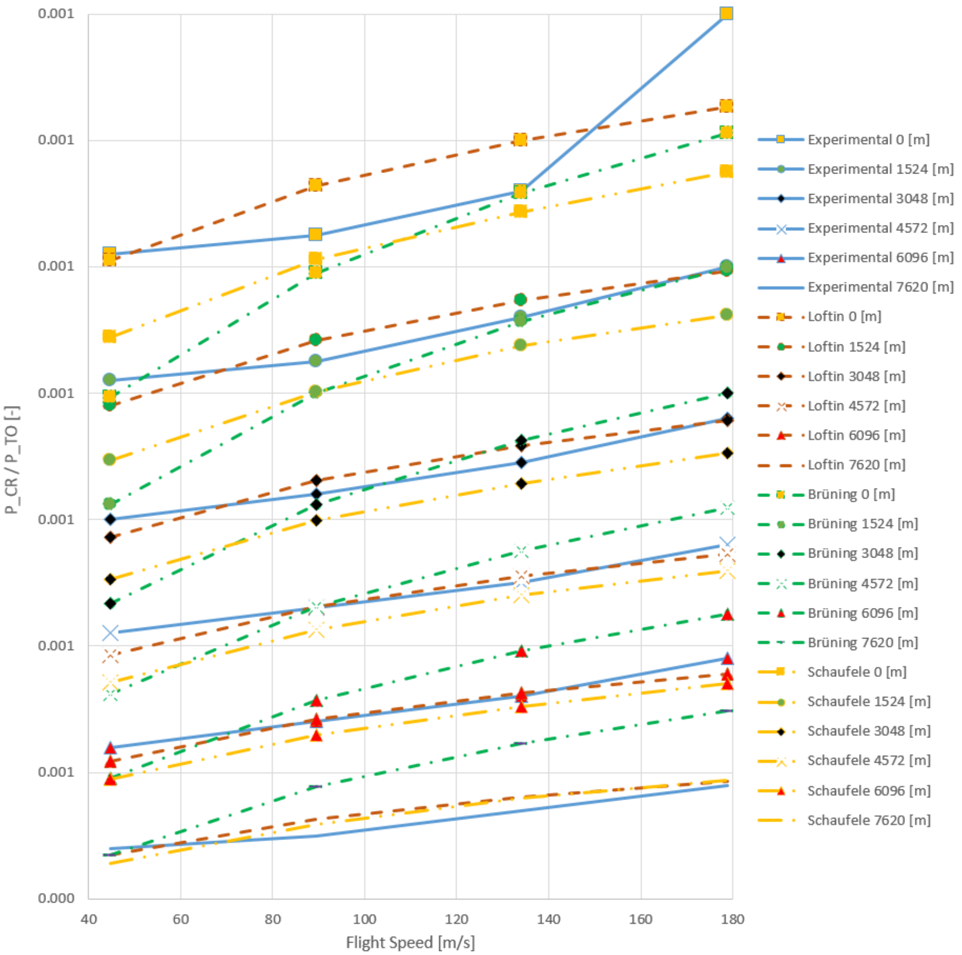

Figure 3.2: Actual flight data [73] is compared against several models ([65],[69],[70],[72],[71]) for different flight speeds and altitudes.

3.1.1. PROPELLER MODEL

Before the aircraft model is explained it is important to establish a model for the propeller as this input is required throughout the various stages of the flight segments that are modelled. Within this section two theoretical models are discussed, the Actuator Disc Theory (ADT) and the Blade Element Method (BEM).

ACTUATOR DISC THEORY

The ADT is a lower order model of the propeller efficiency, by modelling the propeller as a disc with uniform performance properties the efficiency will be ideal. The advantage of using the ADT is that the geometric properties of the propeller do not have to be known. On average experience shows that multiplying the ADT efficiency with 90 [%] gives more reliable results. The ADT assumes irrational, incompressible, steady and continuous flow conditions. The propeller efficiency is dependent on the flight altitude and speed as can be seen in Equation 3.2.

$$\eta_{prop} = \frac{1}{1+\frac{u_a}{u_0}} = \frac{2}{1+\sqrt{1+C_T}} = \frac{2}{1+\sqrt{1+\frac{T_{req}}{0.5\cdot\rho(H)\cdot V_\infty^2\cdot\frac{\pi}{4}\cdot D_{prop}^2}}} \tag{3.2}$$

BLADE ELEMENT METHOD

The BEM is a higher order model of the propeller, by integrating the lift and drag characteristics of several airfoils along the span of the propeller-blade a more accurate result is gained. The propeller used on the ATR72 is the, highly swept back, F568 as is shown by Figure 3.3. The average rotational speed is equal to 1,200 [RPM] and the diameter is 3.93 [m], this results in an Advance Ratio (AR) during cruise conditions (V_∞ = 155 [m/s]) of 0.31 [-].

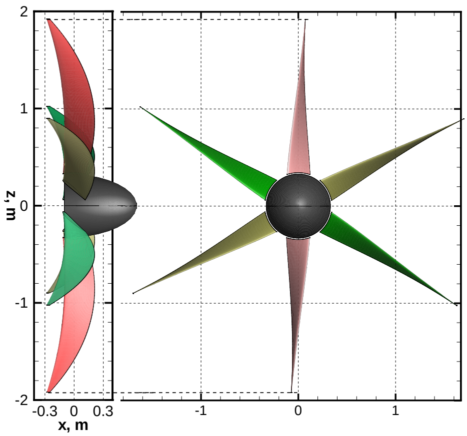

Figure 3.3: The F568 propeller as used on the ATR72 with a diameter of 3.93 [m] and a rotational speed of 1,200 [RPM], derived from [74].

The F568 propeller has been researched in depth by Filippone from the University of Manchester [74]. By reconstructing the geometry of the propeller from photographs and by using standardised supercritical airfoils (SC-1095 and SC-1094) it was possible to construct a rudimentary BEM code. This code is not made public, but the results (Appendix F) can be used to check the validity of the ADT model as is shown in Figure 3.4. Both the originally calculated ADT code as the adjusted (multiplied with a factor 0.89) ADT code are shown. It can be seen that the BEM and ADT show a similar behaviour and trend.

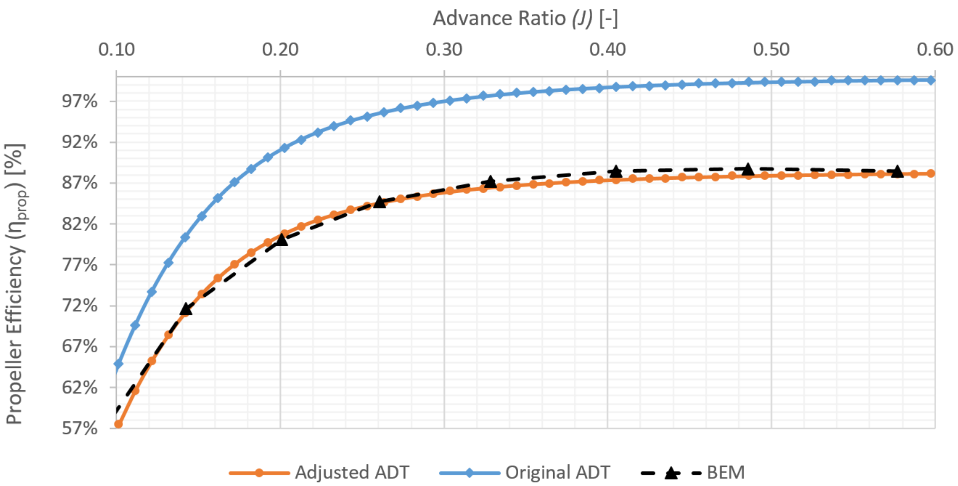

Figure 3.4: Results of BEM analysis performed by [74] compared against ADT analysis.

3.1.2. THRUST

By making use of Equation 3.1 and Equation 3.2 it is possible to calculate the available thrust as a function of altitude and free-stream Mach number. If also the thrust used is known for each phase, it is possible to calculate the thrust setting and therefore the leading engine design parameters.

At low speeds (M<0.7 [-]) a propeller aircraft will perform better than a turbofan aircraft with respect to specific fuel consumption. The actual thrust generated is regulated by the Propeller Electronic Controller (PEC) and the Propeller Control Unit (PCU) onboard the propeller aircraft, [75]. The PEC regulates both propeller pitch and speed, but also a safety-system that includes auto-feathering (decreasing drag in case of engine failure) and automatic under-speed propeller control. The PCU regulates the oil flow that results in a pitch change of the propeller blade.

A turboprop engine is optimised in such a way that the residual thrust coming from the nozzle is minimised and the thrust coming from the propeller is maximised. At higher speeds however, the residual thrust can play a measurable role and is therefore taken into account within this research as can be seen in Figure 3.5.

$$\eta = \eta_g \cdot \eta_m \cdot \frac{T_p + F_g}{P_{shaft}} \cdot V_\infty \tag{3.3}$$

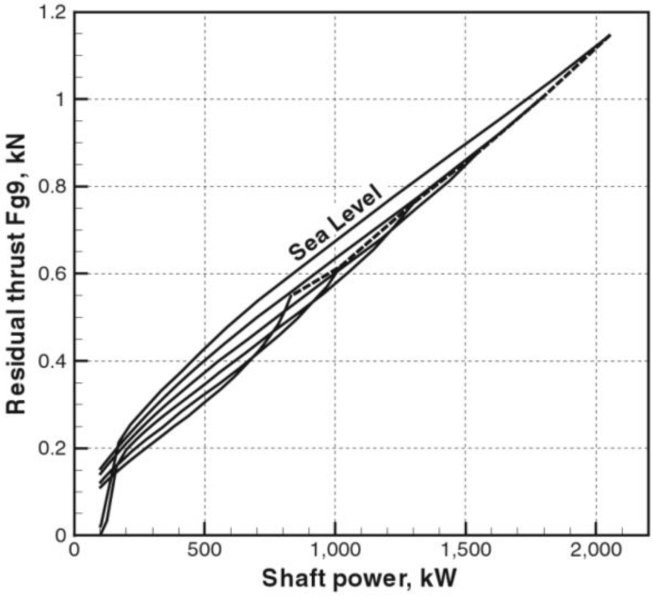

Figure 3.5: Estimated residual thrust versus shaft power for the turboprop engine PW127M used at an ATR72 aircraft [74]. The residual thrust is shown for different altitudes, in steps of 2000 [m] starting at sea-level for the upper line in the figure.

3.2. SIZING ELECTRIC AIRCRAFT ENGINES

Within this chapter the 'basics' of modelling an electric motor are covered. It would go far beyond the scope of this research to cover the entire design process of a highly efficient electric motor. This section will focus mainly on the efficiency (see Equation 3.4), weight and the influence of overall dimensions on these parameters. By interpolating existing data for high performance PM motors it is possible to derive empirical relations for the aforementioned parameters. Several terms that could be considered *jargon* are used throughout this chapter, these (i.e. Ohmic, hysteresis, iron, stray and Eddy current losses) are explained in section 2.4.

$$\eta_{motor} = \frac{P_{mech,out}}{P_{elec,in}} = \frac{\tau \cdot \omega}{I \cdot U} = \frac{[Nm] \cdot [rad/s]}{[A] \cdot [V]} \tag{3.4}$$

The dominant losses in an electric motor can be divided in three groups [76]:

1. Conduction Losses
   (a) I^2R losses in the stator
2. Speed Related Losses
   (a) iron losses in the rotor and stator (hysteresis and Eddy currents)
   (b) frictional losses in the rotor (bearings and aerodynamic effects)
3. Other Losses
   (a) excess losses in the rotor and stator (hysteresis and Eddy currents)

The iron losses are dominant at high speeds, while the conduction losses are dominant at low speeds, [77]. In order to push the boundaries of efficiency, 'normally' the conductor material in both the stator and the rotor is increased in size to achieve a lower coil-resistance (R) and thus lower conduction losses. Furthermore, high quality iron is used at a lower flux density in the stator in order to reduce core losses and the air-gap is increased to reduce the amount of stray losses.

The size of the motor has a direct influence on the overall efficiency, [78]. If all motor dimensions are increased with a factor k, the torque and power output will increase with a factor $k^{3.5}$, while the conduction losses will increase with a factor k^2 and the iron losses will increase with a factor k^3.

While designing a motor for an aircraft, these optimisation 'rules' cannot be applied blindly. Especially the decrease in conductor losses by adding more material will quickly lead to high weight penalties. The conduction losses vary quadratic with the current supplied and are dependent on the resistance measured from phase to the common ground (star-point). This resistance depends on the amount of conducting material used and is therefore different for every motor design.

In order to increase the torque output of the motor, the magnetic field needs to be increased, this can be done by increasing the current (I), the number of windings in the coils (N) or the length (l) of the coils as is shown by the linear relation Equation 3.5. Here μ_0 is the magnetic permeability of free space constant with a value of $4\pi \cdot 10^{-7}$ [H/m]. A similar relation holds between the maximum voltage and the maximum speed ω the motor (with a certain back-EMF) is capable of outputting.

$$B = \frac{\mu_0 \cdot I \cdot N}{L} \tag{3.5}$$

3

Because the electric aerospace industry is very novel, there does not exist much up-to-date data that could be used to find trends. For example literature states that a power density in design exercises should be used of 1.2 [kW/kg], however Siemens developed a high efficiency, low weight, electric motor including gear box [16] in 2013 with a power density of 5 [kW/kg]. Furthermore a lab approved and scalable (to 1[MW]) concept for a generator with a power density of 8 [kW/kg] is already created [79]. These motors in combination with other found examples of electric motors designed for the aerospace industry can be found in Figure 3.6. It is noticeable that the motor weight in the electronic automotive sector is approximately twice as high.

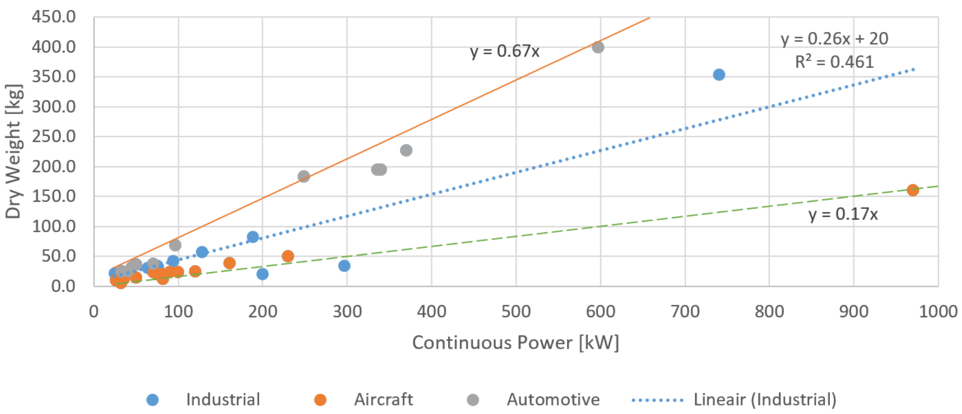

Figure 3.6: The dry weight of different types of PM motors are shown as a function of continuous power [kW]. The motors shown ([16],[80],[81],[82],[83],[84]) are all readily available within the aircraft industry. As a comparison also the current state-of-the-art is shown for the motor weight in the automotive and manufacturing industry ([85],[86],[87],[88],[89],[90],[91],[92]), N=42.

In line with previous chapters, the motor performance will be made dimensionless, however a lower (currently available) and upper (optimistic) value for the power density will be used for the well-to-propeller calculations of respectively 5 [kW/kg] and 8 [kW/kg] [79]. The corresponding efficiencies are 95 and 97 [%].

II

MODELLING

4

Baseline Model

Within this chapter the theoretical model is described that is used to simulate the baseline, the ATR72 aircraft. It should be noted that although the ATR72-500, ATR72-600 and ATR72-210 aircraft have different names, the aircraft are from a technical perspective, similar aircraft [93]. Both the external dimensions as the engines used on these 'different types' of aircraft are all similar. Minor differences can be found in the number of available seats and in the MTOW. For the argument of convenience the baseline aircraft will, in the remainder of this report, be referred to as the ATR72 aircraft. The main purpose of this chapter is to achieve three goals:

1. Find the power required for every flight segment
2. Derive the available power from the ATR72 baseline aircraft
3. Calculate the well-to-propeller efficiency for the baseline aircraft for a specific mission profile

These goals are reached in separate section in this chapter by constructing appropriate models. The performance of an aircraft is highly dependent on the mission profile that is considered; e.g. flight speed, height, payload and range. Therefore the base mission profile that is used for the remainder of this report is described in Table 4.1.

Table 4.1: These parameters are derived for a typical mission profile for the ATR72 aircraft [93]

Parameter	**Value**	**Unit**
Block Range	560	*km*
Reserve Range	160	*km*
Block Fuel Consumption	2000	*kg*
Block Time	120	*min*
Cruise Altitude	5000	*m*
TAS Cruise	140	*m/s*

This mission profile is based on the most flown routes of the ATR72, [94], as described in the literature study by Lenssen, [1]. To get acquainted with the variations in performance that are involved in changing this mission, a sensitivity analysis is performed in section 6.1.

First, the power required is calculated, therefore section 4.1 introduces the ATR72 aircraft and the parameters involved and section 4.2 shows the theoretical model used for the baseline aircraft. Secondly, the power available is calculated in section 4.3 by providing a model for both the engine and the propeller. Thirdly, section 4.4 validates the fuel consumption using several external sources. Finally, in section 4.5 the well-to-propeller efficiency is calculated and section 4.6 is used to draw several intermediary conclusions.

4.1. AIRCRAFT SELECTION

In this research use is made of the propeller aircraft, the ATR72 aircraft (see Figure 4.1).

Figure 4.1: The ATR72 aircraft [95].

This aircraft gives room to a maximum of 70 passengers and can carry a maximum payload of 7,500 kg as is shown in Table 4.2. The most important feature of the aircraft with respect to this research is the fact that there are two PW 127M turboprop engines with propellers present. One of the benefits of a SHEA with respect to a Parallel Hybrid Electric Aircraft (PHEA) is the drag reduction due to the reduction in engine size and thus reduced fuel consumption. In order to exploit this benefit to the fullest, a propeller aircraft requires less design changes as a similar aircraft fitted with gas-turbines. Propellers have a much higher propulsive efficiency than jet engines below a Mach number of 0.7 [-], [67].

Table 4.2: Readily available data of the ATR72 aircraft that is used throughout this thesis [95].

Parameter	**Value**	**Unit**
Type	ATR72	-
Cost (estimate) [94]	28 million	*US$*
Passengers	70	-
Payload Mass	7,500	*kg*
MTOW	22,800	*kg*
MLW	22,350	*kg*
ZWF	20,800	*kg*
OEW	13,500	*kg*
Mach (During Cruise)	0.4	-
Engine	PW127M	-
Number of engines	2	-
Number of propeller blades	6	-

4.2. BASELINE AIRCRAFT MODELLING

Within this chapter the model is introduced that is used to describe the ATR72 aircraft and thereby calculate the required power at every mission segment. Use is made of both sizing tools, actual available flight test data and available literature about the aircraft. The engine model is covered seperately in section 4.3. The total model is implemented in Excel and validated and verified (see section 4.4) by using literary sources.

4.2.1. INPUT PARAMETERS

First, it is important to agree upon a fixed set of parameters that are used as input for the actual model. These 'mission parameters' are shown in Table 4.3

Table 4.3: Readily available data from the ATR72 brochure [95] and the engine manufacturer Pratt & Whitney [96].

Parameter	**Value**	**Unit**	**Source**
Wing surface	61	m^2	brochure [95]
Wing span	27.05	m	brochure [95]
Aspect ratio	12	-	brochure [95]
Weight at start mission	22,800	kg	brochure [95]
Payload	7,500	kg	brochure [95]
Maximum Fuel	5000	kg	brochure [95]
Landing Field Length	1,067	m	brochure [95]
Take-off field Length	1,290	m	brochure [95]
Cruise Altitude	5,000	m	brochure [95]
PW127 Max TO Power (5 min)	2,051,000	W/engine	PW 100 Series [96]
PW127 Normal TO Power (5 min)	1,846,000	W/engine	PW 100 Series [96]
PW127 Max Continuous Power	1,864,000	W/engine	PW 100 Series [96]

4.2.2. LANDING

First the approach speed is calculated using a statistical relation between landing field length as given by FAR 25, [97] and the statistical parameter k_L [66] as given in Equation 4.1. This speed is important as it is used to calculate the wing loading during take-off.

$$V_{Approach} = k_L \cdot \sqrt{s_L} = 1.85 \cdot \sqrt{1067} = 60.4 [m/s] \tag{4.1}$$

The maximum lift coefficient for landing is derived from the ATR72-600 brochure [95] to be 2.44 [-] and is consistent with Roskam [66] as the value is in between 1.6 and 2.6.

4.2.3. TAKE-OFF PHASE

During the take-off phase, two different scenarios can be distinguished All Engines Operative (AEO) and One Engine Inoperative (OEI), both are discussed within this section the latter is visualised by Figure 4.2. First the ground roll and 1st climb segment are discussed. The 2nd, 3rd and 4th segment, as shown in Figure 4.2, are discussed in subsection 4.2.4.

GROUND ROLL & 1ST SEGMENT CLIMB

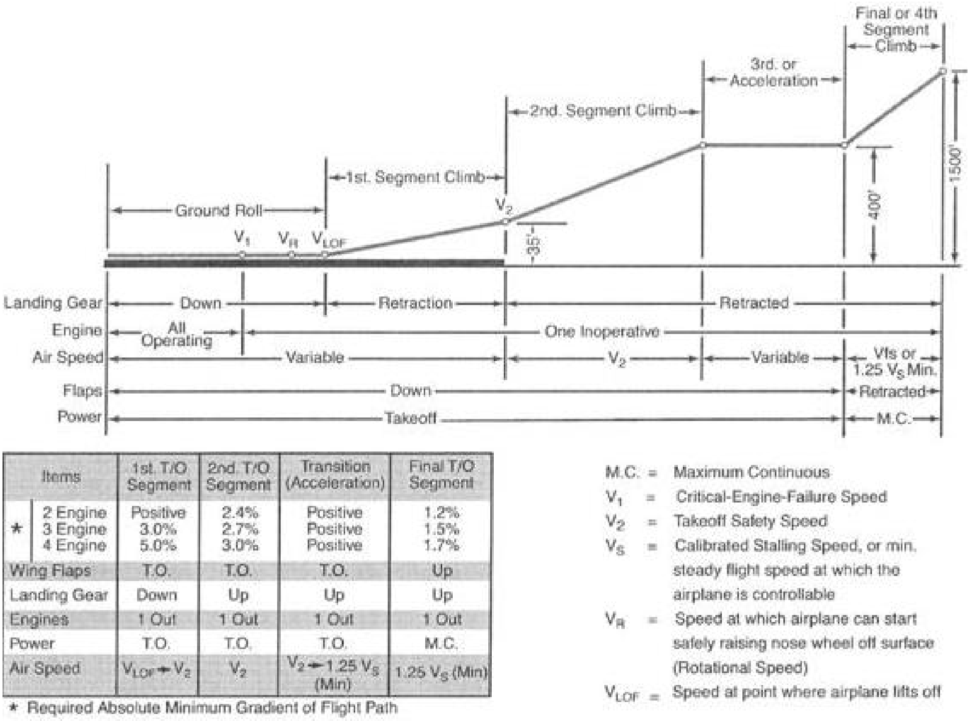

Items	1st. T/O Segment	2nd. T/O Segment	Transition (Acceleration)	Final T/O Segment
* 2 Engine	Positive	2.4%	Positive	1.2%
* 3 Engine	3.0%	2.7%	Positive	1.5%
* 4 Engine	5.0%	3.0%	Positive	1.7%
Wing Flaps	T.O.	T.O.	T.O.	Up
Landing Gear	Down	Up	Up	Up
Engines	1 Out	1 Out	1 Out	1 Out
Power	T.O.	T.O.	T.O.	M.C.
Air Speed	$V_{LOF} \rightarrow V_2$	V_2	$V_2 \rightarrow 1.25\,V_S$ (Min)	$1.25\,V_S$ (Min)

Figure 4.2: The take-off phase is shown in several segments [66].

The speed V_2 indicated in Figure 4.2 can be calculated using Equation 4.4. From literature [98], it is known that the maximum lift coefficient, during take-off, can be estimated as 80 [%] of the maximum landing lift coefficient.

$$V_{S,L} = \frac{V_{Approach}}{1.23} = \frac{60.4}{1.23} = 46.5[m/s] \tag{4.2}$$

$$V_{S,TO} = V_{S,L} \cdot \sqrt{\frac{C_{L,landing}}{0.8 \cdot C_{L,landing}}} = 46.5 \cdot \sqrt{\frac{2.44}{0.8 \cdot 2.44}} = 52.0[m/s] \tag{4.3}$$

The take-off safety speed (V_2) can be calculated by using a factor 1.2 [-] as described by the Federal Aviation Regulations (FAR) CS-25 regulations [97].

$$V_2 = 1.2 \cdot V_{S,TO} = 1.2 \cdot 52.0 = 62.4[m/s] \tag{4.4}$$

Furthermore the average speed during take-off can be calculated using Equation 4.5, where the take-off safety speed ($V2$) is derived from CS-25 regulations as shown in Equation 4.4.

$$V_{Average} = \frac{V_2}{\sqrt{2}} = 41.5[m/s] \tag{4.5}$$

The lift required during the first flight phase can be derived from weight fractions that are based on statistics [66] and are shown in Table 4.4. It can be seen that at the moment of lift-off a minimum lift force of $22347 * 9.81 = 2.19E5[N]$ is required.

Table 4.4: Weight fractions for the ATR72 during the take-off segment, derived from [66] in combination with the MTOW

Phase	**FF**	**MTOW**	**Unit**
Initial	-	22800	*kg*
Engine Start and Warm-up	0.999	22777	*kg*
Taxi	0.999	22754	*kg*
Take-off Ground	0.997	22686	*kg*

The zero-lift drag for the ATR72 is calculated individually for all components of the aircraft by combining results from the university of Hamburg [98],Loftin [65] and by using estimations for High Lift Devices (HLDs). The results for the take-off phase can be found in Equation 4.6 in combination with Figure 4.3.

$$C_{D,0,TO} = C_{D,0,N} + C_{D,0,H} + C_{D,0,V} + C_{D,0,F} + C_{D,0,W} + C_{D,0,LG} + C_{D,0,FL} = 0.050[-] \tag{4.6}$$

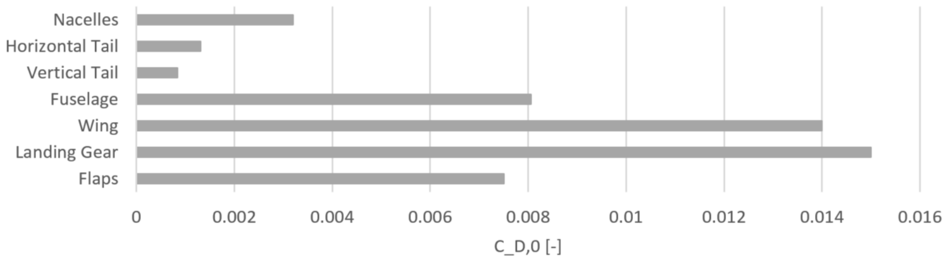

Figure 4.3: Zero lift drag per component for the ATR72 as calculated by the university of Hamburg [98] in combination with sizing theory by Loftin [65].

The total drag coefficient can be calculated (for each flight segment), by adding the corresponding zero-lift-drag and the induced-drag as is shown in Equation 4.7 for the take-off phase. Here the statistical value for the Oswald factor is 0.85 [bron] and the aspect ratio is given in Table 4.3.

$$C_{D,TO} = C_{D,0,TO} + C_{D,i,TO} = C_{D,0,TO} + \frac{{C_L}^2}{\pi \cdot A \cdot e} = 0.050 + 0.031 \cdot {C_L}^2 \tag{4.7}$$

Using this relation the lift-drag polar can be created as can be seen in Figure 4.4.

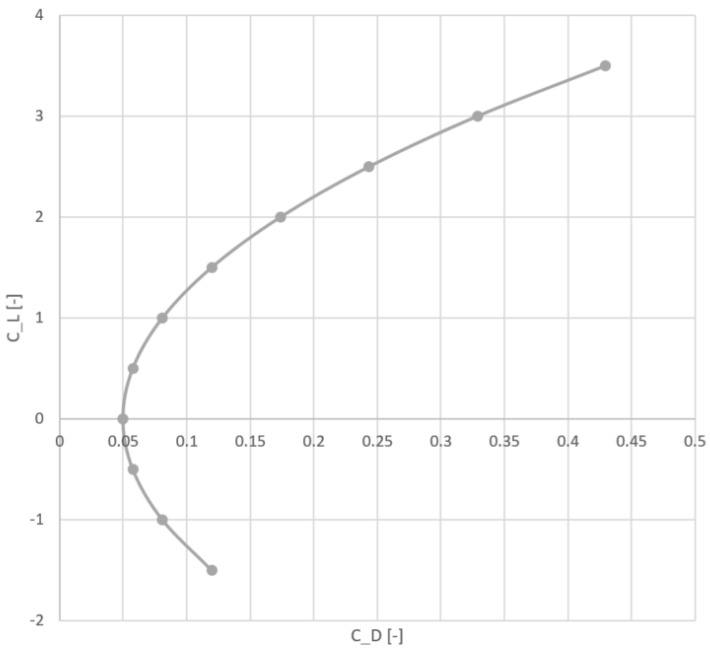

Figure 4.4: The lift drag polar for the take-off phase (flaps and landing gear down), the design point has a lift and drag coefficient of respectively 1.95 [-] and 0.17 [-], [98].

By combining the lift required with the average take-off speed ($V_{Average}$) and the lift-drag-polar, it is possible to calculate the required power in order to overcome the aerodynamic drag at any moment in time during the take-off phase. There are however two other power requirements to overcome:

1. Acceleration of the aircraft-mass up to the maximum take-off speed (V_2)
2. Decreasing friction with the runway as is shown by Equation 4.8
3. Climb Power up to screen height as shown by Equation 4.9

.

The tyre friction coefficient (μ_{TF}) is based on a dry runway and assumed equal to 0.48 [N/kg] [99].

$$P_{TF}(V) = W - \frac{L(V)}{g} \cdot \mu_{fr} \tag{4.8}$$

The power required (Equation 4.9) to reach screen height (35 [ft]) is dependent on the time required to get to the required altitude. Different sources gives an indication of approximately 3-7 [sec] between V_{LOF} and V_2, [100], [101], [98]. In order to maintain a safe design, the time to screen height (t_{scr} is set to 3 [sec].

$$P_{Height} = \frac{E}{t_{scr}} = m_{TO} \cdot g \cdot h_{scr} / t_{scr} \tag{4.9}$$

The resulting power required during the ground phase of the take-off segment can be found in Figure 4.5. It can immediately be seen that the peak loading (3.17 [MW]) occurs during acceleration of the aircraft. For a longer runway, this peak will decrease, however this is not possible due to regulations [97]. It should be noted that the power required shown in the figure is not the same as the power used during the take-off phase. The pilot has more power available and will 'normally' use the maximum thrust setting during take-off.

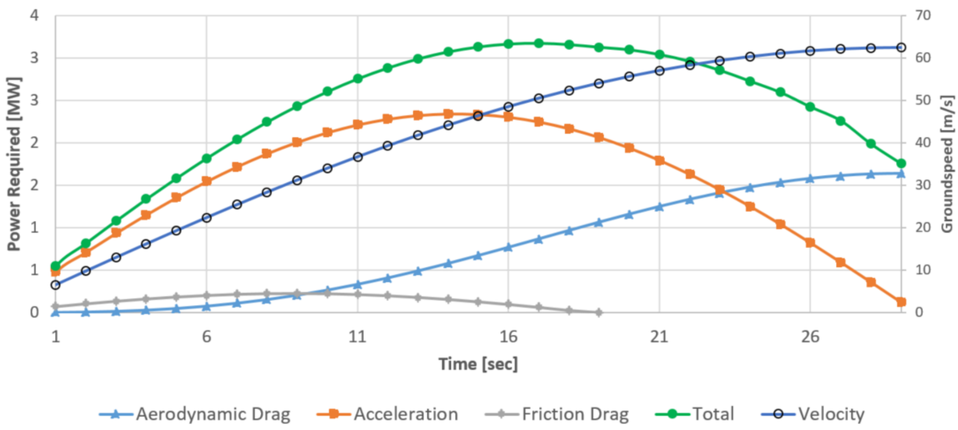

Figure 4.5: The different consumers of power are visualised separately for the first 30 [seconds] of the mission, the take-off phase.

4.2.4. CLIMB & ACCELERATION

Airliners use several climb phases to get to the initial cruise altitude. From literature [74] it is known that 3 'typical' cases exist, within this research the 'standard' case is used:

1. Maximum thrust setting and climb to 300 [m] (part of take-off phase)
2. Thrust cut-back and acceleration
3. At constant Calibrated Airspeed (CAS) (V2) climb to 1 [km]
4. Accelerate to 88 [m/s] CAS
5. At constant CAS climb to cruising altitude

Thus the second segment starts with a climb phase from screen height (10.7 [m]) to acceleration altitude (300 [m]). At the start of this segment the landing gear is retracted and thus the zero-lift-drag coefficient will decrease from 0.050 [-] to 0.035 [-]. The lift coefficient remains constant at 2.05 [-] and the weight of the aircraft varies during the cruise phase as fuel is consumed. The fuel consumption during this phase is mainly dependent on the climb angle and the flight speed chosen and the corresponding thrust setting. Multiple sources indicate that the thrust setting is not changed with respect to the take-off phase (90 [%] Thrust), however the minimum required climbgradient should be in between 2-4 [%], [97].

Directly following the constant velocity climb phase follows the accelerating climb phase at maximum thrust setting, where the altitude and velocity are slowly increased to 1 [km]. Then the aircraft is pitched over and accelerated to a CAS of 88 m/s]. Finally, at constant CAS, the aircraft is brought to cruise altitude and speed as can be seen in Figure 4.6. Within the calculations a standard atmosphere model is used, this can be found in Appendix E. It should be noted that the results found here are highly dependent on the climb angle and thrust setting/flight speed. The optimal climb angle found is unique to the specific mission flown, as is shown in Table 4.1. If however the altitude, payload, velocity or range is altered the corresponding climb angle will change depending on the amount of engine power available.

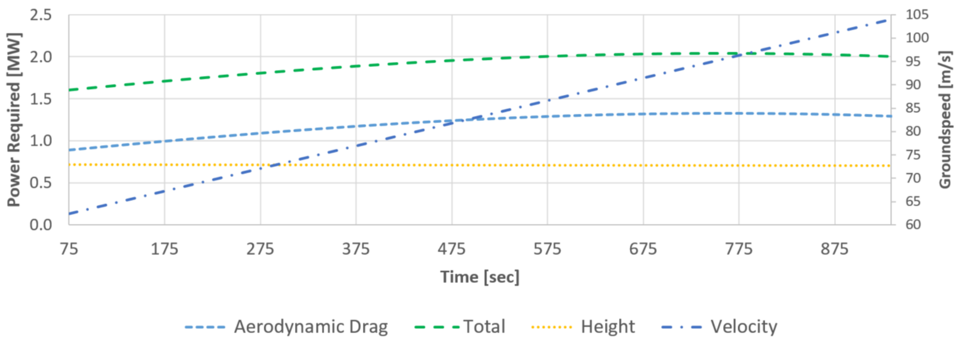

Figure 4.6: The different consumers of power are visualised separately for the second part of the climb and acceleration phase.

It can be seen that in a time-slot of approximately 14 minutes, a constant vertical climb speed of 6 [m/s] is maintained. Because the increase in speed has a higher impact on the drag than the decreasing air-density the drag increases slightly over time.

4.2.5. CRUISE

During the cruise phase, the speed is kept constant at approximately Mach 0.4 [-], Table 4.3. The total drag coefficient can be calculated, by adding the zero-lift-drag and the induced-drag as is shown in Equation 4.10. Here the statistical value for the Oswald factor is 0.85 and the aspect ratio is given in Table 4.3. The weight of the aircraft is assumed to decrease linearly with flight-time from 22,346 [kg] to 21,184 [kg] as is shown in Table 4.1.

$$C_{D,CR} = C_{D,0,CR} + C_{D,i,CR} = C_{D,0,CR} + \frac{{C_L}^2}{\pi \cdot A \cdot e} = 0.0274 + 0.031 \cdot {C_L}^2 \tag{4.10}$$

Using this relation the lift-drag polar can be created as can be seen in Figure 4.7.

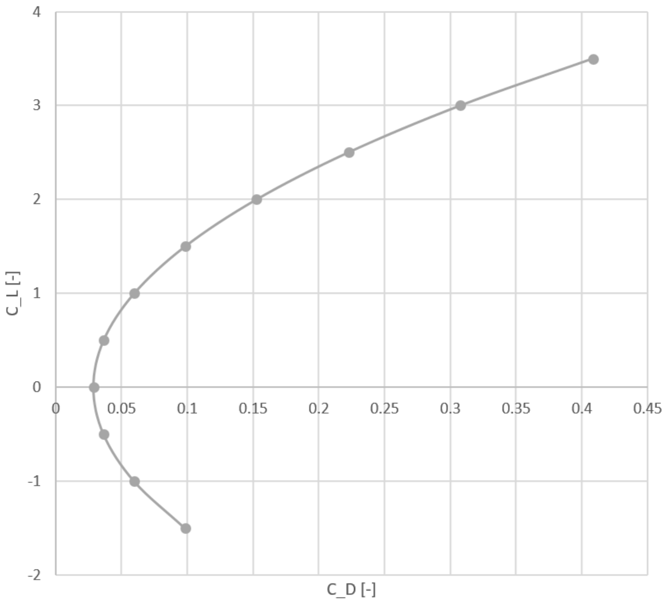

Figure 4.7: The lift drag polar for the cruise phase (flaps retracted and landing gear up), the design point has a clean lift and drag coefficient of respectively 0.81 [-] and 0.048 [-], [98].

The lift and drag coefficient are used extensively trough-out this chapter and have a large impact on the overall model behaviour. Therefore the validation process for both coefficients is covered again using multiple sources from literature in section 4.4. By combining all parameters covered in this section, it is possible to estimate the required power during the cruise phase at an average 1.75 [MW], at an altitude of 5000 [m] and a true airspeed (TAS) of 125 [m/s]. Again this value is highly dependent on the behaviour of the pilot and the mission flown. If the speed is increased at the cost of range, the power required will increase cubed.

Now the available power is known, it is useful to check the validity of this model by first investigating the engine and propeller model in the following section (section 4.3) and then the overall validity of the models used in section 4.4. Finally in section 4.5 the well-to-propeller efficiency is calculated.

4.3. ENGINE MODELLING

4.3.1. ENGINE MODEL

In the previous section the required power is calculated for each segment of the flight of the ATR72, within this section the power available is calculated. With these two sets of data known it is possible to find the specific flight segments where spare power is available but not used. Furthermore the data can be used to calculate the well-to-propeller efficiency of the ATR72 aircraft. Within this section the turboprop engine model is further elaborated upon, it uses the selected model by Loftin [65] as described in section 3.1 for the cruise phase and Table 4.5 provided by Pratt & Whitney on the PW127 engine for the take-off and climb phase. The power available is calculated per flight segment in cohesion with the previous section.

Table 4.5: Engine data as provided by ATR [93] and Pratt & Whitney [96] for various segments of flight. The table shows the advised power settings to the pilot, it is possible to deviate from these 'suggested' power-settings.

Power Setting	**Value**	**Unit**
Max TO Power (5 min)	2.051	MW
Normal TO Power (5 min)	1.846	MW
Max Continuous Power	1.864	MW
Max Climb	1.635	MW

POWER AVAILABLE - TAKE-OFF

Until decision speed V_1 is reached the pilot can choose to use full throttle on both engines or to use a de-rated thrust setting in order to reduce operating costs and improve engine lifespan and reliability. After V_1 is reached two situations can be described AEO and OEI, where only the latter uses maximum engine power available. In both scenarios the maximum shaft-power available is 2.051 [MW] per operating engine. This power is converted into a thrust force by the propeller, the efficiency at which this is done, is discussed in subsection 4.3.2. It should be noted that ATR72 also specifies a nominal take-off power that 'should' be used during take-off, therefore the shaft power available is 1.856 [MW].

POWER AVAILABLE - CLIMB & ACCELERATION

As Table 4.5 shows, the average maximum available power during the climb phase (from screen-height to cruise altitude) is equal to 1.64 [MW] per engine. In order to model the effect of altitude on the climb performance, Loftin [65] as described in section 3.1 is used to interpolate between the take-off phase and the cruise phase.

POWER AVAILABLE - CRUISE

The maximum available power during the cruise phase is described using again the theoretical model by Loftin [65] as described in section 3.1. Depending on the cruising altitude and the flight speed the maximum available power changes, but also the required thrust changes as is shown in the previous sections.

POWER AVAILABLE - LANDING

During the landing phase the available power will slowly increase as the altitude goes down, however the required power will be much lower as the potential energy and momentum of the aircraft can also be used to bring the aircraft down in a controlled manner.

4.3.2. PROPELLER MODEL

The theory behind the propeller model and the selection of the best model for this research is discussed in section 3.1. The parameters of the propeller used for the ATR72 are shown in Table 4.6.

Table 4.6: Parameters for the Hamilton-Sundstrand F568-1 propeller, as is used on the ATR72 aircraft, [74].

Parameter	**Symbol**	**Value**	**Unit**
Rotational Speed	Ω	1200	*RPM*
Diameter	D_{prop}	3.93	m
Number of Blades	B	6	-

If a propeller diameter of 3.93 [m] is used under cruise conditions (see section 4.2) an efficiency of 93.2 [%] can be calculated as can be seen in Figure 3.4. When comparing this value with 85.9 [%], as is calculated by the university of Hamburg [98], it can be seen that the ADT results in a too optimistic value for the efficiency. Therefore it is decided to multiply the ADT model with a factor 0.89 in order to adjust for non-linearity's in the performance properties of the disc (f.e. unsteady or discontinuous flow conditions), this is also shown in section 3.1 in Figure 3.4.

By combining Figure 3.4 and the flight velocity and altitude of the aircraft per segment it is possible to arrive at the efficiencies as shown in Table 4.7.

Table 4.7: Calculated propeller efficiency with and without correction factor per flight segment.

Segment	η_{ADT}	$0.89 \cdot \eta_{ADT}$
Take-off	81%	72%
Climb	96%	85%
Cruise	98%	87%
Descent	97%	86%
Landing	94%	83%

4.3.3. AVAILABLE PERFORMANCE

The aforementioned sections are combined in Table 4.8, where the maximum available power is visualised for AEO. It can be seen that a lot of shaft power is available during the take-off phase, however due to the inefficient performance of the propeller during this segment, the useful power available diminishes rapidly.

Table 4.8: Engine data as provided by ATR [93] and Pratt & Whitney [96] for various segments of flight in combination with the effective power available after incorporating propeller efficiency as shown in Table 4.7.

Segment	$P_{shaft_{avrg}}$	$P_{prop,avrg}$
Take-off	4102	2953
Climb	3114	2647
Cruise	2573	2239
Descent	3114	2678
Landing	3724	3091

The fuel flow can be estimated using Figure 4.8 in combination with Appendix B.

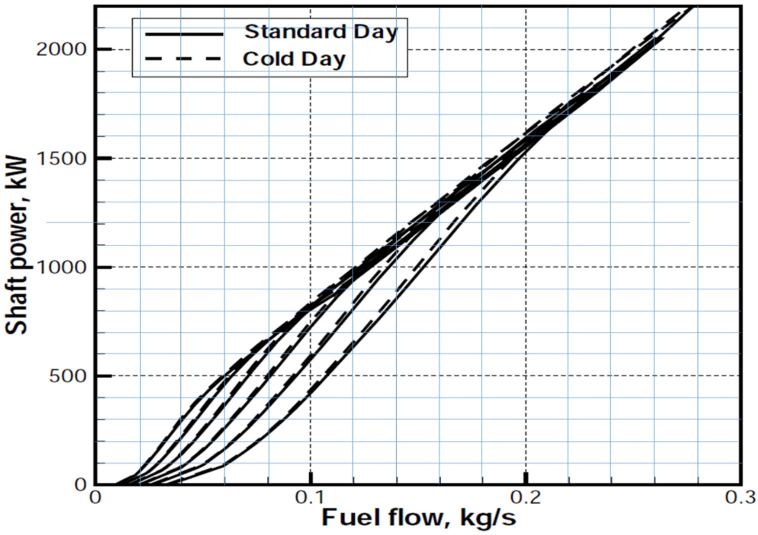

Figure 4.8: Measured fuel flow for the ATR72 turboshaft engine, [74]. The fuel flow is shown for different altitudes, in steps of 2000 [m] starting at sea-level for the upper line in the figure.

4

4.4. VALIDATION OF THE AIRCRAFT MODEL

Within this chapter the consistency of the models used is compared with actual data.

4.4.1. LIFT AND DRAG COEFFICIENTS

As is described in section 4.2 the model is heavily dependent on the values for the lift and drag coefficients. The used values can be found in Table 4.9. It can be seen that during the cruise phase a L/D ratio of 16.87 is used. When comparing this to literature (15.74 [102], 15.61 [103], 16.69 [104]) , an R^2 value of **0.95** can be calculated.

Table 4.9: The lift and drag coefficient are shown for the different flight segments modelled.

Parameters	**Configuration**	C_{D_0}	C_{D_i}	C_D	C_L
Take-Off	Clean(max) + Flap + Landing Gear	0.050	0.131	0.181	2.05
Climb	Clean(max) + Flap	0.035	0.031	0.166	2.05
Acceleration	Clean(max)	0.035	0.059	0.100	1.37
Cruise	Clean(optimum)	0.027	0.020	0.048	0.81
Landing	Clean(max) + Flap + Landing Gear	0.050	0.186	0.236	2.44

4.4.2. ENGINE MODEL

Within this section the engine model is validated against actual flight data. The shaft power model (Loftin [65] was already validated in section 3.1 with an R^2 value of 0.999. Actual data for the fuel consumption of the ATR72 cannot be found, however there is data available for the ATR42 aircraft that has a reduced fuselage size and thus a reduced total weight during cruise (-19 [%]). The data for this aircraft is shown in combination with data from the ATR72 model in Figure 4.9. The data is acquired from flights at different flight altitudes and speeds and can therefore give an accurate insight in the models used.

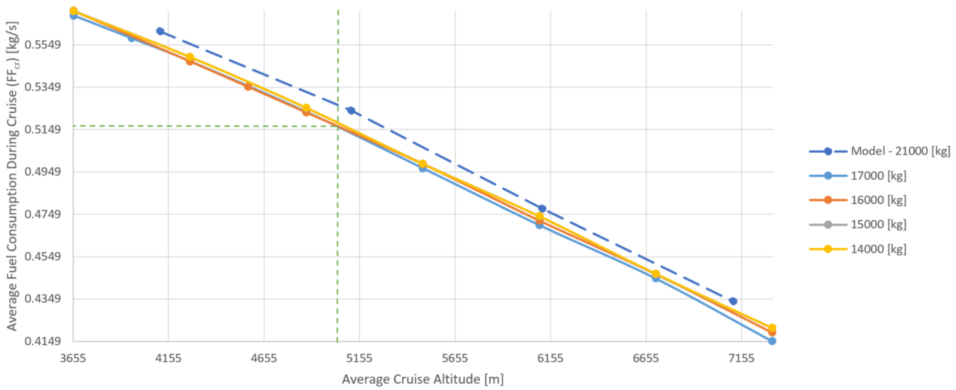

Figure 4.9: Visualisation of flight data of the lighter aircraft the ATR42 in comparison to the ATR72 model used within this Thesis. The dotted (short) line indicates the average cruise altitude of the model, the dotted (long) line shows the fuel consumption of the ATR72 model as a function of altitude. M = 0.5 [-].

It can be seen that the overall gradient of the data points is similar. If the measured data is linearly extrapolated to the model data a fit is achieved of R^2 = 0.941, as is shown by

Equation 4.11. The 6 [%] error can be explained by both errors in the model, in the linear extrapolation and the difference in aircraft type. The fit is however good enough for the remainder of this research. Furthermore by using the specific fuel consumption from [105] and [93] the validity of the engine efficiency is further validated.

$$R^2 = 1 - \frac{\sum \left(FF_{model_i} - FF_{data_i}\right)^2}{\sum \left(\bar{FF}_{model} - FF_{model_i}\right)^2} \tag{4.11}$$

4.4.3. PROPELLER MODEL

As it is highly difficult to assess the performance of the propeller as a separate system (without the interaction with the engines and the airframe), there exists no actual flight data for the F568 propeller. The only source of reference is the elaborate BEM study performed by Filippone [74], as was presented in section 3.1. From Figure 3.4 it can be derived that the R^2 value for the ADT is equal to 0.915.

4.4.4. CERTAINTY OF THE MODEL

The overall proportion of variance in the validation data that is explained by the models used is dependent on the summation of the error of all used models. As modelling an aircraft results in using several models, the resulting total variation can become large, quickly. Table 4.10 shows the summation of all models used within this chapter and an overall baseline model R^2 value of 0.753 is calculated. It should be noted that an unforeseen factor of 0.99 is incorporated in the calculation. This R^2 value is used in section 4.5 to show the accuracy of the models used within this chapter.

Table 4.10: An overview of the different models used in constructing the baseline model. Furthermore the R^2 value for each model is shown with an additional uncertainty factor of 0.99. The R^2 values not covered in this section are estimated or acquired from literature.

Aerodynamics	**0.949**
Geometry	*0.999*
Drag	*0.950*
Weight	**0.940**
Fuel Fractions	*0.999*
Fuel Consumption	*0.941*
Propulsion	**0.852**
WTT Eff	*0.990*
Engine Model	*0.941*
Propeller Model	*0.915*
Total R^2 Value (Including 1 [%] unforeseen)	**0.753**

4.5. WELL-TO-PROPELLER EFFICIENCY

Within this section the Well-to-Propeller Efficiency (η_{WTP}), Equation 4.12, is calculated for the ATR72 conventional propeller aircraft. In order to draw any conclusions with regard to this efficiency, the same ratio is calculated for the electric version of the ATR72 in section 5.3. The η_{WTP} is expressed as $\%_{usefullenergy}$ over $\%_{totalenergy}$ and will therefore be different for different flight phases.

$$\eta_{WTP} = \eta_{WTT} \cdot \eta_{TTP,t} \tag{4.12}$$

The Well-to-Tank Efficiency (η_{WTT}) and the Total Tank-to-Propeller Efficiency ($\eta_{TTP,t}$) are shown by Equation 4.13 and Equation 4.14 respectively. The η_{WTT} is a constant efficiency factor similar for every type of aircraft running on kerosene. The Tank-to-Propeller Efficiency (η_{TTP}) is different for every flight phase and is dependent on both the aircraft and the duration of each phase (t_{FP}). From literature ([106],[107],[1],[108]), it is known that the η_{WTT} efficiency for any petrol based vehicle in Europe is approximately 80 to 88 [%]. This includes extracting crude oil from the ground, refinement into kerosene, transportation and storage in the fuel-tank at the airport.

4

$$\eta_{WTT} = \eta_{extractioncrudeoil} \cdot \eta_{refinement} \cdot \eta_{transportation} \tag{4.13}$$

From the fuel-tank the kerosene is transported to the main engines with a certain fuel flow (FF) and then converted into work and waste heat. This is done by making use of both the propeller (P_p) as the residual thrust (F_g), as is discussed in section 3.1. Approximately 112 [kW] of the converted energy is used in the cabin (P_c), [109]. This energy is not used for propulsion purposes and should thus be subtracted as is shown in Equation 4.14.

$$\eta_{TTP,t} = \int_0^{t_t} (\eta_{TTP})\, dt = \int_0^{t_t} \left(\frac{P_p + F_g \cdot V_\infty}{FF \cdot E^*_{Kerosene} - P_c} \right) dt \tag{4.14}$$

The efficiency for this final process ($\eta_{TTP,t}$) can be calculated using Equation 4.14, the residual thrust can be found in Figure 3.5, the energy density of Kerosene used is 43.3 [MJ/kg], the results can be found in Table 4.11. As can be seen the total well-to-wheel efficiency adds up to $18.1[\%] \cdot 80[\%] = 14.5[\%]$.

Table 4.11: Tank-to-propeller ratios per flight phase as calculated in this chapter are shown. Furthermore the well-to-tank, overall tank-to-propeller and well-to-propeller efficiencies are given.

Segment	η_{TTP}		
Take-off	14.6	η_{WTTker}	80
Climb	17.9	$\eta_{TTP,t}$	18.1
Cruise	18.3	η_{WTP}	14.5
Descent	18.2		
Landing	17.5		

4.6. Intermediary Conclusion Baseline Model

Within this chapter the baseline model is presented for the ATR72 conventional aircraft. A mission profile is outlined and the required power is calculated. Furthermore the available power is calculated by using a model for both the propeller as the turboprop engines. Finally, by combining all models, the well-to-propeller efficiency is calculated with an R^2 accuracy (see Table 4.10) of approximately 0.753 to be 14.3 [%]. Meaning that the well-to-propeller efficiency is in between 12.5 and 16.1 [%].

It should be noted that the results found in this chapter are highly dependent on the 'actions' of the pilot and flown routes by the airliner. For example the take-off phase can be flown using full-thrust or (as some airliners/pilots do) by using a de-rated thrust setting. Overall the found power are consistent with literature and give an estimate of the 'to-be-expected' powers in a HEA as is covered in the following chapter.

5

Series Hybrid Electric Aircraft Model

This chapter is devoted to the modelling of the HEA and its sub-components. This chapter follows the same structure as chapter 4 with the main goal of convenient comparison between the two models. The results of this comparison and a sensitivity analysis of the parameters used can be found in chapter 6. The outcome of this chapter is an overview of all models required and used to model a SHEA. The validation of these models is shown by calculating the overall proportion of variance (R^2 value) with respect to validation data. Furthermore both a theoretical (optimal) design and a practical (currently available technologies) design are presented by calculating the corresponding well-to-propeller efficiency.

The main design philosophy is that that the overall well-to-propeller efficiency of the aircraft can be improved by minimising the size of the gas-turbine with the aid of batteries. Furthermore the gas-turbine is able to run at a constant power requirement (highest efficiency) instead of a variable one.

First, in section 5.1, the individual models used (e.g. motor, inverter, cables, etc.) are introduced. Second, in section 5.2, these models are validated by calculating the R^2 value with respect to validation data from a relevant industry (e.g. automotive, electronics, etc.). Third, the well-to-propeller efficiency is calculated in section 5.3. Finally, in section 5.4, an intermediary conclusion is drawn with respect to the theoretical upper and practical lower limit of the well-to-propeller efficiency.

5.1. Aircraft Modelling

Within this section the different theories used to model the HEA are demonstrated in the reverse order as the flow of energy. First, the propeller model is described briefly, second, the gearbox and the motors that generate the required shaft power are covered. Then, the inverters that control the power settings of the motors are described. Finally the power sources (batteries and the generator) and the cables connecting the electric systems are described. All these components are described from both a weight and an efficiency perspective as these are of trivial importance in modelling a new type of aircraft. In order to provide more structure to this section and to provide background with respect to the theoretical electronical background, chapter 2 is created.

5.1.1. Propeller

Finding an optimum in the geometry of the propeller falls beyond the scope of this research. While neglecting possible changes in interference drag of the propeller with the fuselage or the main and tail-wing due to changes propeller location, it can be assumed that the propulsive efficiency will not change. Therefore the model used within this chapter is identical to the adapted ADT model discussed in section 3.1.

However, because the maximum rotational velocity of a turbo-shaft is limited due to centrifugal forces inside the motor, the shaft speed is fairly constant during the entire flight envelope. Therefore the propeller requires multiple control units (PEC and PCU as described in section 3.1) to control the variable pitch of the blades and thereby the thrust setting. Because electric motors are less sensitive to temporary increases or decreases in rotational velocities, an optimisation is performed with respect to the optimal rotational velocity of the propeller, the results can be found in section 6.1.

5.1.2. Motor

The theory behind high performance PM motors is discussed in section 3.2. It is shown that there exists a quadratic relation between the main losses (conductor) and the current / torque required. Because the model is highly dependent on the specific motor power [W/kg], the model is made dimensionless. For well-to-propeller efficiency calculations a state-of-the-art and future value for the power-density are given in section 3.2 to be 5 and 8 [kW/kg] respectively. The efficiency is shown to be highly independent of motor size, for η_{WTP} efficiency calculation an lower practical limit of 95 [%] and an upper theoretical value of 97 [%] (including gearbox and cooling) is used.

5.1.3. Inverter (Motor Controller)

In order to control the amount of torque (τ) and rotational velocity (ω) of the electric motors and to monitor the status (e.g. temperatures and speed) an inverter is used. As the batteries output a DC and the motors require an AC, the inverter functions both as a DC to AC converter and a controller for the aforementioned parameters. Within this section the theoretical model [110] is described that is used to simulate the motor controller in the electric aircraft model. Use is made of a parametric model that is scalable with current, voltage and power. Both the efficiency and the weight of the inverter can be estimated using the model described. In section 5.2, a validation is given for the model. The model makes use of Insulated-gate bipolar transistor (IGBT) as these are currently considered the most efficient in the industry, [111]. The electrical components (e.g. IGBT, Bipolar Junction Transistor (BJT), Metal-Oxide-Semiconductor Field-Effect Transistor (MOSFET) and others) described in this section are explained in section 2.4.

EFFICIENCY

Both switching and conduction losses are modelled for the diode and the IGBT by using [110]. An IGBT is a cross-product between a MOSFET and a BJT resulting in a higher power gain, higher working voltage and lower input losses, [58]. In the following equations a power factor ($cos(\phi)$) is used equal to 1. The conduction losses (Equation 5.1), only occur when the IGBT is in full conduction, the losses depend on the amount of power required by the motor and the voltage drop in the inverter involved in delivering the required power. Within this equation, $\theta = 2 \cdot \frac{\sqrt{3}}{3} \cdot \frac{U_{Motor}}{U_{In}}$.

$$P_{IGBT,Conduction} = (\frac{1}{2\pi} + \frac{\theta \cdot cos(\phi)}{8}) \cdot \frac{I}{n_{par.}} \cdot U_{CE0} + (\frac{1}{8} + \frac{\theta \cdot cos(\phi)}{3\pi}) \cdot (\frac{I}{n_{par.}})^2 \cdot R_{CE} \quad (5.1)$$

5

Besides conductive losses there are also switching losses involved. These arise from the changing state of the IGBT, from blocking to conducting, with a certain frequency (f_{sw}). During the switching between these states a voltage can be measured across the terminals accompanied by a current trough the circuit, which results in dissipation losses as described by Equation 5.2. Within this equation the frequency (f_{sw}) varies linearly with the rotational velocity of the motor and the number of polepairs (number of magnets/poles divided by two) used inside this motor, $f_{sw} = n_{Motor} \cdot p \cdot k_p$.

$$P_{IGBT,Switching} = E_{T,r} \cdot \frac{I}{I_{Ref}} \cdot (\frac{U_{In}}{U_{CE,Ref}})^{1.4} \cdot f_{sw} \quad (5.2)$$

The IGBT can only handle a positive current, however due to the inductive nature of the motor, current could flow (during switching) in the opposite direction. In order to prevent high voltage peaks, the diode is used in combination with the IGBT. The losses involved are modelled according to Equation 5.3 and Equation 5.4, respectively the conduction and the switching losses.

$$P_{Diode,Conduction} = (\frac{1}{2\pi} - \frac{\theta \cdot cos(\phi)}{8}) \cdot \frac{I}{n_{par.}} \cdot U_{F0} + (\frac{1}{8} - \frac{\theta \cdot cos(\phi)}{3\pi}) \cdot (\frac{I}{n_{par.}})^2 \cdot R_F \quad (5.3)$$

$$P_{Diode,Switching} = \frac{E_D}{\pi} \cdot (\frac{I}{I_{F,Ref}})^{0.6} \cdot (\frac{U_{In}}{U_{F,Ref}})^{0.6} \cdot f_{sw} \quad (5.4)$$

With all losses known it is possible to calculate the total sum of losses $P_{losses} = (P_{IGBT,Cond.} + P_{IGBT,Switching} + P_{Diode,Conduction} + P_{Diode,Switching}) \cdot n_{series} \cdot n_{parallel}$. Here n_{series} is the number of switches in series inside the inverter and respectively $n_{parallel}$ is the number of switches in parallel, as is shown by Equation 5.5. In this relation a redundancy factor (k_r) of 20 [%] is used. Finally, the total inverter efficiency can be estimated using Equation 5.6.

$$n_{series} = \frac{U}{U_{Ref}}; n_{parallel} = \frac{I}{I_{Ref}} \cdot k_r \tag{5.5}$$

$$\eta_{Inverter} = \frac{P_{out}}{P_{out} + P_{Losses}} \tag{5.6}$$

WEIGHT

The weight is calculated by multiplying the individual weight of the sub-components in series and parallel as is shown in Equation 5.7. In this equation m_{switch} is equal to 0.398 [kg] as derived from the datasheet of the IGBT, [112], [113]. Because there are three phases per inverter and each component is used twice per phase, the mass is multiplied with six (see Figure 5.1.

5

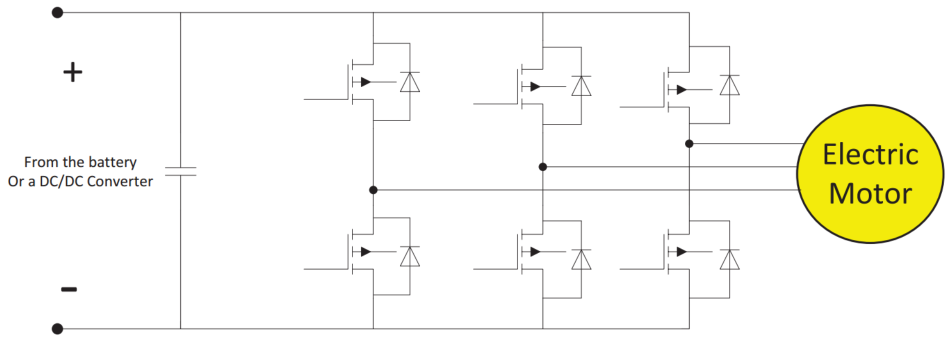

Figure 5.1: Typical inverter schematics, derived from [114]

$$W_{Inverter} = 6 \cdot n_{parallel} \cdot n_{series} \cdot m_{switch} \cdot k_{services} \tag{5.7}$$

5.1.4. CABLES

Everything that is related to getting a certain amount of electric power from geographical location A to location B within the airframe, is discussed in this section. The theoretical background of conductors can be found in section 2.3. Two material properties are of main importance when choosing a material for an electric conductor, these are the material-density (ρ) and the resistivity (σ). Although more exotic materials can be tought of, within this model three different materials are investigated as potential conductor: copper, aluminium and a superconducting material, the specifications are listed in Table 5.1, the literature behind the list can be found in section 2.3.

Table 5.1: Conductor types under investigation

Material	ρ $[g/cm^3]$	σ $[\Omega \cdot mm^2$ **/ m]** @ T = 273 [K]	**Source**
Copper	8.9	$1.67 \cdot 10^{-2}$	[115]
Aluminium {(AlFeMg alloy)}	3.293	$3.00 \cdot 10^{-2}$	[115]
Material	ρ $[g/cm^3]$	σ $[\Omega/m]$ **@ T = 69 [K]**	**Source**
HTS Bi-2223	8.2	$2.00 \cdot 10^{-7}$	[110], [116]

The electric losses through the cable [117] in DC have a quadratic relation with the Ohmic resistance of the conductor I^2R, the higher the current, the higher the losses involved. An AC through a cable will also give rise to a skin effect: the power losses will be higher, in comparison to DC, and increasing with frequency. In order to mitigate the skin-effect a specially woven Litz wire with multiple strands should be used, [118]. The resistance of the cable is dependent on the cross-sectional area, the material temperature and the type of conductor. Increasing the diameter will decrease the resistance, however there is a quadratic weight penalty involved in increasing the diameter of the wire. The relation between the parameters weight and power is described in section 4.5, the *power loading per flight phase* and can be used to find an optimum for the cable diameter. In other words the power loading in a certain flight phase describes the 'cost' in units of Watts of increasing the weight of the aircraft.

5

CONDUCTOR

Three types of cables are modelled in order to give a feeling for certain state-of-the-art and future innovations. First, Equation 5.8 describes the weight of a solid conductor per unit length (W^*), as copper or aluminium.

$$W^*_{cond} = \frac{\pi}{4} \cdot d^2_{cond} \cdot \rho_{cond} \cdot g \tag{5.8}$$

For a superconducting material it is important to know the amount of heat that is generated or the equivalent amount of power that requires dissipation, Equation 5.9. Here the Carnot efficiency is derived from literature [119], to have an upper theoretical limit of 30 [%], T_{sink} is the ambient temperature plus a safety margin of 5 [%]. T_{load} is the operating temperature of the superconductor.

$$P_{cooling} = P_{heat} \cdot \frac{C_{Carnot}}{\eta_{Cooling}} = P_{heat} \cdot \frac{T_{sink} \cdot T_{load}}{T_{load} \cdot \eta_{Cooling}} \tag{5.9}$$

Finally, Equation 5.10 gives the weight of a superconducting material including the weight of the cooling-unit per unit length. The specific weight of the cooling device is 330 [W/kg] [110]. If an ambient temperature of 273 [K] is used in combination with the HTS material Bi-2223 with an operating temperature of 69 [K], a constant supply of approximately 1 [kW] is required.

$$W^*_{supercond} = W^*_{cond} + \frac{W_{cooling}}{l_{supercond}} = W^*_{cond} + \frac{P_{cooling}}{l_{supercond} \cdot 330} \tag{5.10}$$

In order to visualise the effects of both these types of conductors Figure 5.2 shows different methods of sending 1.0 [MW] of power through a cable with varying diameters and voltages, as a function of unit length [m]. It can be seen that aluminium is a good alternative for copper wiring in terms of overall weight [115]. Because the conductivity of copper is 40 [%] higher than the conductivity of aluminium, the diameter will increase with a factor 1.6, however, due to a more preferred material density the overall weight will decrease with 51 [%].

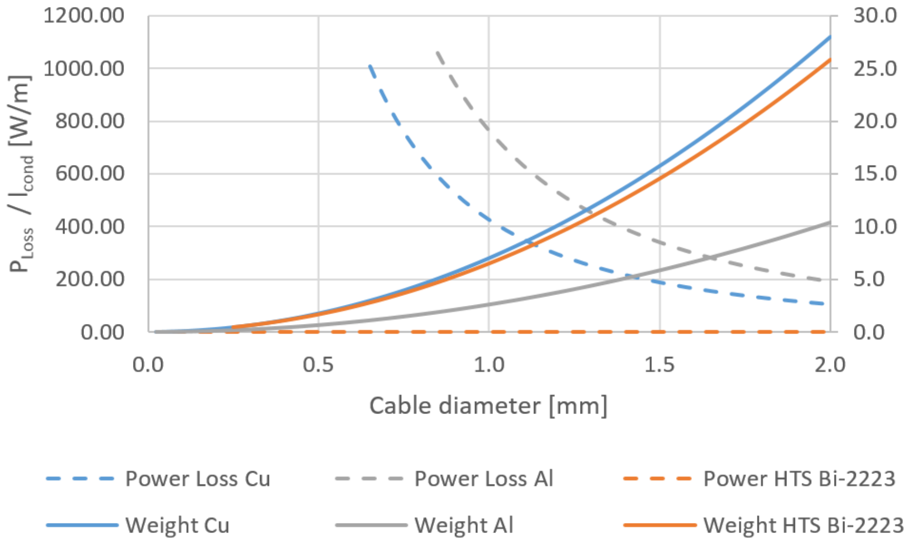

Figure 5.2: Visualisation of the weight and the power losses of a conductor, with varying diameter, transmitting 1.0 [MW] of power at 100 [A] as a function of conductor length [m]. The weight of the superconducting material is calculated including the cryocooler weight according to [110], however excluding the cryocooler power consumption.

In order to find an optimum in cable diameter the 'cost' of adding weight in an aircraft should be used to express a [kg] in units of power [W]. The optimal diameter is calculated (Equation 5.11) by calculating the smallest energy consumption during the cruise phase, the results can be found in Figure 5.3. Here the system is again made independent of cable length (denoted by *). The additional power required as a function of weight is given in Equation 5.11 and the effective power transportation is calculated by Equation 5.12. Here only Ohmic losses are taken into account.

$$P^*_{weight} = W^*_{cond} \cdot \frac{1}{(L/D)_{cr}} \cdot V_{cr} = W^*_{cond} \cdot 7.41 \tag{5.11}$$

$$\eta^*_{cond} = \frac{I \cdot U - P^*_{weight} - I^2 R^*_{cond}(A)}{I \cdot U} \tag{5.12}$$

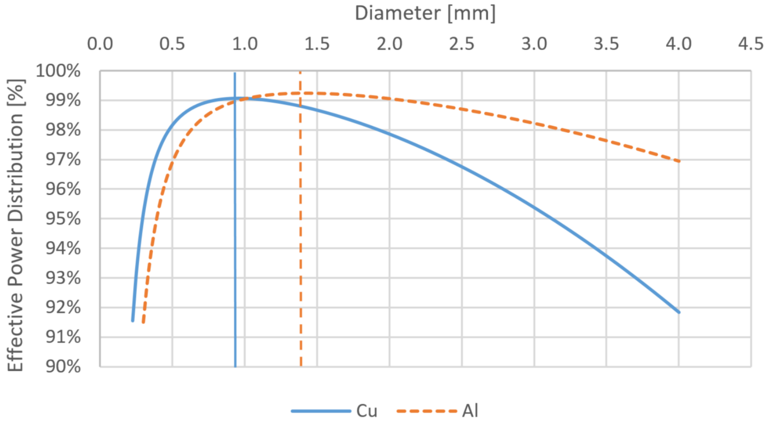

Figure 5.3: The theoretical effective power distribution, for 100 [A_{DC}], as a function of wire diameter is shown for both copper and aluminium as conductor material. The dotted lines indicate the optimum, where the total losses (increase in drag and Ohmic losses) are minimised.

5

It can be seen that for a current of 100 [A] an optimum cable diameter is found of 1.0 [mm]. The Ohmic loss (I^2R) at this diameter is equal to 213 [W/m], which is too high to allow for natural cooling of the cable. The maximum stable temperature of a conductor is dependent on the materials used, the insulating material has the lowest operating temperature (see Table 5.2) and is therefore limiting. The natural convection can be calculated using Equation 5.13, here the ambient temperature (T_a) is set at 293.15 [K] and the limiting temperature (T_{max}) including a safety factor are set to $0.9 \cdot 533$ [K]. It can be shown that a balance in radiative heat losses and generated heat, again for a current of 100 [A], is reached for a diameter of 4.3 [mm]. At this diameter approximately 12 [W] is radiated, the equations used are verified using [120]. Using these calculations it is shown that the leading design parameter is not the minimisation of losses, but the heat dissipation of the conductors. Furthermore it is shown that alternative conductor materials as aluminium can be used to minimise conductor weight. More exotic materials can be taught of as using carbon fibre materials, however investigating the potential of these types of materials fall beyond the scope of this research. The dependency of voltage variations (and thus current variations) is shown in section 6.2.

$$\dot{Q}_{rad} = A \cdot \varepsilon \cdot \sigma (T_a^4 - T_{max}^4) \tag{5.13}$$

Table 5.2: The maximum allowed working temperatures of some types of insulation materials as well as the melting temperatures of aluminium and copper. Derived from [121].

Insulating Material	T_{max} **[K]**	**Insulating Material**	T_{max} **[K]**
PTFE	533	ETFE	428
CETHAX	398	PFA	533
PVC	353	HYTREL	353
FEP	473	Bare Al	660
CETHAX	398	Bare Cu	1085

5.1.5. POWER SUPPLY

Within this section both the gas turbine as the generator are discussed that supply the power to the HEA during flight. Furthermore, a trade-off is made in order to decrease the size of this turbine at the expense of increasing the size of the battery-pack. Finally, also the overall battery design is discussed. The location and main impact of the weight of the main power supply of the HEA is not discussed elaborately in this thesis. Torenbeek [122], however suggests integrating larger APUs in "aerodynamic fairings near the root of the wing, as these can act as Whitcomb bodies". An overall optimisation of the integration of a single or double generator (depending on regulations for OEI), should be performed in future research. Within this research two gasturbines are used, as regulations will most likely stipulate this with the focus on an OEI condition.

GAS TURBINE AND GENERATOR SIZING

Within this section the current trend in engine efficiency and weight as a function of output power is derived. At this moment almost every aircraft is already equipped with an onboard Auxiliary Power Unit (APU). These APUs consist mostly out of a turboshaft engine in combination with a generator. As an electric motor contains the same components as a generator the weight of the latter component can be derived using the same data as used in section 3.2.

By combining the data of 292 engines, Figure 5.4 is created. It can be seen that the linear trend indicates a fixed and variable mass of respectively 30 [kg] and 0.21 [kg/kW] for turboshaft engines. It can be seen that for higher take-off power ratings the data-points are more widespread. The power-density as a function of year of certification can be found in Appendix D. An average increase in power density for turboshaft engines exists equal to +0.24 [kW/kg/year],[123].

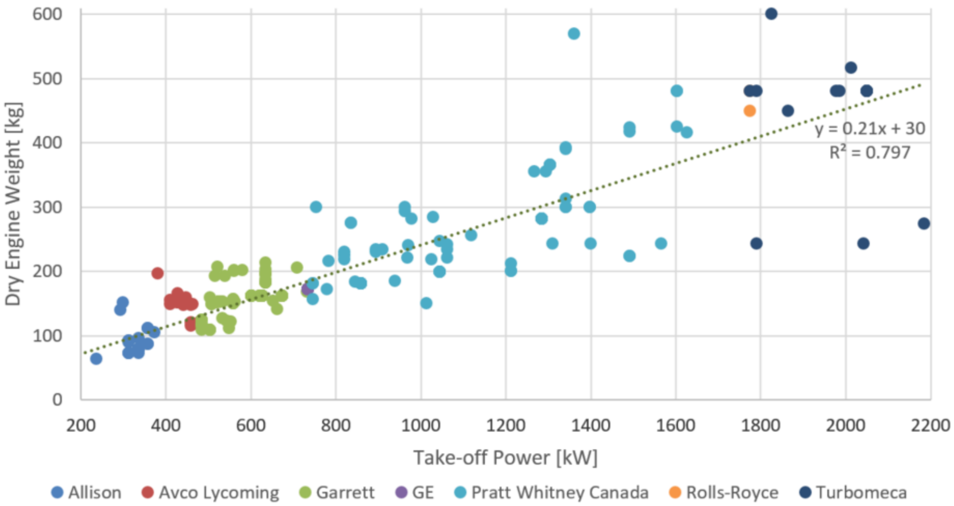

Figure 5.4: The take-off power versus the engine dry-weight are plotted in order to find a linear relation between the two. The engine data is categorised by manufacturer with N=292, R^2=0.797 [124]

Using Figure 3.6 from section 3.2 a fixed and variable weight of respectively 5 [kg] and 0.2 [kg/kW] can be found for the electric generator. The AC to DC conversion is done using an inverter (as covered in subsection 5.1.3) and this weight can be estimated using a fixed weight of 0.76 [kg] in combination with a variable weight of 0.1 [kg/kW]. The models for these components are combined with a contingency (e.g. fairings, bearings, couplings, cables, unforeseen) of 20 [%]. The relation between mass (in [kg]) and power output (in [kW]) of the power supply is shown in Equation 5.14

$$W_{PowerSupply} = 0.61 \cdot P_{output} + 43 \tag{5.14}$$

By integrating the engines in the aerodynamic fairing of the fuselage/wing-root the impact of increasing the engine size will be smaller, therefore additional systems as recuperation could be applied. This could result in a decrease in fuel consumption [125], however beyond the scope of this particular research.

BATTERY SIZING

Because the future of battery energy density is highly uncertain [1], a similar approach is used in modelling the battery as is used in the drive-train design. By parametrisation of the battery model and trade-off, it is possible to arrive at a solution that is independent of technological progress. In order to still be able to give an estimate of the well-to-propeller efficiency, again an upper and lower value for the battery technology is used as discussed in section 2.2. It is interesting to see if the theoretical limit of Li-Ion would suffice or if further research is required in other battery technologies in order to make the concept of electric flight feasible. An overview of the battery technologies discussed in section 2.2 is given in Table 5.3.

5

Table 5.3: Recap from section 2.2, an overview of both the practical and theoretically expected energy density for several battery technologies.

Cell Material	**Energy Density** $[Wh/kg]$	**Theoretical Energy Density** $[Wh/kg]$
Lithium Ion	240	320
Lithium Sulphur	400	2,700
Lithium Oxygen	1,000	15,000

5.1.6. OVERALL SYSTEM OPTIMISATION

Because all aforementioned models are interdependent, an optimisation is required with respect to minimising weight, while optimising efficiency of the overall propulsion system. Variable parameters are: the state of the different technologies used, the main working voltage and the amount of batteries. The weight of the overall aircraft is kept constant within a 10[%] range, the drag is then scaled with the L/D ratio and average speed used during cruise. The percentage heat generated (e.g. 1 - component efficiency) is removed with a theoretical carnot efficiency of 30 [%], comparable to subsection 5.1.4 in this section. The model is implemented in both an Excel as a Matlab environment (Appendix J). Validations of the sub-models are given in section 5.2, verification is done using top-level calculations, these are revisited in chapter 7 for convenience.

5.2. MODEL VALIDATION

Within this chapter the consistency of the models used is compared with actual data. The propeller model is not covered again as the R^2 value of 0.915 is already calculated in section 4.4. The electronic components (motor, inverter, batteries), have never been tested under the exact circumstances as described in this master thesis, therefore data is extrapolated from relevant test-data.

5.2.1. MOTOR

As the best known available motor at the moment (that could be used for reference) for electric aircraft is designed and produced by Siemens and the only available test data for this motor also comes from Siemens, there exists a conflict of interest in the validity of the externally communicated results. Therefore, within this section other high performance PM motors are used for validation purposes. Data could for example be found for a 154 [kW], 95.3 [%] efficient, axial-flux PM motor, [80]. This data is first of all used to show the linear relation between current (I) and torque (τ), Figure 5.5. The figure shows the direct impact of a higher torque output on the copper losses (I^2R). For this specific motor the internal resistance (R) is equal to 0.0401 [Ω], it can be seen that a quadratic trend-line fits the data neatly.

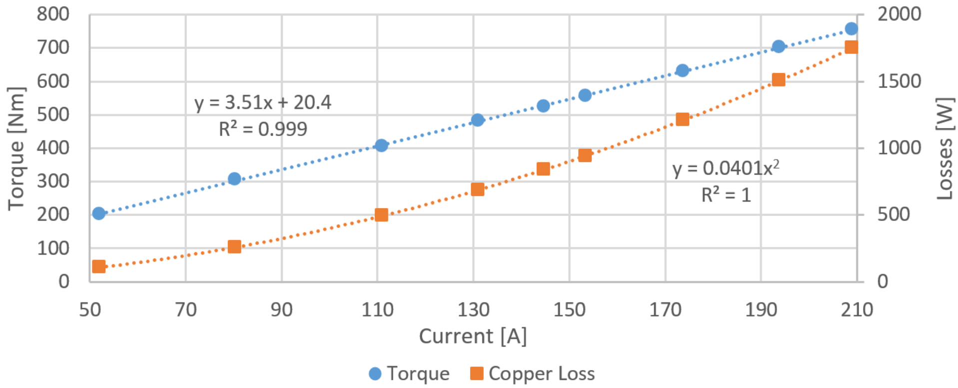

Figure 5.5: Visualisation of the relation between torque, current and the copper losses in a high performance PM motor. Data used for this figure is calculated using [80] and both a linear and a quadratic relation are used to describe the behaviour of the data points.

Secondly several permanent magnet motors are used to find a relation between design power (continuous) and design torque. The results are shown in section 3.2 in Figure 3.6. It can be seen (in this figure) that the motors used in the automotive industry and the aerospace industry show a similar behaviour: an increase of 1 [kW] results in approximately an increase of 0.2 [kg] and 4 [Nm]. However, although the housing weight (static) of electric motors used in the aerospace industry is minimised, weight is of lesser importance in the automotive industry and thus the average starting weight is higher. The R^2 value for the motor weight data is 0.996, the R^2 value for the torque is 0.961. Using a dataset with N=11, the efficiency R^2 value is calculated to be 0.995.

5.2.2. INVERTER (MOTOR CONTROLLER)

Within this section the inverter model (introduced in subsection 5.1.3) is validated. This is done by making use of several readily available inverters from the automotive, agriculture and aerospace industry. By combining the input DC power with the dry-weight (without the cooling system), Figure 5.6 is created. Specifications about the inverters used to create this figure can also be found in Appendix G.

The dotted (red) line is a linear fit to the set of datapoints with an R^2 value of 0.94, the striped (green) line is created by making use of the theoretical inverter model, here the R^2 value between the original data and the model is 0.91. From literature it is known that currently the best inverter has a power density of 11 [kW/kg] [79]. However, the trend seen in Figure 5.6 is equal to $1/0.1044 = 9.6[kW/kg]$. It should be noted that the approximation of the inverters with a lower power (<50 [kW]) shows a much better fit with a low power IGBT from [113] than with the high power [126].

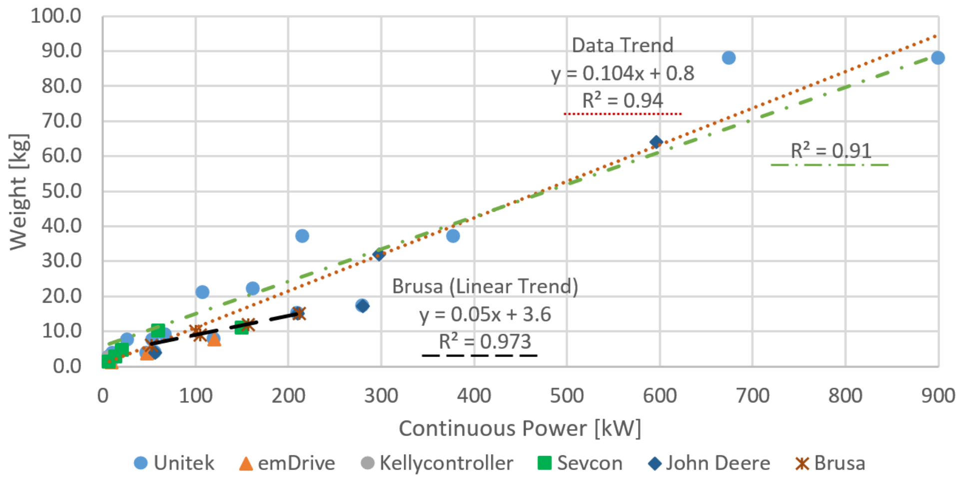

Figure 5.6: By using readily available data on power inverters ([127],[128],[129],[130],[131],[132],[133]), a relation can be shown between the overall weight and the power consumption of the inverter, N=39.

It can be seen that the brand Brusa [132] behaves in a more favourable manner with respect to the power-density. The trendline is shown striped (black) with a R^2 value of 0.973 and when extrapolated, the resulting power density results in 18.45 [kW/kg] which is almost a factor two higher than the main trendline. All other data sets show a similar behaviour with respect to the main trendline. No correlation between inverter power and efficiency could be found and it is estimated (by using N=5 datapoints, [132],[133]), with a 0.99 R^2-certainty, that an optimal design can reach an efficiency of at least 97.5 [%] for a power consumption of 150 [kW] or higher. Practical experience by both [134] and the writer indicate that (at this power consumption or higher) the efficiency could approach 99 [%] as the losses become less significant with respect to the overall power conversion.ef

5.2.3. CABLES (POWER DISTRIBUTION)

The cable weight R^2 value of a solid conductor without shielding is assumed equal to 1, as the material density of copper and aluminium are well known properties. The weight of the shielding, tape-layer and insulation are also well known properties for regular cables, therefore the R^2 value is set at 0.99. The efficiency of sending a DC can be checked by validating the maximum allowable current through the conductor as is shown in Figure 5.7.

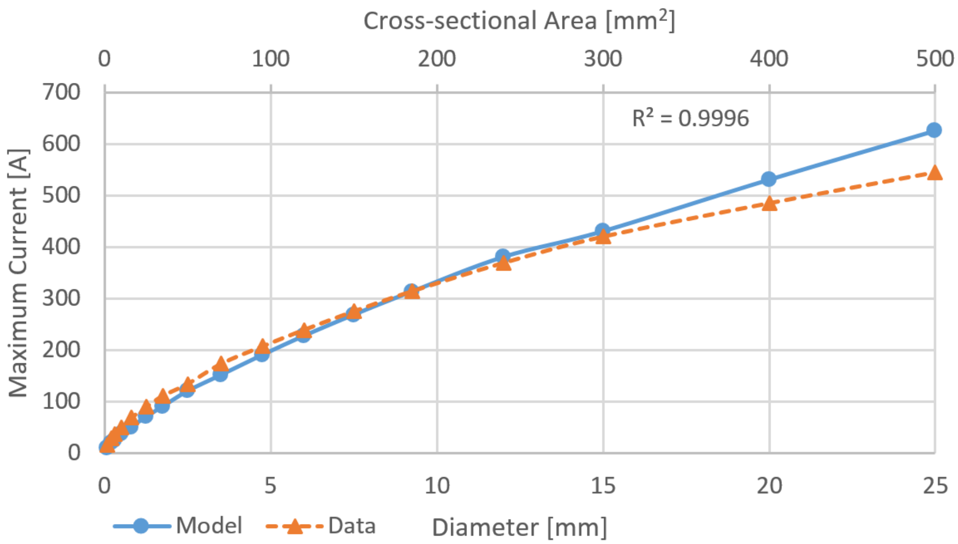

Figure 5.7: The maximum allowable current through a conductor is modelled for similar cable diameters as can be found in validation data [120]. An R^2 value of 0.992 can be calculated for the spreading of the data with respect to the model.

5.2.4. POWER SUPPLY

Within this section the power supply model is compared with the weight found in APUs now-a-days. An overview of APU data can be found in Figure 5.8. The dotted (blue) line is a linear fit to the datapoints with an R^2 value of 0.88, the striped (green) line shows the model introduced in section 5.1.

Although the fit is not optimal for the (low power) datapoints shown, the actual difference, between the model and the linear fit, at a relevant value (1500-2000 [kW]) for the power output shows a difference of 13-14 [%]. This corresponds with an estimate for the power supply weight (at 1500 [kW]) of 958 [kg] and 1100 [kg] for the model and the extrapolation of the linear trend respectively. It should be noted that the difference is mainly found in the gradient, shifting the model with -20 [kg] will create a much better fit (R^2 value changes from 0.57 to 0.85), but the absolute difference at 1500 [kW] remains similar. The R^2 value for the gasturbine efficiency can be derived from section 4.4 in combination with [105] and [93] to be 0.941.

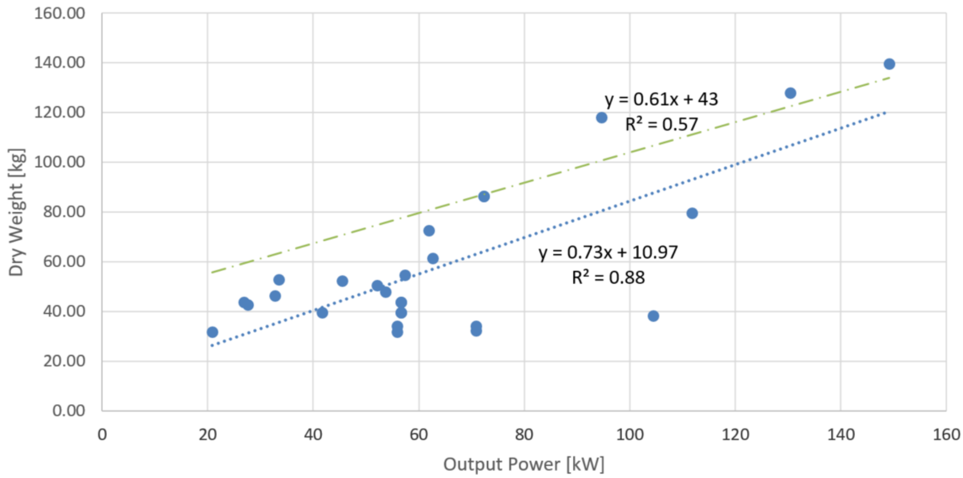

Figure 5.8: By combining data for different types of APUs ([109] and [125]) a linear relation between APU weight and output power is constructed, N=28.

5

5.2.5. CERTAINTY OF THE MODEL

Similar to section 4.4, the overall proportion of variance in the validation data that is explained by the models used is calculated by multiplying the individual R^2 values and incorporating an unforeseen factor of 0.99. The results for this chapter can be found in Table 5.4. The overall certainty is dependent on the summation of the error of all used models, as the number of models used within this chapter is much larger than the number of models use in chapter 4, the variation in data will naturally also be larger. The value of 0.63 for R^2 means that an uncertainty band of 37 [%] surrounds the overall HEA model. Especially the efficiency and the weight of the gasturbine & generator combination are uncertain as no APU exists within the aerospace industry with a similar power rating.

Table 5.4: An overview of the calculated overall proportion of variance between validation data and the models introduced in this chapter. With an R^2 value of 0.77 for the weight modelling and 0.92 for the efficiency modelling, the overall model variance is 0.70.

Weight	**0.77**
Motor	*0.996*
Inverter	*0.91*
Cables	*0.992*
Gasturbine & Generator	*0.852*
Efficiency	**0.92**
Motor	*0.99*
Inverter	*0.995*
Cables	*0.99*
Gasturbine & Generator	*0.941*
Total R^2 Value (Including 1 [%] unforeseen)	**0.70**

5.3. Well-to-Propeller Efficiency

In order to get energy from well to battery, several conversions are required. The electric efficiency of the grid is dependent on the source as is shown in Table 5.5. The charging efficiency [%] of batteries is assumed equal to 90 [%] [135]. For this research a worst-case-scenario is used; η_{WTT} efficiency for kerosene is 80 [%] as discussed in chapter 4 and η_{WTT} efficiencies for electricity of 37 and 77 [%] are used for respectively natural gas and renewables as source.

The energy required in the process of constructing a powerplant is not taken into account in the well-to-tank calculations. The construction energy is not well defined in literature [136] and averages out between different sources of energy (e.g. wind, solar, natural gas). Extraction and conversion losses are present in transforming raw material to usable energy carriers (f.e. from crude oil to kerosene). As the source of energy for renewable forms of energy is considered infinite, the extraction and conversion efficiencies do not apply.

5

In the model described in this research the efficiency of renewable sources of energy does not have an influence on the well-to-tank efficiency. It might be of interest to investigate, in future research, the influence of this assumption.

Table 5.5: Several sources, indicate different η_{WTT} efficiencies from different sources as well as an average for the entire grid in the USA, [135], [137], [138]

Energy Source	Extraction	Conversion	Transportation	Charging	Total
Renewable	-	-	86-92	90	77-83
Natural Gas	90-92	53-60	86-92	90	37-46
Coal	98	44.2	86-92	90	34-36
Average Grid	95	42.7	86-92	90	31-34

Due to the absence of residual thrust, the equation for the η_{TTP} efficiency simplifies to Equation 5.15. The fuel flow (FF) to the generator is a function of the required power as shown by Equation 5.16. This relation is shown in section 4.2 and derived from [68].

$$\eta_{TTP,t} = \int_0^{t_t} (\eta_{TTP})\, dt = \int_0^{t_t} \left(\frac{P_p}{FF \cdot E^*_{Kerosene} - P_c} \right) dt \tag{5.15}$$

$$FF = f\left(P_{required}\right) = f\left(\frac{T \cdot V_\infty}{\eta_{prop} \cdot \eta_{inv} \cdot \eta_{cables} \cdot \eta_{gen} \cdot \eta_{motor}} \right) \tag{5.16}$$

A sensitivity analysis of the different variables used within the model is discussed in chapter 6. Within this section both a best-case (theoretical) and a state-of-the-art (currently available) calculation is performed for the η_{TTP} efficiency. A summary of all efficiencies derived within this chapter can be found in Table 5.6.

Several different configurations (including the baseline model from chapter 4) are calculated and shown in Table 5.7. The bus-voltage and battery size are optimised, such that the generator mass is minimised. Furthermore two cases are covered, where first the electricity required is generated using natural gas, and the second is generated in a sustainable manner. It can be seen that the by not adding batteries to a HEA, the overall efficiency goes down rapidly. Furthermore the effect of increasing the battery technology from 240 [Wh/kg] to 1,000 [Wh/kg] is best demonstrated by the larger difference in η_{WTP} for the theoretical case with respect to the currently available case.

Table 5.6: Efficiencies and energy densities used in the overall model. It should be noted that only the maxima and minima are mentioned in this table, in reality these numbers are interdependent and variable.

	Currently Available		**Theoretical**	
	Efficiency [%]	Energy Density	Efficiency [%]	Energy Density
Motor	95	5000 [W/kg]	97	7000 [W/kg]
Inverter	97.5	9600 [W/kg]	99	11000 [W/kg]
Generator	95	5000 [W/kg]	97	7000 [W/kg]
Gasturbine	25.2	1364 [W/kg]	26.6	1566 [W/kg]
Battery	90	400 [Wh/kg]	95	1000 [Wh/kg]

Within these results the added battery weight is optimised such that the gasturbine and generator size is minimised. This means that the take-off and climb power production constraints placed on these components is lower, because power is also supplied by the batteries. The column in Table 5.7 named $\eta_{TTP_{nobatteries}}$ shows the η_{WTP} without batteries. The battery technologies used for the currently available and theoretical scenarios are respectively Li-Ion at 240 [Wh/kg] and Lithium Oxygen at 1,000 [Wh/kg]. For both these energy densities, an increase in battery mass results in an increase in well-to-propeller efficiency. However the total mass of the aircraft and thus the drag also increase. As the L/D ratio is linearised, the weight would keep on increasing infinitely as the increase in drag is less than the increase in efficiency. A maximum of 10 [%] increase in overall weight with respect to the baseline aircraft is allowed. Furthermore, it is seen that the model converges to an aea for a battery energy density of 2,802 [Wh/kg], both the fuel weight and the generator weight are then brought back to zero.

Table 5.7: Both the theoretical maximum as the currently available State-of-the-Art (SotA) η_{TTP} are shown for different flight segments with the corresponding time.

η_{TTP}	**No Batteries**	**Currently Available**	**Theoretical**
Take-off	11.8	14.2	15.9
Climb	13.8	17.6	19.3
Cruise	13.6	16.6	20.2
Descent	13.7	16.8	17.8
Landing	17.1	16.5	18.5
$\eta_{WTT_{ker}}$	80	80	80
$\eta_{WTT_{elec}}$	-	37-77	37-77
$\eta_{TTP,t}$	13.6	16.7	19.4
η_{WTP}	10.8	13.2-13.3	14.4-15.5

By combining the results for the η_{WTP} with the uncertainty factor found in section 5.2, both Table 5.8 and Figure 5.9 are created.

Table 5.8: Numerical results chapter 5, both the well-to-tank as the tank-to-propeller ratios are shown for different cases.

Well-to-propeller Efficiency	R^2	Lower Value	Mean Value	Upper Value
$\eta_{WTP_{baseline}}$	0.75	12.5	14.3	16.1
$\eta_{WTP_{nobatteries}}$	0.70	9.2	10.8	12.4
$\eta_{WTP_{current,naturalgas}}$	0.70	11.2	13.2	15.2
$\eta_{WTP_{current,renewable}}$	0.70	11.3	13.3	15.3
$\eta_{WTP_{theoretical,naturalgas}}$	0.70	12.2	14.4	16.6
$\eta_{WTP_{theoretical,renewable}}$	0.70	13.1	15.5	17.9

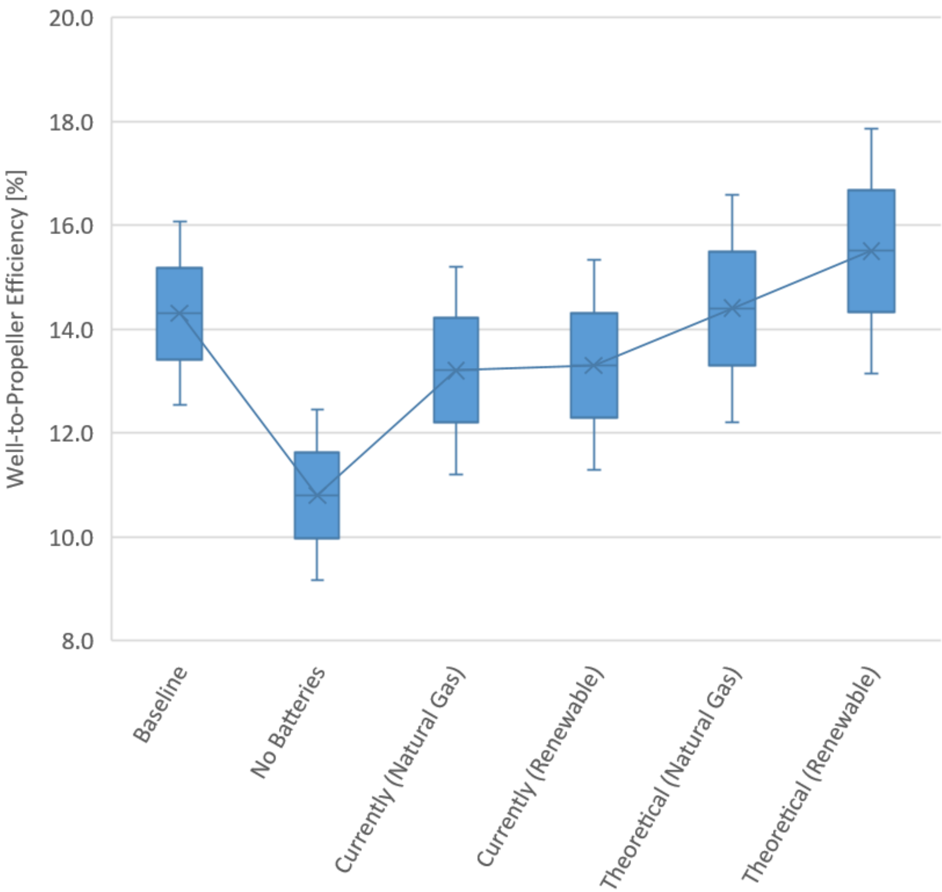

Figure 5.9: Box-plot of well-to-propeller efficiencies of different HEA configurations including the baseline model. The data used is similar to Table 5.8.

5.4. INTERMEDIARY CONCLUSION SERIES HYBRID ELECTRIC AIRCRAFT MODEL

The analysis of the series hybrid electric aircraft showed first of all that the expected advantages of the concept are 'small'. The electric energy used to charge the batteries should first of all come from a renewable source of energy to make the concept feasible. Second, the theoretical limits of technology should be approached in order for the well-to-propeller efficiency to exceed that of the conventional ATR72 aircraft. It is seen that the model converges to an all electric version of the ATR72 if the battery energy density is increased to 2,802 [Wh/kg]. It is also seen that the HEA concept does not work without the use of batteries, the combined efficiencies of all additional pars (e.g. motors, inverters, cables, etc.) has, in this specific case, a decremental effect on the overall efficiency.

Furthermore, a higher voltage can best be chosen, this will result (depending on the working voltage of the electric motor) in a lower efficiency of the motor controller (dc to ac converter), however a much higher efficiency of the cables. An important side-effect of this decrease in current through the cable is the reduction in magnetic field and thus health effects related to the distribution of power throughout the airframe [1]. An important limiting factor is the shielding material of the cable. As Dr. ir Polinder [134] explains: "a practical voltage to work with in the transportation sector (e.g. trams and trains) is 25 [kV], above this voltage the shielding at component interfaces becomes to difficult".

For the limiting case (theoretical technological limit), the well-to-propeller efficiency increases with approximately 2 [%]. Especially the technology of superconducting is required in order to keep the cable weight within an acceptable limit. It is clearly shown that the battery technology is leading in the acceptance of hybrid or all electric aircraft. With the theoretical energy density of 1,000 [Wh/kg] the aircraft will increase 10 [%] in weight, but the well-to-propeller efficiency does increase with approximately 2[%]. Although this could have a large influence on the total carbon emissions in the aerospace industry, several factors have not been covered. For example the impact of initial cost, operating cost and maintenance are not taken into account. Furthermore the impact of the footprint of the battery technology should be investigated before the overall environmental impact can be calculated. Finally, costs involved in design, changes in infrastructure and training of personnel [134] (e.g. to be able to work with high voltages) have also not been taken into account.

5

III

Results

6

Results and Analysis

In this chapter the results of this master thesis are presented. In chapter 4 and chapter 5 intermediate results are shown in combination with an uncertainty analysis (R^2). In order to further investigate the validity of the theoretical models and the results presented in this master thesis, a sensitivity analysis is performed. The robustness of the overall model is checked by investigating the impact of change of variables on the results. A systematic approach is chosen where the following parameters are varied:

1. Propulsion (section 6.1)
   (a) Number of Propellers
   (b) Ideal Rotational Velocity
2. Electronics (section 6.2)
   (a) Bus Voltage
   (b) Technology Used
3. Mission Profile (section 6.3)
   (a) Range
   (b) Cruise Altitude

Finally, chapter 7 will use the results presented in this chapter to arrive at an answer to the main research question and provide a conclusion.

6.1. SENSITIVITY ANALYSIS - PROPULSION

As discussed in chapter 4 the amount of power required in a OEI condition is equal to 2051 [kW]. The amount of installed engines has a direct impact on the total available power of the aircraft during AEO flight conditions. The main advantage of electric engines, as discussed in chapter 5, the specific power of electric motors is less sensitive to changes in design power than is the case with conventional turboprops. Therefore it is possible to increase the amount of engines per wing and thereby create a more relaxed OEI boundary condition. In order to assess the viability of this change in design it is important to take into account the additional devices, cables, fairings, aerodynamic drag and other relevant changes to the design as discussed in section 5.1.

6.1.1. DISTRIBUTED PROPULSION

The optimal number of propellers driven by an electric motor per wing ($No_{prop,opt}$) is dependent on the changes in weight and the change in drag. The weight change will consist out of an increase in weight due to the electric system (ΔW_{elec}) and a decrease in weight due to the smaller vertical tail (ΔW_{VT}) and the removal of the original propulsion system ($\Delta W_{prop,old}$). The change in drag will originate from the decrease in vertical tail drag (D_{VT}) and a change in propeller area depending on the amount of propellers. This top-level relation between optimal number of propellers, weight and drag is shown in Equation 6.1.

6

$$No_{prop,opt} = f(W_{elec}, D) \tag{6.1}$$

The weight of the electrical system consists out of a fixed part (independent on amount of propellers) and a variable part (dependent on the amount of propellers), this is shown by Equation 6.2 and Equation 6.3. Both these parts of the total weight are still variable with all parameters indicated in previous chapters.

$$W_{elec,fixed} = W_{generator} + W_{battery} \tag{6.2}$$

$$W_{elec,var} = n \cdot W_{motor} + n \cdot W_{inverter} + W_{cables} + n \cdot W_{prop} \tag{6.3}$$

AERODYNAMIC ALTERATIONS

In case of a OEI take-off flight condition, the aircraft will show two types of behaviour that need to be countered in order to end up with a stable flight. First, as Figure 6.1 shows, a yawing moment will exist around the Centre of Gravity (CG) that needs to be counteracted by the vertical tail. The surface area of the vertical tail depends largely on this specific flight condition and potential gains in efficiency can be found here when introducing multiple engines per wing. Furthermore, due to the yawing motion of the aircraft the engine active wing will experience a higher lifting force as the engine inactive wing, therefore a rolling motion will accompany the yawing motion. This rolling motion is to be counteracted by use of the ailerons, however the ailerons are not sized according to this specific flight condition. Therefore the main benefit will be the decrease of the vertical tail height and thus surface area and its aerodynamic effect on the overall drag during all flight conditions.

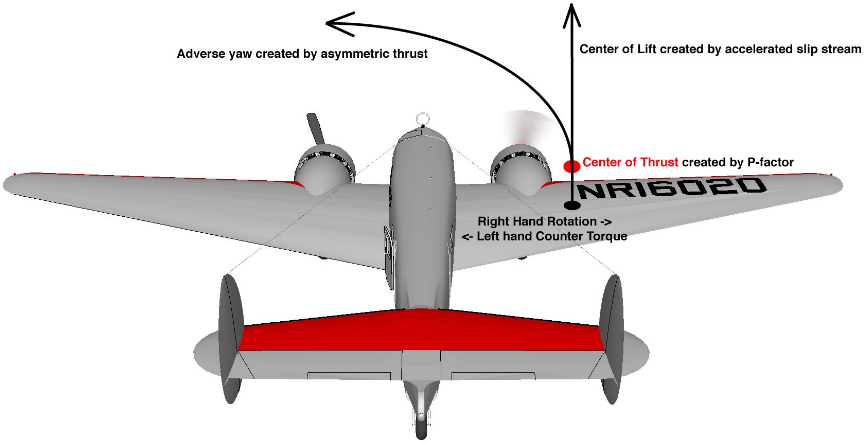

Figure 6.1: Visualisation of the yawing and rolling moment produced by the OEI flight condition [139].

The total moment experienced by the aircraft is the sum of the moments created by the in-balance in thrust, measured from the CG and the additional drag [140] created by the in-operational engine (approximately 25 [%] of the total moment). This moment can be calculated using Equation 6.4 to be 102 [kNm]. Where the $V_{TO,avg}$ cannot exceed $1.2 \cdot V_S$ as stated by FAR25 regulations [97] and calculated in section 4.2 to be 65.4 [m/s].

6

$$M_{OEI,Engine} = 1.25 \cdot M_{In-balancedThrust} = 1.25 \cdot \frac{\eta_{prop} \cdot d_{cog-engine} \cdot P_{TO,engine}}{V_{TO,avg}} \tag{6.4}$$

The size of the rudder (and vertical tail) required to counteract this moment can be calculated using the DATCOM [98] method as shown by Equation 6.5. FAR25 regulations [97] state that the maximum rudder deflection (δ_F) during this manoeuvre cannot exceed 25 [deg].

$$M_{OEI,VTail} = \frac{1}{2} \cdot \rho \cdot V_{TO,avg}^2 \cdot \delta_F \cdot \left(\frac{C_{L,\delta}}{(C_{L,\delta})_{theory}} \cdot (C_{L,\delta})_{theory} \right) \cdot K' \cdot K_\Lambda \tag{6.5}$$

The term in between brackets in Equation 6.5 describes the increase of the lift coefficient of the rudder due to the deflection δ_F. The value of this term is dependent on the ratio c_f/c, where c_f is the chord length of the rudder, while c is the Mean Aerodynamic Chord (MAC) of the vertical tail. Several sources give different values for the ratio of c_f/c as can be seen in Table 6.1, therefore the average value of 0.36 will be used.

Table 6.1: Different sources for the average ratio c_f/c by Roskam, Schaufele and the average between both methods. Because the numbers are based on empirical data it is not possible to use them for sizing an innovative concept, but they give a good estimate for validation [141].

Parameter	**Value**	**Unit**	**Source**
c_f/c	0.32 - 0.44	-	Roskam
c_f/c	0.25 - 0.45	-	Schaufele
c_f/c	0.36	-	Average

RESULTS

To find the optimal number of propellers for a HEA, the added weight (Equation 6.3) and the amount of fuel saved, should balance in favour of the latter. In this trade-off the reduction in fuel consumption is exaggerated by removing the drag produced by the OEI constraint completely. Due to stability reasons the vertical tail can only decrease from 14.1 [m^2] to 9.6 [m^2], [74]. Furthermore it is assumed that the aircraft experiences no side-winds during the entire mission-profile. This results, with a constant mission-profile, in a reduction of fuel of 92 [kg] or approximately 5 [%] of the total fuel consumption. This figure is validated by looking at the fraction of vertical tail drag versus overall drag, [142].

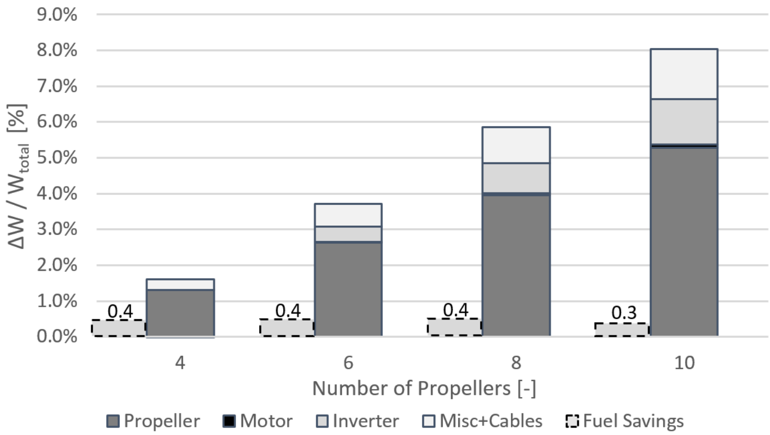

Figure 6.2: Percentage weight addition versus percentage fuel weight reduction for varying number of propellers with a diameter of 3.93 [m].

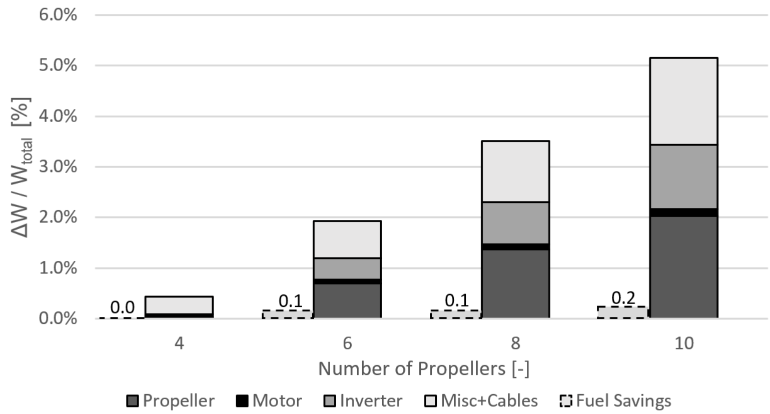

Figure 6.3: Percentage weight addition versus percentage fuel weight reduction for varying number of propellers with a diameter of 2.0 [m].

As the number of propellers increases, the power required per motor and inverter decreases and thus the effective losses per motor increase, making the parts less efficient. This trend is validated by [134]. Furthermore per motor, inverter and propeller a certain amount of mass is added per propeller. If the diameter of the propellers is decreased (and thereby the added propeller weight) the overall system efficiency is also decreased and thus the fuel consumption increased as can be seen in Figure 6.2 and Figure 6.3.

It can immediately be seen that the weight of the motor decreases in contrary to expectations. This is due to the reduced maximum power requirement as the OEI conditions are less stringent. Overall it is however seen that the added mass and decrease in efficiency of the sub-components used, do not balance with the reduction in fuel consumption due to the smaller vertical tail. There is a large decrease in efficiency involved with the distribution of power over multiple propellers. Other benefits of distributed propulsion could be taken into account in order to make this innovation work on the ATR72, however these benefits have not yet been identified and that research would fall beyond the scope of this thesis.

6.1.2. DEPENDENCY ON ROTATIONAL VELOCITY PROPELLER

For electric motors it is less complicated (in comparison to gasturbines) to vary the speed of the shaft (ω). However in order to keep the shaft power (P_{shaft}) constant, the torque (τ) will vary with a change in shaft speed ($P_{shaft} = \tau \cdot \omega$), therefore the efficiency will also change as is explained in section 3.2. In order to find an optimum a sub-optimisation is performed including the propeller, motor and inverter models. The variation of propeller efficiency can be seen in Figure 6.4, here the drivetrain-efficiency is equal to $\eta_{motor} \cdot \eta_{inv} \cdot \eta_{prop}$. Turbulence effects are not taken into account, however the striped (black) line at 1200 [RPM] corresponds with a tip-Mach-velocity of 0.8.

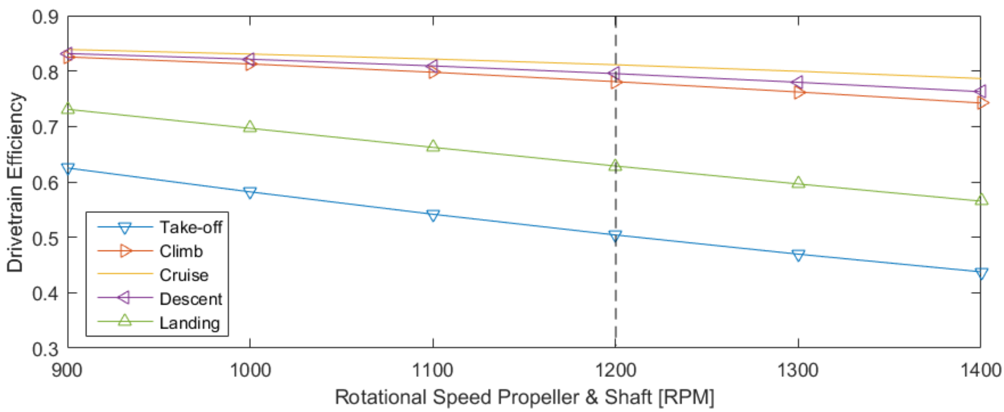

Figure 6.4: The drivetrain efficiency is shown as a function of propeller speed for different segments of flight. The original rotational velocity of the propeller is 1200 [RPM] (denoted in black striped) [96], the tip-mach-speed is 0.8 for this velocity [98], therefore substantial turbulence effects should be expected above this speed, thereby further decreasing the drivetrain efficiency.

The change in propeller efficiency is due to the change in AR, the changes in motor and inverter efficiency are mainly found in the Ohmic losses due to a change in torque. The torque and current drawn by these two devices vary linearly, while the losses involved with the change in current vary quadratically. It can be seen that a reduction in propeller RPM could (independently of the flight-phase) result in an increase in overall efficiency. As the motors are designed for a certain speed and torque combination it is not possible to variably increase the torque, as the motors would become more heavy as they require more copper, [134]. It is however interesting to reduce the rotational speed only during the climb phase, as the motors can temporarily be over-loaded. The limit in overloading is reached when the internal temperature increase beyond the glass-transition temperature of the materials used inside the motor (commonly, high temperature epoxy at 303 [K] surrounding the coils in the stator of the motor). The climb phase is chosen as the relative increase in efficiency is the highest for this flight segment.

The overall conclusion that can be drawn is that the optimal speed of the propeller will change for electric motors. In order to find this optimal shaftspeed a more elaborate aerodynamic analysis should be performed in combination with the expected losses in the electronic devices (e.g. motors and inverters).

6.2. SENSITIVITY ANALYSIS - ELECTRONICS

Within this section a sensitivity analysis is performed on the electric part of the design. First the impact of the working voltage on the bus is discussed. The impact is shown by taking multiple models that are used in the HEA as example. Furthermore the influence of energy density and power density on the performance of the models is shown.

6.2.1. DEPENDENCY ON BUS VOLTAGE

In electronics design the most dominant losses are in most cases Ohmic losses (I^2R), the current required is directly dependent on the chosen working voltage ($P = U \cdot I_{DC}$), therefore it is of interest to investigate the overall system efficiency as a function of working voltage. In this section, first the most remarkable sub-system performances as a function of voltage are discussed, after which the influence of bus voltage on the overall efficiency is researched.

INVERTER (MOTOR CONTROLLER)

Both the efficiency as the weight of the inverter vary with the chosen voltage as can be seen in Figure 6.5. It can be seen that the trend is however not smooth, this is due to the fact that the model functions in a discrete manner; increasing the voltage or current beyond a certain threshold value can result in a stepwise increase of the weight or losses due to the addition of a component. In general it is shown that a higher voltage results in both a lower inverter weight and a higher efficiency. However a stagnating effect can be seen beyond 1500 to 2500 [V], where a further increase in voltage does not necessarily result in a decrease in weight.

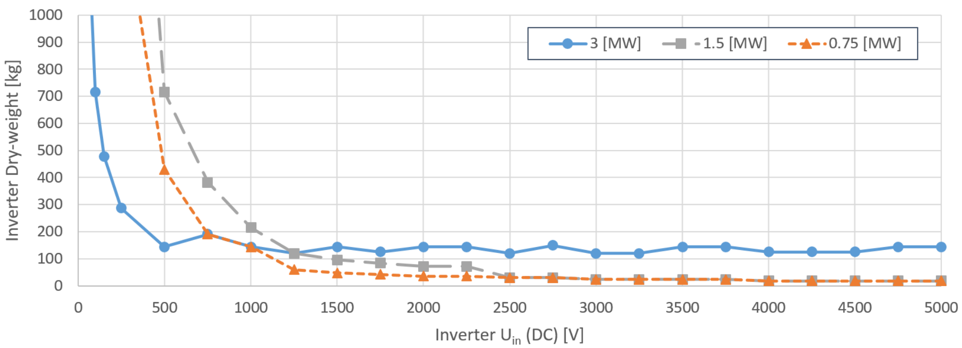

Figure 6.5: By varying the voltage used by the inverter model (see section 5.1), the effect of a decrease in voltage on the overall weight can be shown. Three different power settings have been modelled.

CABLES

The cables experience two dominant types of losses: Ohmic losses (DC & AC) and skin effect (AC). By increasing the voltage both types of cables will experience less losses as is already shown in subsection 5.1.4. As there exists a difference in potential between for example the ground and the live wire, isolation is required to prevent short circuiting, [134]. With increasing voltage the isolation requirements will increase quadratically and thus an optimum exists between weight addition and voltage increase.

6

Batteries

In section 2.2, the influence of battery architecture (connecting battery cells in series and/or parallel) is discussed. Within this section the sensitivity of overall model performance as a function of the battery architecture and other battery parameters (U_{nom}, I_{max}, Wh/kg and Wh) is discussed. For a fixed battery weight in combination with the energy density of the cell technology, it is possible to calculate the amount of cells required as is shown by Equation 6.6.

$$n_{total} = n_{series} \cdot n_{parallel} = \frac{m_{allowed} \cdot E^{*}}{E_{cell}} \tag{6.6}$$

By dividing the required bus-voltage by the cell-voltage, the number of cells in series can be calculated. By combining these two parameters the number of cells in parallel is also known and by combining this given with the internal cell resistance, the respective battery resistance can be calculated. The total internal losses of the battery are given by Equation 6.7. As the losses go down linearly ($R_{internal}$) but up quadratically (I^2), the total battery efficiency goes up with increasing voltage.

$$P_{loss,batt} = I^2 \cdot R_{internal} = I^2 \cdot \frac{n_{series}}{n_{parallel}} \cdot R_{cell} \tag{6.7}$$

6

Overall Performance

As can be seen the efficiency of all components goes up for an increasing voltage. This is in line with trends seen in the electricity grid where the voltage is slowly raised every year. As explained the main limitation in raising the voltage is the shielding of components with an electric potential with respect to other components. For wires, the isolation thickness can be calculated relatively straightforward, however for connection points in between components (for example the wires to the inverter) the isolation can proof to be difficult and a maximum practical voltage of 25 [kV] is advised, [134].

6.2.2. Development of Technologies

Within this section the dependency of the model is tested for different states of technologies (e.g. changes in Wh/kg, W/kg, etc.).

Energy Density

It is shown that for an energy density for the batteries of 2,790 [Wh/kg] the model converges into an AEA. On the other end of the spectrum a battery density of 2,402 [Wh/kg] is required in combination with other parts (e.g. motor, inverter, cables, etc.) at current technology. If future technology is used a battery density of 710 [Wh/kg] would equal a brake-even point with the conventional ATR72 well-to-propeller efficiency.

Power Density

An increase in 10 [%] in power density of the electric motors results in approximately 2 [%] increase in well-to-propeller ratio. This increase, is lower for a higher power density (e.g. 1.8 at 8,000 [W/kg] and 2.1 at 5,000 [W/kg]). This could mainly have to do with the quadratic nature of the losses involved in the system.

6.3. SENSITIVITY ANALYSIS - MISSION PROFILE

Within this section the dependency of the model on flight mission characteristics is discussed. The influence of increasing the range, cruise altitude or velocity are covered in separate sections. The influence of choosing a different type of aircraft is considered beyond the scope of this research. The model investigated is the SHEA using renewable energy sources and electronics working at the theoretical limit as discussed in chapter 5. Due to the small perturbations, the variance of the well-to-propeller efficiency is considered linear around the design point. The range of the design point is slightly decreased, such that a well-to-

6.3.1. DEPENDENCY ON RANGE

Increasing the range (without altering any other flight parameter) has a decremental effect on the overall well-to-propeller performance of the hybrid electric aircraft. This is mainly due to the fact that all components have to be carried over a larger distance. Furthermore, the ratio $\frac{E_{batt}}{E_{kerosene}}$ decreases with increasing range. On average an energy consumption can be derived from the model of 13.2 [MJ] per flown kilometre in the cruise phase. This number is dependent on a large number of parameters but most sensitive to weight. As the range is increased, either kerosene or batteries need to be added which thus have a direct impact on the well-to-propeller efficiency. Increasing the range with 1 [%] results in an average decrease of the η_{WTP} of 0.2 [$\%_{WTP}/\%_{Range}$]. Decreasing the range with 1 [%] results in an average increase of the η_{WTP} of 0.3 [$\%_{WTP}/\%_{Range}$].

6

6.3.2. DEPENDENCY ON CRUISE ALTITUDE

The climb phase is leading in the design of all propulsion components (e.g. motors, inverters, etc.) and thus has a direct impact on the weight of the propulsion system. As the cruise altitude is increased without allowing more flight time in the climb phase and the climb angle is thus increased, the weight of the propulsion system will increase. Due to the change in altitude the drag reduces, however due to the additional weight the overall amount of power required increases. The result is shown in Figure 6.6.

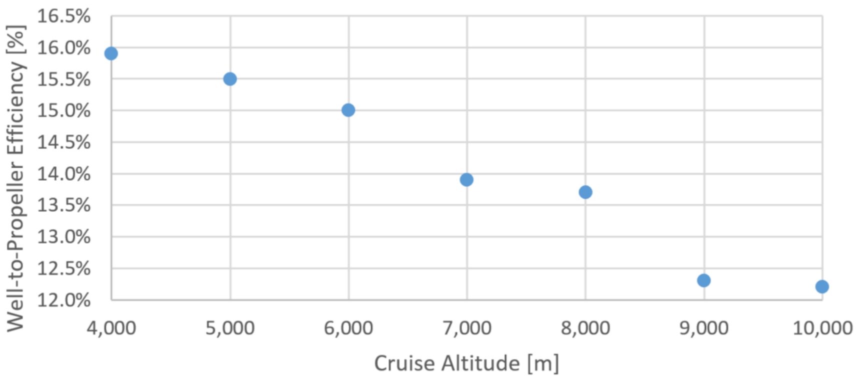

Figure 6.6: By varying the cruise altitude, but thereby increasing the climb angle, the well-to-propeller efficiency decreases.

In reality the climb time or distance (if a similar speed is assumed) will not be constant for different cruise altitudes and an optimisation is performed. Mission profile optimisation is a field of research on its own [143] and taking into account all parameters would fall beyond the scope of this research. Therefore a more top-level optimisation method is used to find the dependency of well-to-propeller efficiency on cruise altitude. If the flight time per segment is made variable and the energy consumption per unit distance is optimised (dE/ds [J/km]), it can be seen that the climb phase time is increased. Furthermore, it is shown that increasing the cruising altitude has a beneficial effect on the overall well-to-propeller efficiency as can be seen in Figure 6.7. An optimum in efficiency is found for an altitude of 7,000 [m], above this altitude the weight of the propulsion system increases again. It is recommended that further research is performed on the topic of mission profile optimisation for hybrid and all electric aircraft.

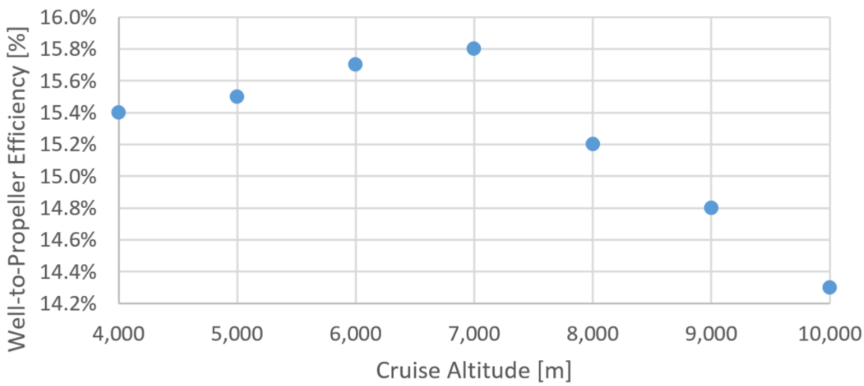

Figure 6.7: Varying cruising altitude versus well-to-propeller efficiency.

7

Conclusion

In this chapter the final conclusion is drawn with respect to the research question. This chapter is build up in the same way as section 1.1, first intermediary conclusions are drawn with respect to the sub-questions after which these results are used to come up with a final conclusion. Finally, recommendations are given that indicate areas of high interest that could be used for future research.

7.1. What is the well-to-propeller efficiency of a conventional ATR72 aircraft?

In chapter 4 it is shown that the Well-to-Propeller Efficiency (η_{WTP}) can be calculated by multiplying the Well-to-Tank Efficiency (η_{WTT}) and the Tank-to-Propeller Efficiency (η_{TTP}) efficiencies. It is shown that a relatively high η_{WTT} efficiency of 80 [%] can be achieved for petroleum based fuels as kerosene. The η_{TTP} efficiency for the ATR72, for a mission profile with a range of 560 [km], is equal to 17.9 [%]. By combining these two efficiencies, the η_{WTP} can be calculated to be 14.3 [%] with an R^2 value for the models of 0.753. Meaning that the η_{WTP} is in between 12.5 and 16.1 [%]. It is shown that fuel could be saved at the expense of safety by decreasing the power setting during take-off to 90 [%], thereby making use of the full runway length. Furthermore increasing the flight altitude has a direct positive impact. It is shown that the constraint on the maximum power of the engines is posed by different segments in the following order: One Engine Inoperative (OEI) take-off segment, climb phase, All Engines Operative (AEO) take-off segment, cruise, descent, landing. Energy from batteries in the Hybrid Electric Aircraft (HEA) concept is applied in a similar order to the different segments, such that the Series Hybrid Electric Aircraft (SHEA) concept is utilised the fullest.

7.2. WHAT IS THE WELL-TO-PROPELLER EFFICIENCY OF A SHEA VERSION OF THE ATR72?

In chapter 5 it is shown that the η_{WTPs} for an HEA using currently available and theoretically possible technologies are respectively 13.3 and 15.5 [%]. The η_{WTT} efficiency is highly dependent on the use of natural gas or renewable energy as source of energy. While the former is shown infeasible, the latter is required in combination with the theoretical limits in technology to make the concept of SHEA feasible. The validity of the models is checked against available data from related industries as the agriculture, transportation (automotive) and electric power (grid) industry to have an R^2 value of 0.70.

The Direct Current (DC) electricity created by the generators should be transported by using High Temperature Superconducting (HTS) cables as copper and even aluminium wiring requires either too much cooling or becomes too heavy. The inverter and electric motor are place at the location of the original turboprop engine and are combined with the original propeller in order to keep the centre of gravity constant.

The scientific community often refers to HTS materials, although the practical implementation on a commercial scale is viable for direct current cables. Rotating machinery and alternating currents in combination with HTS still require a lot of research, [134]. Furthermore the interfacing between different components is difficult and the functionality of the system rely fully on the reliability of the cooling system. From a regulations point of view this is not 'advised' and a dual or triple redundant system configuration can be expected.

Using these partial conclusions it is shown that the concept of HEA is both at this moment in time as in the near future <35 years, rendered infeasible. As soon as electric aircraft are a viable option it is advised to immediately scale to an all electric aircraft.

7.3. IN WHAT CATEGORY SHOULD POTENTIAL BENEFITS OF SHEA BE STUDIED?

A sensitivity analysis is performed in chapter 6; it is shown that the efficiency of all components decreases as the power per component decreases. Especially the propeller and the inverter experience a significant decrease in operating efficiency, while the total mass of the system increases. These two trends lead to the conclusion that, while distributed propulsion does allow for a more relaxed OEI design condition, the overall model does not show improvement for an increase in propulsive systems.

It is seen that temporarily lowering the velocity of the propeller at take-off increases the propeller efficiency with approximately 9 [%], the overall well-to-propeller efficiency would change with less then 1 [%], as the efficiency of the electronics decrease. It should however be noted that in this specific case the motors are overloaded as the current drawn by the inverter is temporarily higher in order to produce the same amount of power ($P = \omega \cdot \tau$). The potential gain of overloading is the highest during the take-off and climb phase segments.

One of the potential benefits of SHEA as mentioned in [1], is the reduction of noise at and around airports. This phenomena is not researched in this thesis, however due to the presence of two turboshaft engines the noise levels might be comparable to currently used APUs. Integration in fairings and the removal of residual thrust might have an influence, however this thesis cannot give a clear answer to these sub-research-questions.

Overall it is seen that the system performance improves with increasing working voltage. This is due to the dominant Ohmic losses (I^2R) that are found in all electric devices used. The cost involved with ever increasing voltages will increase when working with 1 [kV] or more as specially trained (more expensive) personal is required to design and build this type of electric installations.

Almost all components used are currently under-performing. While gasturbines have a power-density of 5 [kW/kg], the motor and inverter combination have a combined power-density of 3.4 [kW/kg]. Increasing the power-density of the motor and the inverter with 10 [%] each, results respectively in a 7 and 3 [%] combined increase power-density increase. The expected values for 2050 for both these components would have to be reached to equal the power-density of current gasturbines.

The component that requires the highest amount of improvement because it has the highest impact on the overall well-to-propeller efficiency is the battery. Current battery technology should improve with a factor 4 in order for the concept of HEA to be feasible. It is not calculated within this thesis, but a further increase would be required in order to balance the relative advancements that could be made in gasturbine technology.

Finally a sensitivity analysis with respect to the flight mission shows that decreasing the range immediately increases the potential of the HEA concept. The relation between η_{WTP} and range is shown to be -0.3 [$\%_{WTP}/\%_{Range}$].

7.4. HOW DOES THE WELL-TO-PROPELLER EFFICIENCY CHANGE BETWEEN A CONVENTIONAL AIRCRAFT AND A SHEA?

As shown by the previous sections, the concept of series hybrid electric aircraft is from a technological perspective not an advised topic of development. If the theoretical limits of technologies are reached (especially with respect to battery technology) a 2 [%] improvement can be achieved on the well-to-propeller efficiency. However as the latter concept becomes viable, a more sustainable concept would be to immediately create an all electric aircraft as adding more battery weight results in an increase in well-to-propeller efficiency. In order to accelerate the transition to a HEA within the smallest time-frame, research should be focused on battery technology and the use of an alternating current in superconducting materials both in cables and in rotating machinery.

7.5. RECOMMENDATIONS

Due to the large amount of models used, the first advise would be to further elaborate some of the models used within this thesis. This can be done systematically by looking at the R^2 value that is presented in every chapter of this thesis. The models with the lowest R^2 value are either immature technologies (e.g. the differences per product/manufacturer in performance are still high), or are models that require more complexity. The main focus within this thesis is to bridge the gap between the aerospace industry and electrical engineering. Therefore more time is allocated to the latter type of models as can be seen in the corresponding R^2 values.

The calculations for the well-to-tank efficiency are currently in line with literature. It could however be interesting to take into account the efficiency and/or size of renewable energy sources, as these parameters are currently not taken into account.

The gasturbine model could be expanded and techniques as recuperation could be researched, thereby further optimising the efficiency of this component. A topic for future thesis research could be the aerodynamic optimisation of a propeller in combination with the design space of an electric motor; the feasible rotational shaft velocity range is much larger than is currently seen in conventional gasturbines.

From an electrical engineering perspective more research could be performed in the area of superconducting and the distribution of electricity in an airframe. A risk-management-analysis should be performed on the use of superconducting materials in flight critical systems.

Finally, a full mission profile optimisation in combination with an analysis of the commercial aviation flight routes should be performed. This could result in valuable insight in potential short range flight routes. An optimised hybrid or all electric aircraft in combination with a required infrastructure could then be designed specifically for that route.

IV

Appendices

A

Practical and Theoretical Limits Battery Technology

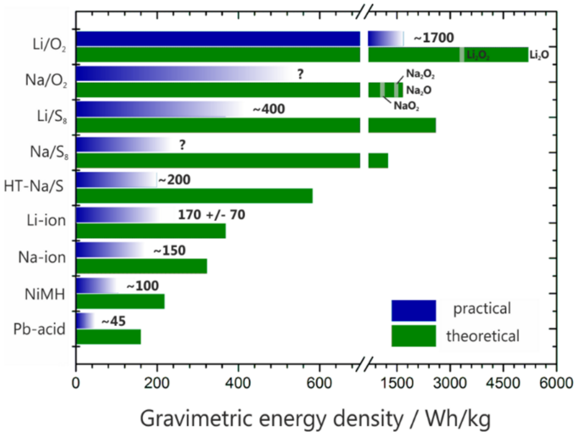

Figure A.1: Theoretical and (estimated) practical energy densities of different rechargeable batteries in the year 2015 [49].

B

ENGINE MODEL

WITHIN Matlab an elaborate turbofan engine model exists that is both capable of calculating design and off-design engine parameters as Specific Fuel Consumption (SFC), thrust settings and Mass Flow Rate (MFR). The model is dependent on a large set of internal and external settings (for example velocity and altitude of the aircraft). Such a model does not yet exist for a turboprop engine model. In order to integrate the ATR72 aircraft it is decided to create an engine model for turboprop engines.

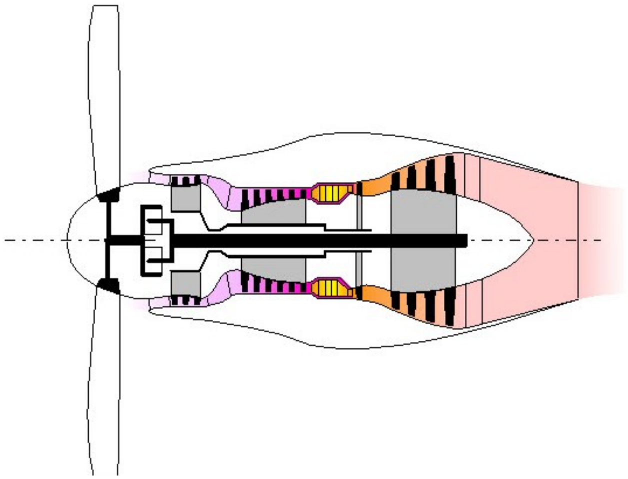

Figure B.1: Visualisation of a two spool turboprop engine. [144]

The turboprop engine used in the ATR72-600 is a PW 127-M with a maximum shaft power of 2051 [kW] [96]. As is displayed in Figure B.1 the PW 127-M engine has a two-spool configuration. Meaning the Low Pressure Turbine (LPT) drives both the Low Pressure Compressor (LPC) and the High Pressure Compressor (HPC), the High Pressure Turbine (HPT) drives the propeller. Furthermore the exhaust gas through the nozzle might also provide (residual) thrust up to 10 [%] as is shown in section 5.3. The propeller and the shaft are connected through a 30-to-1 reduction gearbox as the shaft speed is in the order of 30.000 [RPM] and the propeller turns with 1.212 [RPM] [75]. A table summing up all engine characteristics can be found in Table B.1.

Table B.1: Details PW 127-M turboprop engine that is used on the ATR 72-600 aircraft. [96]

Parameter	**Value**	**Unit**
Manufacturer	Pratt Whitney Canada	-
Type	PW127-M	-
Max Power at T/O	2051	kW
Number of Spools	2	-
LPC Stages	1	-
HPC Stages	1	-
HPT Stages	2	-
LPT	2	-
Length	2.13	m
Width / Diameter	0.84	m
Weight	481	kg

The original design point of the engine can be approached by calculating 'station' by 'station' the engine characteristics as shown in Figure B.2. First air is compressed in the compressor(s) *(station 2 to 3)*, then at constant pressure heat is added in the combustion chamber *(station 3 to 4)*, then heat is extracted in an isentropic expansion process in the turbine(s) *(station 4 via gg to 5)* and finally heat is rejected at constant pressure to the environment. This cycle is also known as the Brayton cycle and the energy extracted from the flow in between station 4 and 'gg' is equal to the energy required by the compressor(s).

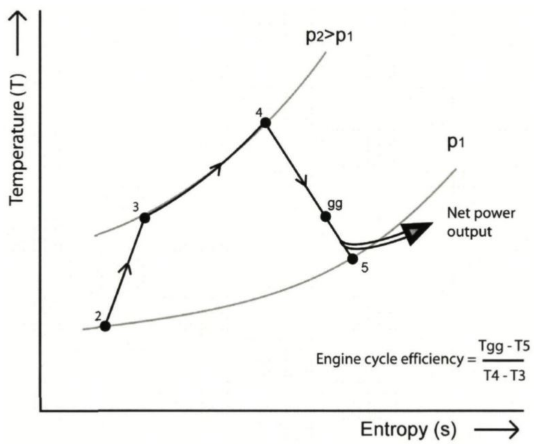

Figure B.2: The Brayton cycle. Figure taken from lecture slides of the course Gas Turbines from the Delft University of Technology (DUT) [67].

Inlet Conditions

The inlet of the turboprop engine is located behind the propeller, this results in a slightly higher pressure at the inlet then ambient conditions would suggest. The velocity is assumed equal to the free-stream velocity, resulting in the relations shown in Equation B.1 and Equation B.2. A typical number for the pressure recovery over the inlet for modern aero-engines is 1-3 [%] [bron].

$$p_{t,2} = p_{s,1} \cdot (1 + \frac{\gamma - 1}{2} \cdot M_0^2)^{\frac{\gamma}{\gamma-1}} \tag{B.1}$$

$$T_{t,2} = T_{s,1} \cdot (1 + \frac{\gamma - 1}{2} \cdot M_0^2) \tag{B.2}$$

Compressor

The PW 127-M has two compressor stages, a LPC and a HPC both assumed to compress air in an ideal isentropic fashion, as is shown by relations Equation B.3 and Equation B.4. In reality the real cycle does result in an increase in entropy, the total pressure remains similar, however the power requirement for compression is higher. Typically a factor 85-93 [%] [bron] is seen between the ideal and the real case, dependent on the number of stages.

$$p_{t,3} = PR_3 \cdot p_{t,2} \tag{B.3}$$

$$T_{t,3} = T_{t,2} \cdot PR_3^{\frac{\gamma-1}{\gamma}} \tag{B.4}$$

Most modern engines can achieve a pressure ratio for a single stage of 1.15 to 1.28, whilst the polytropic efficiency of such a stage reaches values of 90-92 [%] [bron].

Combustion Chamber

Inside the combustion chamber heat is added in order to provide energy to keep the engine cycle going. Typically the efficiency of the Combustion Chamber (CC) (η_{cc}) is 98-99 [%] and given by Equation B.5, where LHV is the Lower Heating Value (LHV) of kerosene in [MJ/kg]. The Pressure Ratio (PR) is mostly in the order of 92-98 [%].

$$\eta_{cc} = \frac{(\dot{m}_3 + \dot{m}_f) \cdot C_{p,a} \cdot T_{t,4} - \dot{m}_3 \cdot C_{p,a} \cdot T_{t,3}}{\dot{m}_f \cdot LHV} \tag{B.5}$$

Turbine

Typically in the turbine of a turboshaft or turboprop-engine 75 [%] of the energy generated is used for the compressor and 25 [%] is available for an external load as a propeller or a generator. [bron]. The PR over this particular stage in combination with a certain mass flow results in a temperature ratio (τ) which is a representation of the energy generated in the turbine stages. The energy generated in the HPT is used to power the HPC and the LPC, whilst the energy (W) generated in the LPT is available for an external load as shown in Equation B.9. The pressure and temperature at these stages can be calculated

B

using Equation B.8 and Equation B.7 for the HPT and Equation B.10 and Equation B.11 for the LPT. Here p_5 is derived from the nozzle efficiency and the ambient pressure p_a.

$$W_{HPT} = \frac{W_{HPC} + W_{LPC}}{\eta_m} \tag{B.6}$$

$$T_{t,45} = T_{t,4} - \frac{W_{HPT}}{\dot{m}_4 \cdot C_{p,g}} \tag{B.7}$$

$$p_{t,45} = p_{t,4} \cdot (1 - \frac{1 - \frac{T_{t,45}}{T_{t,4}}}{\eta_{is,HPT}})^{\frac{\kappa_g}{\kappa_g - 1}} \tag{B.8}$$

$$W_{shaft} = W_{LPT} = \dot{m}_{45} \cdot C_{p,g} \cdot (T_{t,45} - T_{t,5}) \tag{B.9}$$

$$p_{t,5} = p_{t,4} \cdot (1 - \frac{1 - \frac{T_{t,45}}{T_{t,4}}}{\eta_{is,HPT}})^{\frac{\kappa_g}{\kappa_g - 1}} \tag{B.10}$$

$$T_{t,45} = T_{t,4} - \frac{W_{HPT}}{\dot{m}_4 \cdot C_{p,g}} \tag{B.11}$$

C

Validation Well-to-Propeller Efficiency

In this master thesis all sub-models are validated in separate sections, however due to the absence of previous research on the topic of SHEA no validation of the overall model is available in literature. Therefore in this appendix, by means of a 'back-of-the-envelop' calculation in combination with sources that are available in literature the η_{WTP} of both the baseline and the SHEA are validated. In the automotive industry the well-to-wheel efficiency has been researched extensively. The well-to-tank efficiency can be derived from those sources in literature as is shown in section C.1 and section C.3. The baseline and hybrid electric aircraft are covered in separate sections.

C.1. Validation Well-to-Tank Efficiency Baseline

Multiple sources in literature exist to validate the well-to-tank efficiency, these are covered in section 4.5. From literature ([106],[107],[1],[108] and [136]), it is known that the η_{WTT} efficiency for any petrol based vehicle in Europe is approximately 80 to 88 [%]. This includes extracting crude oil from the ground, refinement into kerosene, transportation and storage in the fuel-tank at the airport.

C.2. Validation Tank-to-Propeller Efficiency Baseline

In line with literature [145], the total efficiency can be calculated using Equation C.1 to be approximately 27.7 [%] at cruise conditions and 25.4 [%] at take-off conditions (see Table C.1. A segmentation of losses is performed by [146], as can be seen in Figure C.1.

$$\eta_{gas,turbine} = \frac{P_{shaft}}{FF \cdot E^*_{kerosene}} \tag{C.1}$$

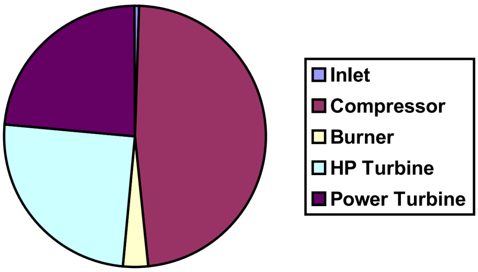

C

Figure C.1: Percent of lost shaft work in power turbine per major component [146]

Table C.1: Validation data PW120 engine [145]. Motor 1 and Motor 2 show actual flight test data.

Parameter	TO	Cruise	Unit
FF Motor 1	437.6	266.4	*kg/h*
FF Motor 2	456.2	281.1	*kg/h*
FF Model	482.2	289.6	*kg/h*
FF Average	458.7	279.0	*kg/h*
Power Motor 1	5,263	3,204	*kW*
Power Motor 2	5,487	3,381	*kW*
Power Model	5,800	3,483	*kW*
Power Average	5,517	3,356	*kW*
Shaft Power Motor 1	1,358	929	*kW*
Shaft Power Motor 2	1,391	930	*kW*
Shaft Power Model	1,454	927	*kW*
Shaft Power Average	1,401	929	*kW*
Efficiency Motor 1	25.8	29.0	*%*
Efficiency Motor 2	25.4	27.5	*%*
Efficiency Model	25.1	26.6	*%*
Efficiency Average	25.4	27.7	*%*

The data presented in Table C.1 belongs to the PW120 type engine, while the ATR72 makes use of a PW127 engine. In this validation section it is assumed that all engines in the PW100 series have a similar efficiency; as shown in [96] all engines have similar characteristics, however the maximum power available differs with approximately 30 [%].

C.3. VALIDATION WELL-TO-TANK EFFICIENCY SHEA

The well-to-tank efficiency can be validated using data from the automotive industry as is shown in section 4.5. For petrol based energy carriers the efficiency is similar as for the baseline model, for electric energy a distinction is made between renewable and non-renewable sources of energy.

C.4. VALIDATION TANK-TO-PROPELLER EFFICIENCY SHEA

One of the main goals of this master thesis is to find an accurate model for an (hybrid) electric aircraft, such that the well-to-propeller efficiency can be determined. This is of interest as such models do not yet exist for series hybrid electric aircraft. In literature, the term well-to-wheel efficiency is researched in-depth for the automotive industry, however the term well-to-propeller efficiency is still unknown in the aircraft industry.

D

POWER DENSITY OF TURBOSHAFT ENGINES TREND

The power density of turboshaft engines as a function of year of certification. An average increase of 0.24 [kW/kg/year] can be found, [123].

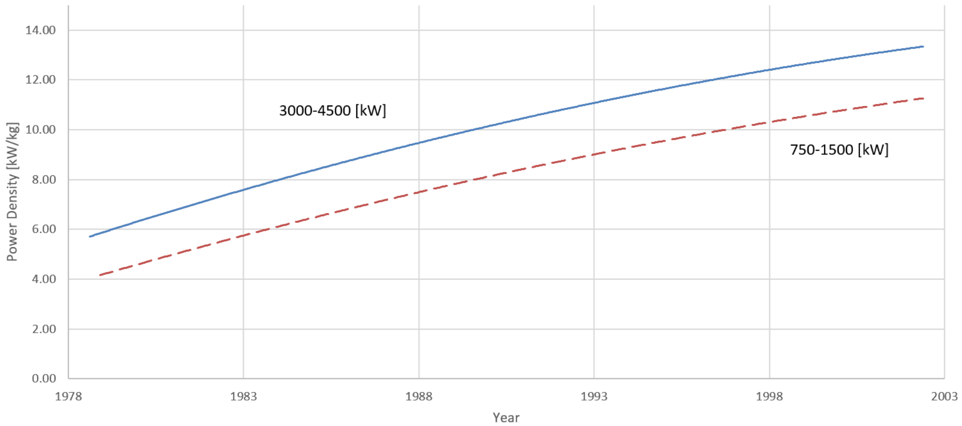

E

STANDARD ATMOSPHERE

Altitude [m]	Temperature [K]	Pressure [Pa]	Density $[kg/m^3]$	Speed of sound [m/s]
0.00000	288.150	101325	1.22500	340.294
250.000	286.525	98357.5	1.19587	339.333
500.000	284.900	95460.8	1.16727	338.370
750.000	283.275	92633.6	1.13920	337.403
1000.00	281.650	89874.6	1.11164	336.434
1250.00	280.025	87182.5	1.08460	335.462
1500.00	278.400	84556.0	1.05807	334.487
1750.00	276.775	81994.0	1.03203	333.510
2000.00	275.150	79495.2	1.00649	332.529
2250.00	273.525	77058.5	0.981435	331.546
2500.00	271.900	74682.5	0.956859	330.560
2750.00	270.275	72366.3	0.932757	329.570
3000.00	268.650	70108.5	0.909122	328.578
3250.00	267.025	67908.2	0.885948	327.583
3500.00	265.400	65764.1	0.863229	326.584
3750.00	263.775	63675.1	0.840958	325.583
4000.00	262.150	61640.2	0.819129	324.579
4250.00	260.525	59658.3	0.797737	323.571
4500.00	258.900	57728.3	0.776775	322.560
4750.00	257.275	55849.2	0.756236	321.547
5000.00	255.650	54019.9	0.736116	320.529
5250.00	254.025	52239.4	0.716408	319.509
5500.00	252.400	50506.8	0.697106	318.486
5750.00	250.775	48821.0	0.678204	317.459
6000.00	249.150	47181.0	0.659697	316.428
6250.00	247.525	45586.0	0.641579	315.395
6500.00	245.900	44034.8	0.623844	314.358
6750.00	244.275	42526.7	0.606487	313.317
7000.00	242.650	41060.7	0.589501	312.274
7250.00	241.025	39635.9	0.572882	311.226
7500.00	239.400	38251.4	0.556624	310.175
7750.00	237.775	36906.3	0.540721	309.121
8000.00	236.150	35599.8	0.525168	308.063

E

F

Results Blade Element Method Propeller

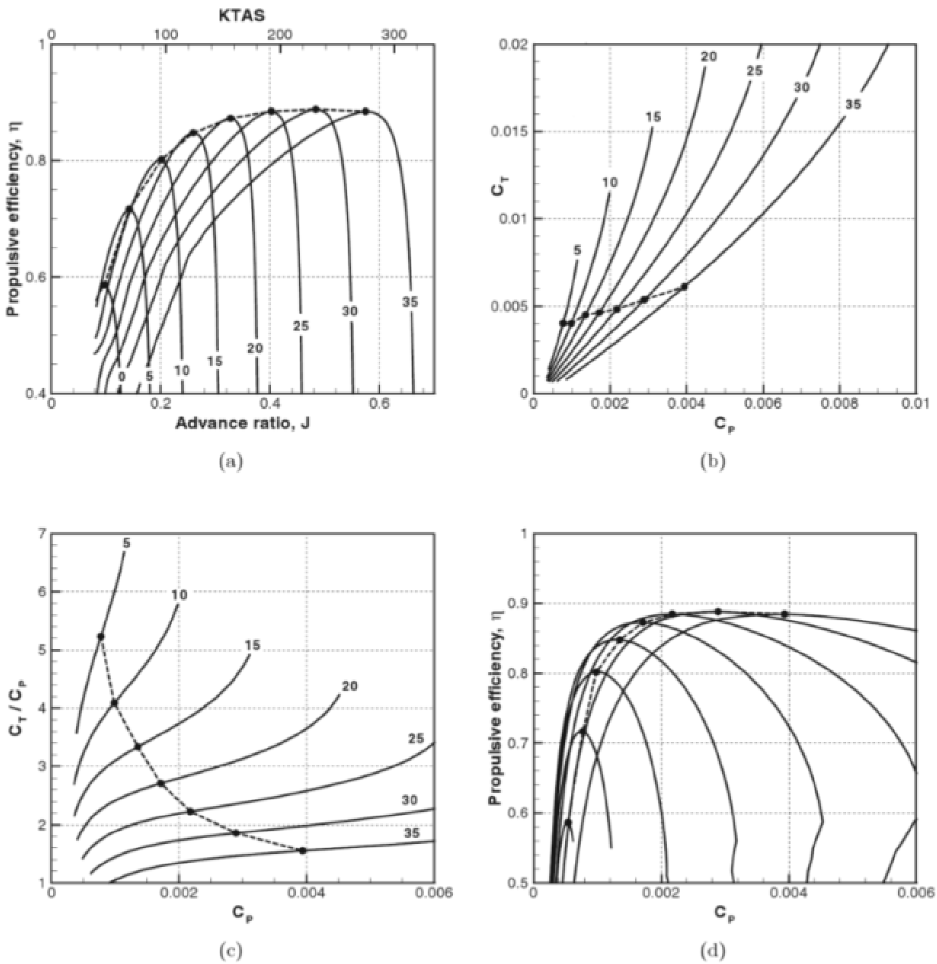

Figure F.1: Results of Blade Element Method (BEM) analysis performed by [74]

G
VALIDATION DATA INVERTER

Validation data for several high performance inverters available in the industry.

Manufacturer	**Type**	$I_{DC,Cont}$ **[A]**	$I_{DC,Max}$ **[A]**	P_{Cont} **[kW]**	**Weight [kg]**
Kellycontroller [127]	KLS7275D	200	500	14.4	2.4
Kellycontroller [127]	KLS7250D	160	400	11.52	2.4
Kellycontroller [127]	KLS7240D	140	350	10.08	2.4
Kellycontroller [127]	KLS6050D	160	400	9.6	2.4
Kellycontroller [127]	KLS6040D	140	350	8.4	2.4
Kellycontroller [127]	KLS4850D	160	400	7.68	2.4
Kellycontroller [127]	KLS4840D	140	350	6.72	2.4
Unitek [128]	P3 400/450-15	15	30	6.75	2.8
Unitek [128]	P3 400/450-25	25	50	11.25	3.6
Unitek [128]	P3 400/450-40	40	80	18	3.9
Unitek [128]	P3 400/450-60	60	120	27	7.5
Unitek [128]	P3 400/450-120	120	240	54	7.5
Unitek [128]	P3 400/450-150	150	300	67.5	8.9
Unitek [128]	P3 400/450-240	240	480	108	21.0
Unitek [128]	P3 400/450-360	360	720	162	22.0
Unitek [128]	P3 400/450-480	480	960	216	37.0
Unitek [128]	P3 400/450-840	840	1680	378	37.0
Unitek [128]	P3 400/450-1500	1500	3000	675	88.0
Unitek [128]	P3 400/450-2000	2000	4000	900	88.0
Emsiso [129]	emDrive150	150	250	9	1.2
Emsiso [129]	emDrive 400	400	600	48	3.7
Emsiso [129]	emDrive H300	300	450	120	7.7
Sevcon [130]	Gen4Size10	375	750	150	10.9
Sevcon [130]	Gen4Size8	250	500	60	10.0
Sevcon [130]	Gen4Size6	180	360	22	4.6
Sevcon [130]	Gen4Size4	120	240	14	2.7
Sevcon [130]	Gen4Size2	60	120	7	1.2
John Deere [131]	PD80	80	100	56	4.0
John Deere [131]	PD 300	300	300	210	15.0
John Deere [131]	PD 400 Single	400	500	280	17.3
John Deere [131]	PD 550 Single	425	550	298	32.0
John Deere [131]	PD 550 Dual	850	1100	596	64.0
Brusa [132]	DMC 534	337	450	157	12.0
Brusa [132]	DMC 524	225	300	105	9.0
Brusa [132]	DMC 514	112	150	52	6.0
Brusa [132]	DMC 544	450	600	212	15.0
Brusa [132]	MES TIM600	110	280	100	10.0
TM4 [133]	CO150	375	575	150	12.2
TM4 [133]	CO150-HV	425	375	170	12.2

G

H

PANASONIC - NRC18650 CELL

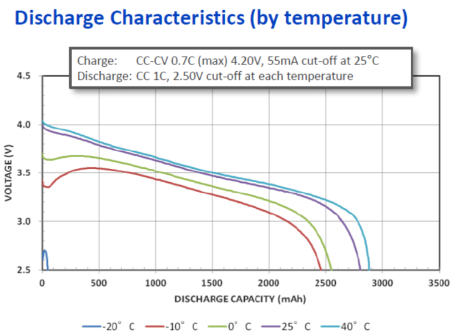

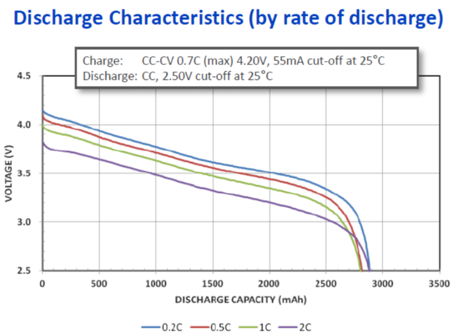

I

IGBT - CHARACTERISTICS

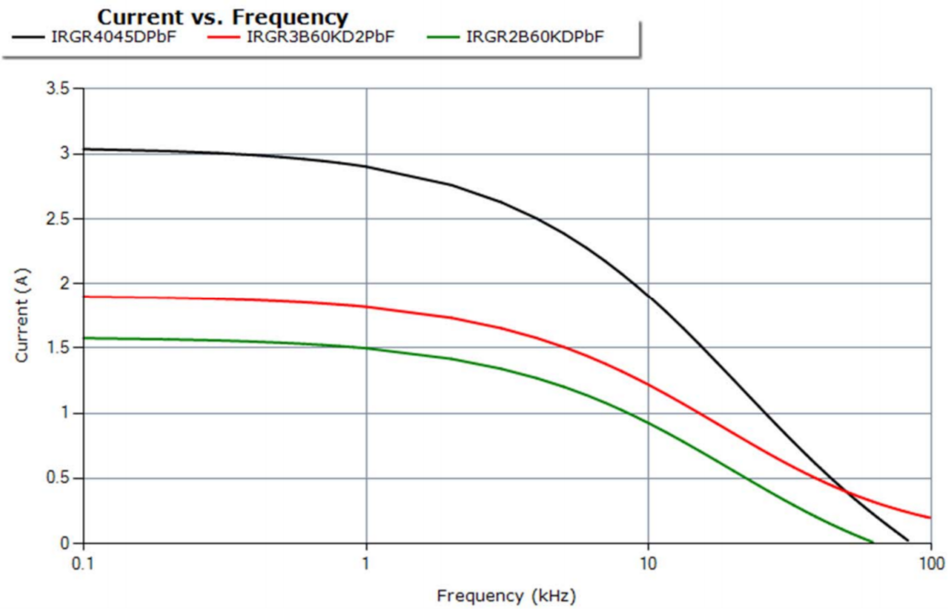

Figure I.1: The effect of increasing the efficiency on the amount of current passing through the IGBT is shown, [147]

J

Matlab Program - Well-to-Propeller Efficiency

Main Program

```
%% Optimiser
% Written by: R.H. Lenssen (TU Delft)
% Date: 1st of May 2016
% Master Thesis Supervisor: Ir. J.A. Melkert (TU Delft)
% Faculty: Aerospace Engineering
% Chair: Flight Performance & Propulsion
% -------------------------------------------------------
% Purpose of program is to find the optimum well-to-propeller
%% Initialise
clc
clear all
close all
%% Initial vector
design_init = [15000 ... %U_DC
               2 ...     %D_cable
               3.93 ...  %D_prop
               1200 ...  %RPM
               5000 ...  %h_cruise
               ];
design      = ones(1, length(design_init));
%% Boundaries to Design Vector
% Lower Bound
lb          = [5000 ...  %U_DC
               0.1 ...   %D_cable
               1 ...     %D_prop
               800 ...   %RPM
               4000 ...  %h_cruise
               ] ./ design_init;
% Upper Bound
ub          = [50000 ... %U_DC
               20 ...    %D_cable
               4 ...     %D_prop
               2000 ...  %RPM
               6000 ...  %h_cruise
               ] ./ design_init;
% Initialise Solver
PlotFun                         = {@optimplotfval};
options                         =
optimoptions('fmincon','Display','iter','PlotFcn',PlotFun,'Algori
thm','SQP','DiffMinChange',0.04,'DiffMaxChange',0.1,'TolX',1e-
3,'TolFun',1e-3);
[design_vector,J_final,iter,output] = fmincon(@(design)
objective(design),design,[],[],[],[],lb,ub,[],options);
design_final                    = design_vector .*
design_init;
```

Objective Function

```
%% Main
% Written by: R.H. Lenssen (TU Delft)
% Date: 1st of May 2016
% Master Thesis Supervisor: Ir. J.A. Melkert (TU Delft)
% Faculty: Aerospace Engineering
% Chair: Flight Performance & Propulsion
% ------------------------------------------------------
% Purpose of program is to find the well-to-propeller efficiency
of
% different type of aircraft

function [J] = objective(design)
design_init = [15000 ... %U_DC
               2 ...     %D_cable
               3.93 ...  %D_prop
               1200 ...  %RPM
               5000 ...  %h_cruise
               ];
design_vector = design .* design_init;
U_dc     = design_vector(1);
D_cable  = design_vector(2);
D_prop   = design_vector(3);
RPM      = design_vector(4);
h_cruise = design_vector(5);

%% Inputs
% Variables
no_props    = 2;    % Total number of propellers
no_gasturb  = 2;    % Total number of Gas Turbines
celltype    = 5;    % 1 & 2 Li-Ion, 3 & 4 Li-S8, 5 & 6 Li-O
[eff_motor, w_kg_motor] = technology(2); %1 = Practical, 2 =
Theoretical
WTT_ker     = 0.8;  % Eff transport incl. filling tank
WTT_elec    = 0.77; % Eff generation * Eff_grid * Eff_batt_charge

% Constants
% Weight baseline aircraft at start Segment [kg]
W_to        = 22754;
W_climb     = 22686;
W_cruise    = 22346;
W_descent   = 21184;
W_landing   = 20866;
W_end       = 20762;

% Average Flight Velocity aircraft per segment [m/s]
V_to        = 44.1;
```

```
V_climb     = 100;
V_cruise    = 125;
V_descent   = 110;
V_landing   = 60.4;

% Average Flight Altitude [m]
h_to        = 15;
h_climb     = h_cruise/2;
h_descent   = h_cruise/2;
h_landing   = 15;

% Length Flight Segment [m]
s_to        = 6;
s_cruise    = 355;
s_climb     = 56;
s_descent   = 80;
s_landing   = 22;

% Electronic Model Constants
l                = 50;         % Total Length cables
k_r              = 1.2;        % [-] Inverter Model
m_switch         = 398;        % [g] Inverter Model
k_service        = 2.5;        % [-] Inverter Model
I_ref            = 300;        % [A] Inverter Model
U_CE             = 650;        % [V] Inverter Model

% Physics and Aircraft related constants
g                = 9.81;       % Gravitational Acceleration [m/s2]
E_ker            = 43.3E6;     % [J/kg Kerosene]
S                = 61;         % Reference Area [m^2]
P_c              = 120000;     % Cabin power required
P_cont           = 3728000;    % [W_cont] from turboshaft total
f_tyr            = 0.48;       % [N/kg]
W_prop           = 150;        % Weight of propeller [kg]
[~,a_0,~,rho_0] = atmosisa(0);% Standard Atmosphere at Sea Level
%% Calculations
% Time per Segment (not taken into account vertical distance)
[sec]
t_to        = 3600 * s_to      / (3.6 * V_to);
t_climb     = 3600 * s_climb   / (3.6 * V_climb);
t_cruise    = 3600 * s_cruise  / (3.6 * V_cruise);
t_descent   = 3600 * s_descent / (3.6 * V_descent);
t_landing   = 3600 * s_landing / (3.6 * V_landing);
t_total = t_to + t_climb + t_cruise + t_descent + t_landing;
%total time
s_total = s_to + s_cruise + s_climb + s_descent + s_landing; %
total distance
```

```
% Standard Atmosphere at flight altitude per segment
[T_to,~,~,rho_to]             = atmosisa(h_to);
[T_climb,~,~,rho_climb]       = atmosisa(h_climb);
[T_cruise,~,~,rho_cruise]     = atmosisa(h_cruise);
[T_descent,~,~,rho_descent] = atmosisa(h_descent);
[T_landing,~,~,rho_landing] = atmosisa(h_landing);

%% Power Calculations
% Cruise
W_cruise_avg      = (W_cruise + W_descent) / 2; % Average weight
segment
cl_cruise         = (W_cruise_avg * g) / (0.5 * rho_cruise *
V_cruise^2 * S);
[cd_cruise]       = drag_coefficient(cl_cruise,'cruise');
T_cruise          = 0.5 * rho_cruise * V_cruise^2 * S * cd_cruise;
P_cruise          = T_cruise * V_cruise / no_props;
[eff_prop_cruise] =
propeller(P_cruise,V_cruise,rho_cruise,D_prop);
P_motor_cruise    = no_props * P_cruise / eff_prop_cruise;
P_motor_cruise2 = P_cont * (rho_cruise/rho_0)^0.728;

% Take-off
W_to_avg          = (W_to + W_climb) / 2;
cl_to             = (W_to_avg * g) / (0.5 * rho_to * V_to^2 * S);
[cd_to]           = drag_coefficient(cl_to,'to');
T_to              = 0.5 * rho_to * V_to^2 * S * cd_to + W_to_avg *
f_tyr / 2 + W_to_avg * V_to / (2 * t_to);
P_to              = T_to * V_to / no_props;
[eff_prop_to]     = propeller(P_to,V_to,rho_to,D_prop);
P_motor_to        = no_props * P_to / eff_prop_to;
P_motor_to2       = 3692000;

% Climb
W_climb_avg        = (W_climb + W_cruise) / 2;
cl_climb           = (W_climb_avg * g) / (0.5 * rho_climb *
V_climb^2 * S);
[cd_climb]         = drag_coefficient(cl_climb,'climb');
T_climb            = 0.5 * rho_climb * V_climb^2 * S * cd_climb;
P_climb            = T_climb * V_climb / no_props;
[eff_prop_climb] = propeller(P_climb,V_climb,rho_climb,D_prop);
P_motor_climb      = no_props * P_climb / eff_prop_climb;
P_motor_climb2     = P_cont * (rho_climb/rho_0)^0.728;

% descent
W_descent_avg      = (W_descent + W_landing) / 2;
```

```
cl_descent        = (W_descent_avg * g) / (0.5 * rho_descent *
V_descent^2 * S);
[cd_descent]      = drag_coefficient(cl_descent,'descent');
T_descent         = 0.5 * rho_descent * V_descent^2 * S *
cd_descent;
P_descent         = T_descent * V_descent / no_props;
[eff_prop_descent] =
propeller(P_descent,V_descent,rho_descent,D_prop);
P_motor_descent   = no_props * P_descent / eff_prop_descent;
P_motor_descent2 = P_cont * (rho_descent/rho_0)^0.728;

% landing
W_landing_avg     = (W_landing + W_end) / 2;
cl_landing        = (W_landing_avg * g) / (0.5 * rho_landing *
V_landing^2 * S);
[cd_landing]      = drag_coefficient(cl_landing,'landing');
T_landing         = 0.5 * rho_landing * V_landing^2 * S *
cd_landing;
P_landing         = T_landing * V_landing / no_props;
[eff_prop_landing] =
propeller(P_landing,V_landing,rho_landing,D_prop);
P_motor_landing   = no_props * P_landing / eff_prop_landing;
P_motor_landing2 = P_cont * (rho_landing/rho_0)^0.728;

%% Propeller Model
weight_prop       = W_prop * no_props * 3.93 / D_prop; %Dependent
on diameter

%% Motor Model
max_power_motor = max([P_motor_to P_motor_climb P_motor_cruise
...
                        P_motor_descent
P_motor_landing]/no_props);
weight_motor     = no_props * (5 + max_power_motor / w_kg_motor);
%Total weight motors
%% Inverter Model
[P_loss_motor] = motor(P_motor_to / no_props,RPM); % Motor Ohmic
Losses

% Calculate inverter power required by dividing by motor
efficiency
P_inv_to        = P_motor_to      / (no_props * eff_motor);
P_inv_climb     = P_motor_climb   / (no_props * eff_motor);
P_inv_cruise    = P_motor_cruise  / (no_props * eff_motor);
P_inv_descent   = P_motor_descent / (no_props * eff_motor);
P_inv_landing   = P_motor_landing / (no_props * eff_motor);
```

```
P_inv_max      = max([P_inv_to P_inv_climb P_inv_cruise
P_inv_descent P_inv_landing]);

% Mass [kg]
mass_inv     = no_props * 6
*(ceil(k_r*(P_inv_max/U_dc)/I_ref))*(ceil(U_dc/U_CE))*m_switch*k_
service/1000; %Total weight inverters

% Efficiency [%]
[P_inv_loss_to,     eff_inv_to,     mass_inv_to]      =
inverter(U_dc,P_inv_to);
[P_inv_loss_climb,  eff_inv_climb,  mass_inv_climb]   =
inverter(U_dc,P_inv_climb);
[P_inv_loss_cruise, eff_inv_cruise, mass_inv_cruise]  =
inverter(U_dc,P_inv_cruise);
[P_inv_loss_descent,eff_inv_descent,mass_inv_descent] =
inverter(U_dc,P_inv_descent);
[P_inv_loss_landing,eff_inv_landing,mass_inv_landing] =
inverter(U_dc,P_inv_landing);

%% Cables Model
% Calculate cable power required by dividing by motor efficiency
P_cable_to       = P_inv_to      / eff_inv_to;
P_cable_climb    = P_inv_climb   / eff_inv_climb;
P_cable_cruise   = P_inv_cruise  / eff_inv_cruise;
P_cable_descent  = P_inv_descent / eff_inv_descent;
P_cable_landing  = P_inv_landing / eff_inv_landing;

% Mass [kg]
[~,mass_cable,P_cooling] = cable(l,D_cable,3,T_cruise);

% Efficiency [%]
P_cable_loss_to       = P_cooling + (P_cable_to      / U_dc)^2 *
cable(l,D_cable,3,T_to);
P_cable_loss_climb    = P_cooling + (P_cable_climb   / U_dc)^2 *
cable(l,D_cable,3,T_climb);
P_cable_loss_cruise   = P_cooling + (P_cable_cruise  / U_dc)^2 *
cable(l,D_cable,3,T_cruise);
P_cable_loss_descent  = P_cooling + (P_cable_descent / U_dc)^2 *
cable(l,D_cable,3,T_descent);
P_cable_loss_landing  = P_cooling + (P_cable_landing / U_dc)^2 *
cable(l,D_cable,3,T_landing);

%% Battery Model
weight_battery = 5000;
error = 1;
while error ~= 0
```

```
[eff,ser,par,P_batt,I_nom] =
battery(U_dc,weight_battery,celltype);

%% Generator Model
% Define the driving flight segment for the generator sizing
P_driving = sort([P_cable_to P_cable_climb P_cable_cruise
P_cable_descent P_cable_landing]);
P_diff    = diff(P_driving);

if P_batt <= P_diff(4)
    P_batt2 = P_batt;
    P_batt1 = 0;
    P_batt3 = 0;
    P_batt4 = 0;
    P_batt5 = 0;
elseif P_batt <= P_diff(4) + P_diff(3)
    P_batt2 = P_diff(4);
    P_batt1 = P_batt - P_diff(4);
    P_batt3 = 0;
    P_batt4 = 0;
    P_batt5 = 0;
elseif P_batt <= P_diff(4) + P_diff(3) + P_diff(2)
    P_batt2 = P_diff(4);
    P_batt1 = P_diff(3);
    P_batt3 = P_batt - P_diff(4) - P_diff(3);
    P_batt4 = 0;
    P_batt5 = 0;
elseif P_batt <= P_diff(4) + P_diff(3) + P_diff(2) + P_diff(1)
    P_batt2 = P_diff(4);
    P_batt1 = P_diff(3);
    P_batt4 = P_diff(2);
    P_batt3 = P_batt - P_diff(4) - P_diff(3) - P_diff(2);
    P_batt5 = 0;
else
    P_batt2 = P_diff(4);
    P_batt1 = P_diff(3);
    P_batt4 = P_diff(2);
    P_batt3 = P_diff(1);
    P_batt5 = P_batt - sum(P_diff);
end

% Calculate Generator Power for each segment
P_gen_to       = ((P_cable_to      + P_cable_loss_to)      *
no_props - P_batt1) / no_gasturb;
P_gen_climb    = ((P_cable_climb   + P_cable_loss_climb)   *
no_props - P_batt2) / no_gasturb;
```

```
P_gen_cruise    = ((P_cable_cruise  + P_cable_loss_cruise)  *
no_props - P_batt3) / no_gasturb;
P_gen_descent   = ((P_cable_descent + P_cable_loss_descent) *
no_props - P_batt4) / no_gasturb;
P_gen_landing   = ((P_cable_landing + P_cable_loss_landing) *
no_props - P_batt5) / no_gasturb;

% Make generator efficiency equal to motor efficiency
eff_gen         = eff_motor;

% Electric generator Model
P_gasturb_to        = P_gen_to      / eff_gen;
P_gasturb_climb     = P_gen_climb   / eff_gen;
P_gasturb_cruise    = P_gen_cruise  / eff_gen;
P_gasturb_descent   = P_gen_descent / eff_gen;
P_gasturb_landing   = P_gen_landing / eff_gen;

% Mass [kg]
mass_gasturbine =(0.61 * P_gasturb_to / 1000 + 43) * no_props;
if round(mass_gasturbine,0) <= 0
    mass_gasturbine = 0;
end
%% Gasturbine Model
% Residual Thrust for baseline model
F_g_to      = no_props * residual(P_motor_to      / (1000 *
no_props));
F_g_climb   = no_props * residual(P_motor_climb   / (1000 *
no_props));
F_g_cruise  = no_props * residual(P_motor_cruise  / (1000 *
no_props));
F_g_descent = no_props * residual(P_motor_descent / (1000 *
no_props));
F_g_landing = no_props * residual(P_motor_landing / (1000 *
no_props));

% Fuel Fractions
FF_to       = no_gasturb * gasturbine(h_to,      (P_motor_to
- (F_g_to * V_to))            / (no_props * 1000));
FF_climb    = no_gasturb * gasturbine(h_climb,   (P_motor_climb
- (F_g_climb * V_climb))      / (no_props * 1000));
FF_cruise   = no_gasturb * gasturbine(h_cruise,  (P_motor_cruise
- (F_g_cruise * V_cruise))    / (no_props * 1000));
FF_descent  = no_gasturb * gasturbine(h_descent, (P_motor_descent
- (F_g_descent * V_descent)) / (no_props * 1000));
FF_landing  = no_gasturb * gasturbine(h_landing, (P_motor_landing
- (F_g_landing * V_landing)) / (no_props * 1000));
```

```
FF_hea_to         = no_gasturb * 0.8 * gasturbine(h_to,
P_gasturb_to       / 1000);
FF_hea_climb      = no_gasturb * 0.8 * gasturbine(h_climb,
P_gasturb_climb    / 1000);
FF_hea_cruise     = no_gasturb * 0.8 * gasturbine(h_cruise,
P_gasturb_cruise   / 1000);
FF_hea_descent    = no_gasturb * 0.8 * gasturbine(h_descent,
P_gasturb_descent / 1000);
FF_hea_landing    = no_gasturb * 0.8 * gasturbine(h_landing,
P_gasturb_landing / 1000);

if round(mass_gasturbine,0) <= 0
    FF_hea_to = 0;
    FF_hea_climb = 0;
    FF_hea_cruise = 0;
    FF_hea_descent = 0;
    FF_hea_landing = 0;
end
%% Well-to-propeller Calculations
%Well-to-propeller calculation HEA
TTP_hea_to        = (no_props * P_to      ) / (FF_hea_to      *
E_ker - P_c);
TTP_hea_climb     = (no_props * P_climb   ) / (FF_hea_climb   *
E_ker - P_c);
TTP_hea_cruise    = (no_props * P_cruise ) / (FF_hea_cruise  *
E_ker - P_c);
TTP_hea_descent = (no_props * P_descent) / (FF_hea_descent *
E_ker - P_c);
TTP_hea_landing = (no_props * P_landing) / (FF_hea_landing *
E_ker - P_c);
TTP_hea_total     = (TTP_hea_to   * t_to       + ...
                     TTP_hea_climb    * t_climb    + ...
                     TTP_hea_cruise   * t_cruise   + ...
                     TTP_hea_descent * t_descent + ...
                     TTP_hea_landing * t_landing)/ (t_total);
WTP_hea_total1    = WTT_ker * TTP_hea_total;
WTP_hea_total2    = WTT_elec * TTP_hea_total;
WTP_hea_total = (WTP_hea_total1 * sum([P_gasturb_to
P_gasturb_climb P_gasturb_cruise P_gasturb_descent
P_gasturb_landing]) + ...
                (WTP_hea_total2 * P_batt)) / (sum([P_gasturb_to
P_gasturb_climb P_gasturb_cruise P_gasturb_descent
P_gasturb_landing]) + P_batt);
J = 1 - WTP_hea_total;
%Well-to-propeller calculation baseline
TTP_to       = (no_props * P_to       + F_g_to       * V_to)       /
(FF_to       * E_ker - P_c);
```

```
TTP_climb   = (no_props * P_climb   + F_g_climb   * V_climb)   /
(FF_climb   * E_ker - P_c);
TTP_cruise  = (no_props * P_cruise  + F_g_cruise  * V_cruise)  /
(FF_cruise  * E_ker - P_c);
TTP_descent = (no_props * P_descent + F_g_descent * V_descent) /
(FF_descent * E_ker - P_c);
TTP_landing = (no_props * P_landing + F_g_landing * V_landing) /
(FF_landing * E_ker - P_c);
TTP_total   = (TTP_to      * t_to      + ...
    TTP_climb   * t_climb   + ...
    TTP_cruise  * t_cruise  + ...
    TTP_descent * t_descent + ...
    TTP_landing * t_landing)/ (t_total);
WTP_total   = WTT_ker * TTP_total;
%% Check Weights
% Take-Off
Wfuel_to       = t_to * no_gasturb * FF_hea_to;
Wfuel_climb    = t_climb * no_gasturb * FF_hea_climb; % Climb
Segment
Wfuel_cruise   = t_cruise * no_gasturb * FF_hea_cruise; % Cruise
Segment
Wfuel_descent  = t_descent * no_gasturb * FF_hea_descent; %
Descent Segment
Wfuel_landing  = t_landing * no_gasturb * FF_hea_landing; %
Landing Segment
% Total Fuel Weight
Wfuel_total = Wfuel_to + Wfuel_climb + Wfuel_cruise +
Wfuel_descent + Wfuel_landing;
%% Optimimisation
% Weight addition until battery weight == fuel weight baseline +
10%
total_weight = weight_prop + weight_battery + weight_motor +
mass_inv + mass_cable + mass_gasturbine + Wfuel_total;
total_allowed_weight = 1.1 * (1997 + 1300 + 2*150 +
(0.21*(2.051e6)/1000+30)*2); %fuel + prop + generators
error = round(total_allowed_weight - total_weight,0);
disp(error)
% Alter weight battery and return in loop
if error > 0
    weight_battery = weight_battery + 1;
elseif error < 0
    weight_battery = weight_battery - 1;
end
disp(weight_battery)
end
end
```

Cable Model

```
%% Cable
% Written by: R.H. Lenssen (TU Delft)
% Date: 1st of May 2016
% Master Thesis Supervisor: Ir. J.A. Melkert (TU Delft)
% Faculty: Aerospace Engineering
% Chair: Flight Performance & Propulsion
% -------------------------------------------------------
% Purpose of program is to calculate the conductor properties
depeding on
% the material type choosen

function [R,W,P] = cable(l,D,material,T)
eff_cool = 0.3; % Carnot efficiency of 30 [%]

if     material == 1
    density = 3.293; % Aluminium [g/cm^3]
    conduct = 0.029985007; % Conductivity
    P = 0;              % Cooling Power required is zero
elseif material == 2
    density = 8.9;    % Copper [g/cm^3]
    conduct = 0.016730801 + 0.00393*(T-273);
    P = 0;              % Cooling Power required is zero
elseif material == 3
    density = 8.2;    % Superconducting Material & Temperature
    conduct = 0.0000001; % Set resistance artificially low
    P = 1.05 * T * 69 / (69 * eff_cool); % Power required for
cooling
end

% Calculations
A           = pi*(D/2)^2;          % Area conductor
W           = l * A * density;     % Weight conductor
R           = l * 2 * conduct / A;  % Resistance conductor
end
```

Battery Model

```
% Written by: R.H. Lenssen (TU Delft)
% Master Thesis Supervisor: Ir. J.A. Melkert (TU Delft)
% Faculty: Aerospace Engineering Flight Performance & Propulsion
% -------------------------------------------------------
% Purpose of program is to find the battery performance
function [eff,ser,par,P,I] = battery(U,kg_battery,celltype)
    if celltype == 1 %Li-Ion practical
        wh_kg_cell = 240; %[Wh/kg]
        U_cell     = 3.6; %[V]
        wh_cell    = 46.5 * wh_kg_cell / 1000;
        I_nom      = wh_cell / U_cell;
        R_cell     = 0.055;
    elseif celltype == 2 %Li-Ion theoretical
        wh_kg_cell = 320; %[Wh/kg]
        U_cell     = 3.6; %[V]
        wh_cell    = 46.5 * wh_kg_cell / 1000;
        I_nom      = wh_cell / U_cell;
        R_cell     = 0.045;
    elseif celltype == 3 %Li-Sulphur lab
        wh_kg_cell = 400; %[Wh/kg]
        U_cell     = 3.6; %[V]
        wh_cell    = 46.5 * wh_kg_cell / 1000;
        I_nom      = wh_cell / U_cell;
        R_cell     = 0.025;
    elseif celltype == 4 %Li-oxygen theoretical
        wh_kg_cell = 1000; %[Wh/kg]
        U_cell     = 3.6; %[V]
        wh_cell    = 46.5 * wh_kg_cell / 1000;
        I_nom      = wh_cell / U_cell;
        R_cell     = 0.015;
    elseif celltype == 5 %Li-oxygen theoretical
        wh_kg_cell = 1802; %[Wh/kg]
        U_cell     = 3.6; %[V]
        wh_cell    = 46.5 * wh_kg_cell / 1000;
        I_nom      = wh_cell / U_cell;
        R_cell     = 0.015;
    end
    ser = round(U / U_cell,0);
    cells = kg_battery * wh_kg_cell / wh_cell;
    par = round(cells / ser,0);
    P = par * I_nom * U; %Wh
    R_ser = R_cell * ser;
    R_batt = 1 / (par * 1 / R_ser);
    P_loss = R_batt * I^2;
    eff = (P - P_loss) / P;
end
```

Drag Coefficient

```
%% Drag Coefficient
% Written by: R.H. Lenssen (TU Delft)
% Date: 1st of May 2016
% Master Thesis Supervisor: Ir. J.A. Melkert (TU Delft)
% Faculty: Aerospace Engineering
% Chair: Flight Performance & Propulsion
% -------------------------------------------------------
% Purpose of program is to find the drag coefficient by combinin
the
% zero-lift-drag (cd0) and the induced-drag (cdi) with the lift
(cl)

function [cd] = drag_coefficient(cl,segment)
%% Constants
% Zero Lift Drag Coefficients per segment [-]
cd0_to      = 0.05;
cd0_climb   = 0.035;
cd0_cruise  = 0.027;
cd0_descent = 0.027;
cd0_landing = 0.05;

% Induced Drag Coefficient per Segment [-]
cdi_to      = 0.0312;
cdi_climb   = 0.07;
cdi_cruise  = 0.0205;
cdi_descent = 0.04;
cdi_landing = 0.0312;

%% Calculations
if      strcmp(segment,'to')
    cd = cd0_to + cdi_to * cl^2;
elseif strcmp(segment,'climb')
    cd = cd0_climb + cdi_climb * cl^2;
elseif strcmp(segment,'cruise')
    cd = cd0_cruise + cdi_cruise * cl^2;
elseif strcmp(segment,'descent')
    cd = cd0_descent + cdi_descent * cl^2;
elseif strcmp(segment,'landing')
    cd = cd0_landing + cdi_landing * cl^2;
end
```

Inverter Model

```
%% Inverter Model
% Written by: R.H. Lenssen (TU Delft)
% Date: 1st of May 2016
% Master Thesis Supervisor: Ir. J.A. Melkert (TU Delft)
% Faculty: Aerospace Engineering
% Chair: Flight Performance & Propulsion
% -----------------------------------------------------
% Calculate all losses involved in the inverter. Using
% these properties the efficiency and the weight are determined
function [P_inv_loss_total, eff_inv, mass_inv] = inverter(U,P)
    %% Constants & Inputs
    U_CE0       = 0.8;     % [-]
    k_r         = 1.2;     % [-]
    m_switch    = 398;     % [g]
    k_service   = 2.5;     % [-]
    I_ref       = 300;     % [A]
    U_CE        = 650;     % [V]
    Res         = 0.002;   % [Ohm]
    E_switch    = 0.053;   % [J]
    f           = 20000;   % [Hz] Motor Frequency
    %% Calculations
    I                         = P / U; %Direct Current required
    Theta                     = 2 * sqrt(3) * 500 /(3 * U);
    n_parallel                = ceil(k_r * I / I_ref);
    n_series                  = ceil(U/U_CE);
    % Conduction and switching losses
    P_inv_loss_IGBT_cond      = (0.5/pi + Theta / 
8)*I*U_CE0/n_parallel + ((1/8)* Theta 
/(3*pi))*(I/n_parallel)^2*Res;
    P_inv_loss_IGBT_switch    = E_switch*(I/I_ref)*(U/U_CE)^1.4*f;
    P_inv_loss_diode_cond     = ((0.5/pi-
Theta/8)*I*1.1/n_parallel+(1/8-
Theta/(3*pi))*(I/n_parallel)^2*0.00171);
    P_inv_loss_diode_switch = 
(0.053/pi)*(I/300)^0.6*(U/2.64)^0.6*f;
    % Total losses
    P_inv_loss_total          = P_inv_loss_IGBT_cond   + ...
                                P_inv_loss_IGBT_switch + ...
                                P_inv_loss_diode_cond  + ...
                                P_inv_loss_diode_switch;

    mass_inv                  = 6 * n_parallel * n_series * 
m_switch / 1000;
    eff_inv                   = (U * I - P_inv_loss_total) / (U * 
I);
end
```

Motor Ohmic Losses

```
%% Motor
% Written by: R.H. Lenssen (TU Delft)
% Date: 1st of May 2016
% Master Thesis Supervisor: Ir. J.A. Melkert (TU Delft)
% Faculty: Aerospace Engineering
% Chair: Flight Performance & Propulsion
% -------------------------------------------------------
% Purpose of program is to find the Ohmic losses

function [P_loss_motor] = motor(P,RPM)
% Equation for torque does not result in [Nm]! Therefore RPM
should be in
% units of [rad/s]

% Torque constant based on motor model thesis
T = 1750600 / 1200;
I = 1750600 / 5000;
T_I = I / T;

% Required torque and current
T_new = P / RPM;
I_new = T_I * T_new;

% Total Ohmic losses motor
P_loss_motor = 0.0401 * I_new^2;
end
```

Propeller Model

```
function [eff_prop] = propeller(P,V,rho,D)

% Actuator Disc Theory scaled with a factor 0.885
eff_prop = 2 * 0.885 / ...
       (1+sqrt(1 + ((P / V)  / (0.5 * rho  * V^2  * 0.25 * pi *
D^2))));

end
```

Residual Thrust Model

```
%% Residual Thrust
% Written by: R.H. Lenssen (TU Delft)
% Date: 1st of May 2016
% Master Thesis Supervisor: Ir. J.A. Melkert (TU Delft)
% Faculty: Aerospace Engineering
% Chair: Flight Performance & Propulsion
% -------------------------------------------------------
% Purpose of program is to find the residual thrust for the
baseline

function [F_res] = residual(P)

F_res = -0.00000000000000000006*P^6 + 0.00000000000000042849*P^5
- 0.00000000000116569590*P^4 + 0.00000000146944927629*P^3 -
0.00000082289623301969*P^2 + 0.00067632807840948200*P +
0.05290556502275710000;
F_res = F_res * 1000;

end
```

Technology

```
%% Technology
% Written by: R.H. Lenssen (TU Delft)
% Date: 1st of May 2016
% Master Thesis Supervisor: Ir. J.A. Melkert (TU Delft)
% Faculty: Aerospace Engineering
% Chair: Flight Performance & Propulsion
% -------------------------------------------------------
% Purpose of program is to alter constants for theoretical or
practical
% state of technology
function [eff_motor, w_kg_motor] = technology(state)
if state == 1
    % Efficiencies
    eff_motor        = 0.95; % Motor Efficiency [%]
    % Energy Densities
    w_kg_motor       = 5000; %[W/kg]

elseif state == 2
    % Efficiencies
    eff_motor        = 0.97; % Motor Efficiency [%]
    % Energy Densities
    w_kg_motor       = 8000; %[W/kg]
end
end
```

REFERENCES

[1] R.H. Lenssen. Project plan and literature study used for the course research methodologies ae4010 at the delft university of technology should be read in cohesion with this report. Literature Study, January 2016.

[2] Ali Emadi, Young Joo Lee, and Kaushik Rajashekara. Power electronics and motor drives in electric, hybrid electric, and plug-in hybrid electric vehicles. *Industrial Electronics, IEEE Transactions on*, 55(6):2237–2245, 2008.

[3] Chris Mi, M Abul Masrur, and David Wenzhong Gao. *Hybrid electric vehicles: principles and applications with practical perspectives*. John Wiley & Sons, 2011.

[4] Omonowo D Momoh and Michael O Omoigui. An overview of hybrid electric vehicle technology. In *Vehicle Power and Propulsion Conference, 2009. VPPC'09. IEEE*, pages 1286–1292. IEEE, 2009.

[5] JY Hung and Luis Felipe Gonzalez. On parallel hybrid-electric propulsion system for unmanned aerial vehicles. *Progress in Aerospace Sciences*, 51:1–17, 2012.

[6] Ryan M Hiserote and Frederick G Harmon. *Analysis of hybrid-electric propulsion system designs for small unmanned aircraft systems*. PhD thesis, Defense Technical Information Center, 2010.

[7] Frederick G Harmon, Ryan M Hiserote, Matthew D Rippl, and Joseph K Ausserer. Parallel hybrid-electric propulsion systems for unmanned aircraft, February 15 2012. US Patent App. 13/396,760.

[8] J Van Bogaert. Student delft university of technology. http://repository.tudelft.nl/view/ir/uuid%3A0fc7019f-d988-45c1-a7e2-55825f4f90ca/, december 2015.

[9] He Zhang, Christophe Saudemont, Benoit Robyns, and Marc Petit. Electrical features comparison between more electric aircrafts and hybrid electric vehicles. *Electromotion*, 16(3), 2009.

[10] RI Jones. The more electric aircraft: the past and the future? In *Electrical Machines and Systems for the More Electric Aircraft (Ref. No. 1999/180), IEE Colloquium on*, pages 1–1. IET, 1999.

[11] Mike Howse. All electric aircraft. *Power Engineer*, 17(4), 2003.

[12] J. Wilson H.D. Perkins and D.P. Raymer. An evaluation of performance metrics for high efficiency tube-and-wing aircraft entering service in 2030 to 2035. November 2011.

[13] S.M. Amin. Toward a smart grid: power delivery for the 21st century. *IEEE Power & Energy Magazine*, 3(5):34–41, 2005.

[14] The third industrial revolution. *The Economist Newspaper Limited*, April 2012.

[15] Japan Aerospace Exploration Agency. Electric and hybrid propulsion system for aircraft, April 2015. visited on 14-12-2015.

[16] Aviation Week & Space Technology. Eads, siemens plot way to hybrid-electric propulsion. http://aviationweek.com/awin/eads-siemens-plot-way-hybrid-electric-propulsion, October 2013. visited on 14-12-2015.

[17] European Commission Whitepaper. Roadmap to a single european transport area – towards a competitive and resource efficient transport system. March 2011.

[18] Stphen Shankland CNET. Electric aircraft start finding a foothold in aviation industry.

[19] Ockels W. Terzi A., Melkert J. Superbus: A novel concept for safe, fast and sustainable mobility. *SAE Technical Paper*, January 2009.

[20] Martin Hepperle German Aerospace Center. Electric flight – potential and limitations. page 30, 2012.

[21] NL TenneT. 66kv systems for offshore wind farms. 2015.

[22] Philippe J Masson, Cesar Luongo, et al. High power density superconducting motor for all-electric aircraft propulsion. *Applied Superconductivity, IEEE Transactions on*, 15(2):2226–2229, 2005.

[23] Chung-Yi Li Gilles Thériault. Risks of leukaemia among residents close to high voltage transmission electric lines. *Occupational and Environmental Medicine*, 54, May 1997.

[24] Savitz DA Ahlbom A. Feychting M, Kaune WT. Estimating exposure in studies of residential magnetic fields and cancer: importance of short-term variability, time interval between diagnosis and measurement, and distance to power line. *Epidemiology*, July 1996.

[25] David A. Savitz and Dana P. Loomis. Magnetic field exposure in relation to leukemia and brain cancer mortality among electric utility workers. *American Journal of Epidemiology*, 141(2):123–134, 1995.

[26] IARC Working Group on the Evaluation of Carcinogenic Risks to Humans, World Health Organization, and International Agency for Research on Cancer. *Non-ionizing Radiation: Static and extremely low-frequency (ELF) electric and magnetic fields*. IARC monographs on the evaluation of carcinogenic risks to humans. IARC Press, 2002.

[27] P J Masson, G V Brown, D S Soban, and C A Luongo. Hts machines as enabling technology for all-electric airborne vehicles. *Superconductor Science and Technology*, 20(8):748, 2007.

[28] The Washinton Times. Editorial: Unplug the volt - liberals burn tax money on flammable cars. http://www.washingtontimes.com/news/2012/jan/17/unplug-the-volt/, January 2012. visited on 2016-01-31.

[29] J. Goldberg. Paying for playthings for the rich. http://articles.chicagotribune.com/2010-08-10/opinion/ct-oped-0810-goldberg-20100810_1_electric-cars-chevy-volt-ev1, August 2010. visited on 2016-01-31.

[30] J. Wilson. Overhyped electric cars and ethanol are 'greenwashed' scams that ultimately cause more pollution than fossil fuels. http://www.naturalnews.com/049504_electric_cars_ethanol_greenwashing.html, April 2015. visited on 2016-01-31.

[31] S.J. Cho. All-electric cars: Not so eco-friendly. http://www.cnbc.com/2014/12/16/all-electric-cars-not-so-eco-friendly.html, December 2014. visited on 2016-01-31.

[32] Cesar Luongo, Philippe J Masson, Taewoo Nam, Dimitri Mavris, Hyun D Kim, Gerald V Brown, Mark Waters, David Hall, et al. Next generation more-electric aircraft: a potential application for hts superconductors. *Applied Superconductivity, IEEE Transactions on*, 19(3):1055–1068, 2009.

[33] P. Ziogas J.P. Vandelac. A novel approach for minimizing high frequency transformer copper losses. In *Power Electronics Specialists Conference, 1987 IEEE*, pages 355–367. IEEE, 1987.

[34] J.A. Ferreira. Improved analytical modeling of conductive losses in magnetic components. *Power Electronics, IEEE Transactions on*, 9(1):127–131, 1994.

[35] Y. Takeda S. Morimoto, Y. Tong and T. Hirasa. Loss minimization control of permanent magnet synchronous motor drives. *Industrial Electronics, IEEE Transactions on*, 41(5):511–517, 1994.

[36] Y. Maryanka. Wiring reduction by battery power line communication. In *Passenger Car Electrical Architecture (Ref. No. 2000/088) IEE Seminar*, pages 8–1. IET, 2000.

[37] T. Kamata. High-strength light-weight conductor and twisted and compressed conductor, June 10 2003. US Patent 6,576,844.

[38] Vinay Bhaskara. Program analysis: Airbus a380 struggles but a business case exists for neo. http://airwaysnews.com/blog/2015/01/21/program-analysis-airbus-a380-struggles-but-a-business-case-exists-for-neo/, January 2015. visited on 2016-07-13.

[39] The Guardian Karl West. Airbus's flagship plane may be too big to be profitable. http://uk.businessinsider.com/airbuss-flagship-plane-may-be-too-big-to-be-profitable-2014-12?r=US&IR=T, December 2014. visited on 2016-07-13.

[40] Dominic Gates. Will 787 program ever show an overall profit? analysts grow more skeptical. http://www.seattletimes.com/business/boeing-aerospace/will-787-program-ever-show-an-overall-profit-analysts-grow-more-skeptical October 2015. visited on 14-12-2015.

[41] Chuck Squatriglia. Q&a - renault-nissan ceo pledges 5.6 billion dollar for evs. http://www.wired.com/2011/06/qa-with-carlos-ghosn/, June 2011. visited on 14-12-2015.

[42] W. La Jeunesse. Electric car subsidies transferring wealth from the poor to the rich? http://www.foxnews.com/politics/2012/01/09/electric-car-subsidies-transferring-wealth-from-poor-to-rich.html, January 2012. visited on 2016-01-31.

[43] E. Behrmann. Green batteries' graphite adds to china pollution. http://www.bloomberg.com/news/articles/2014-03-14/teslas-in-california-help-bring-dirty-rain-to-china, May 2014. visited on 2016-01-31.

[44] G. Wong. Elektra one: the electricity-powered plane. http://www.ubergizmo.com/2011/03/elektra-one/, March 2011. visited on 14-12-2015.

[45] M. Hanlon. Yuneec-e430 electric aircraft. http://www.gizmag.com/yuneece430-electric-aircraft/12036/, June 2009. visited on 14-12-2015.

[46] Panasonic. Lithium ion nrc18650b. http://industrial.panasonic.com/cdbs/www-data/pdf2/ACA4000/ACA4000CE240.pdf, 2012. visited on 14-12-2015.

[47] Abbas Fotouhi, Daniel J. Auger, Karsten Propp, Stefano Longo, and Mark Wild. A review on electric vehicle battery modelling: From lithium-ion toward lithium–sulphur. *Renewable and Sustainable Energy Reviews*, 56:1008 – 1021, 2016.

[48] Petr Novák. A reality check on battery materials development. In *18th International Meeting on Lithium Batteries (June 19-24, 2016)*. Ecs, 2016.

[49] Philipp Adelhelm, Pascal Hartmann, Conrad L. Bender, Martin Busche, Christine Eufinger, and Juergen Janek. From lithium to sodium: cell chemistry of room temperature sodium–air and sodium–sulfur batteries. *Beilstein Journal of Nanotechnology*, 6:1016–1055, 2015.

[50] Mark Prigg. Tesla boss elon musk gives away firm's electric car secrets in bid to boost market. June 2014.

[51] Cableizer Damian Aegerter and Stephan Meier. Jet engine specification database. https://az772942.vo.msecnd.net/features_cable_editor.png?v=0, 2016. visited on 2016-06-09.

[52] Toshio Ogawa. Responses of atmospheric electric field and air-earth current to variations of conductivity profiles. *Journal of atmospheric and terrestrial physics*, 46(5):431–445, 1984.

[53] The Gale Group Inc. The great soviet encyclopedia 3rd edition. http://encyclopedia2.thefreedictionary.com/Atmospheric+Conductivity, 1970-1979. visited on 2016-07-13.

[54] Burnice Doyle Bedford and Richard Gibson Hoft. *Principles of inverter circuits*. John Wiley & Sons, 1964.

[55] Sylveste Campbell. *Solid-State AC Motor Controls: Selection and Application*, volume 56. CRC Press, 1987.

[56] Ralph L Jaeschke. *Controlling power transmission systems*. Penton/IPC, 1978.

[57] Charles Seymour Siskind. *Electrical control systems in industry*. Glencoe/McGraw-Hill School Pub Co, 1963.

[58] Carl Blake and Chris Bull. Igbt or mosfet: choose wisely. *International Rectifier*, 2001.

[59] Hamid A Toliyat and Gerald B Kliman. *Handbook of electric motors*, volume 120. CRC press, 2004.

[60] John S Hsu, John D Kueck, Mitchell Olszewski, Don A Casada, Pedro J Otaduy, and Leon M Tolbert. Comparison of induction motor field efficiency evaluation methods. *Industry Applications, IEEE Transactions on*, 34(1):118, 1998.

[61] Dean Patterson and Rene Spee. The design and development of an axial flux permanent magnet brushless dc motor for wheel drive in a solar powered vehicle. *Industry Applications, IEEE Transactions on*, 31(5):1054–1061, 1995.

[62] Magnetic field of a moving charge: which way to the north pole. https://www.physicsforums.com/threads/magnetic-field-of-a-moving-charge-which-way-to-the-north-pole.766573/, August 2014. visited on 2016-04-16.

[63] Naresh Tummalapalli. How can i measure the impedance and resistance of a bldc motor. https://qph.is.quoracdn.net/main-qimg-04eab9257a23bc5bfd32cef0e67142f9?convert_to_webp=true, September 2015. visited on 2016-04-16.

[64] Shen Wang, Michael Andrew De Rooij, Willem Gerhardus Odendaal, Jacobus Daniel Van Wyk, and Dushan Boroyevich. Reduction of high-frequency conduction losses using a planar litz structure. *Power Electronics, IEEE Transactions on*, 20(2):261–267, 2005.

[65] Laurence K Loftin Jr. Subsonic aircraft: Evolution and the matching of size to performance. *Hampton, VA. Langley: National Aeronautics and Space Administration, Research Center*, 1980.

[66] J Roskam. Airplane design, part i: Preliminary sizing of airplanes, design. *Analysis and Research Corporation, Lawrence, Kansas*, 1997.

[67] L.L.M. Veldhuis. Propeller propulsion aerodynamics. https://blackboard.tudelft.nl/bbcswebdav/pid-2522532-dt-content-rid-9068954_2/courses/35340-151601/Lecture%20Propeller%20Propulsion-V2%281%29.pdf, June 2013. part of lecture series AE4130 given in 2015.

[68] Mihaela Florentina Nita. *Aircraft Design Studies Based on the ATR 72*. PhD thesis, 2008. Project, Hamburg University of Applied Sciences Department of Automotive and Aeronautical Engineering.

[69] Roger D Schaufele. *The elements of aircraft preliminary design*. Aries Publications Santa Ana, 2000.

[70] Gerhard Brüning, Xaver Hafer, and Gottfried Sachs. *Flugleistungen: Grundlagen, Flugzustände, Flugabschnitte. Aufgaben und Lösungen*. Springer-Verlag, 2013.

[71] J Russell. *Performance and stability of aircraft*. Butterworth-Heinemann, 1996.

[72] Barnes Warnock McCormick, Barnes Warnock McCormick, and Barnes Warnock McCormick. *Aerodynamics, aeronautics, and flight mechanics*, volume 2. Wiley New York, 1995. p. 351.

[73] Barnes Warnock McCormick. *Aerodynamics, aeronautics, and flight mechanics*. Wiley, 1979.

[74] Antonio Filippone. *Advanced aircraft flight performance*, volume 34. Cambridge University Press, 2012.

[75] Antonio Filippone and Zulfaa Mohamed-Kassim. *Multi-disciplinary simulation of propeller-turboshaft aircraft flight*. Cambridge University Press, December 2012.

[76] J. Petro CTO. Achieving high electric motor efficiency. *EEMODS*, (60):1–12, 2011.

[77] Bimal K Bose and Bimal K Bose. *Power electronics and variable frequency drives: technology and applications*, volume 996. IEEE press New York, 1997.

[78] Jacek F Gieras. *Permanent magnet motor technology: design and applications*. CRC press, 2002.

[79] PJ Masson, GV Brown, DS Soban, and CA Luongo. Hts machines as enabling technology for all-electric airborne vehicles. *Superconductor Science and Technology*, 20(8):748, 2007.

[80] Rong-Jie Wang, Maarten J Kamper, Kobus Van der Westhuizen, and Jacek F Gieras. Optimal design of a coreless stator axial flux permanent-magnet generator. *Magnetics, IEEE Transactions on*, 41(1):55–64, 2005.

[81] Enstroj Electric Motor Innovation. Emrax 268 technical data table. http://www.enstroj.si/Electric-products/emrax-268.html, January 2014. visited on 2016-05-21.

[82] Enstroj Electric Motor Innovation. Emrax 200 technical data table. http://www.enstroj.si/Electric-products/emrax-200.html, January 2014. visited on 2016-05-21.

[83] Enstroj Electric Motor Innovation. Emrax 228 technical data table. http://www.enstroj.si/Electric-products/emrax-228-motorsgen.html, January 2014. visited on 2016-05-21.

[84] Pipistrel d.o.o. Ajdovscina. Aircraft technical data. http://wattsup.pipistrel.si/aircraft/#techdata, May 2016. visited on 2016-05-21.

[85] QS MOTOR. 3000w-8000w electric car hub motor(273 model). http://www.qs-motor.com/product/3000w-8000w-electric-car-hub-motor273-model/, 2014. visited on 2016-05-21.

[86] Protean Electric. Protean drive™ specifications. http://www.proteanelectric.com/specifications/, 2016. visited on 2016-05-21.

[87] Elaphe Ltd. M700, m1100, l-type, marine, lev. http://in-wheel.com/product-category/motors/, 2016. visited on 2016-05-21.

[88] Onvolts. 48v 3000w hub motor met enkelzijdige as. http://www.onvolts-onderdelen.nl/a-36361214/hub-motoren-naaf-motoren/48v-3000w-hub-motor-met-enkelzijdige-as/, 2016. visited on 2016-05-21.

[89] YASA Motors 2016. Yasa-400. http://www.yasamotors.com/products/yasa-400/, 2016. visited on 2016-07-24.

[90] Launchpoint Technologies Inc. Electric machines for propulsion. http://www.launchpnt.com/portfolio/aerospace/electric-machines-for-propulsion, 2016. visited on 2016-07-24.

[91] DRS Technologies Inc. Permanent-magnet axial (pa) series pm motors and generators. http://www.drs.com/products-and-services/permanent-magnet-axial-pa-series-pm-motors-and-generators/, 2016. visited on 2016-07-24.

[92] GKN. Electric motor and generator technology. http://tinyurl.com/nh8a4vc, 2016. visited on 2016-07-24.

[93] ATR DC/E and Pratt & Whitney Canada. Atr-500 series. http://www.atraircraft.com/datas/download_center/34/fiches_500_septembre2014_34.pdf, September 2014. visited on 14-04-2016.

[94] The flying engineer. Why the atr72 is outselling the q400. http://aeroblogger.com/home/blog/atr-72-bombardier-q400/, March 2012.

[95] ATR. Atr72-600. http://www.atraircraft.com/products_app/media/pdf/Fiche_72-600_septembre%202014.pdf, September 2014. visited on 20-02-2016.

[96] European Aviation Safety Agency Pratt & Whitney Canada. Type-certificate data sheet - pw100 series. http://tinyurl.com/zr86mld, June 2014. visited on 01-03-2016.

[97] Federal Aviation Regulations. Far-25. *US Federal Aviation Authority, Washington, DC, USA*.

[98] Mihaela Florentina Nita. Aircraft design studies based on the atr72. *Hochschule fur Angewandte Wissenschaften Hamburg*, June 2008.

[99] Thomas J Yager and John L Mccarty. Friction characteristics of three 30 by 11.5-14.5, type 8, aircraft tires with various tread groove patterns and rubber compounds. 1977.

[100] I. Wakefield and C. Dubuque. Exceeding tire speed rating during takeoff. *Boeing Aero*, April 2009.

[101] The Flying Engineer. Q400 vs atr72. http://theflyingengineer.com/aircraft/proud-to-fly-a-turboprop-q400-vs-atr72/, March 2012. visited on 12-05-2016.

[102] Pierluigi Della Vecchia. Development of methodologies for the aerodynamic design and optimization of new regional turboprop aircraft. 2013.

[103] Caldarelli G. Atr-72 accident in taiway. In SAE Aircraft & Engine Icing International Conference, Oktober 2008. ICE 13, Sevilla, Spain.

[104] Raffi Babikian, Stephen P Lukachko, and Ian A Waitz. The historical fuel efficiency characteristics of regional aircraft from technological, operational, and cost perspectives. *Journal of Air Transport Management*, 8(6):389–400, 2002.

[105] S. Campilongo T. Donateo, M.G. De Giorgi. Greenin the propulsion: A comparative analysis of advanced more electric solutions for aircraft. https://www.researchgate.net/publication/284169912_GREENING_THE_PROPULSION_A_comparative_analysis_of_advanced_more_electric_solutions_for_aircraft, November 2015. visited on 2016-04-12.

[106] S Ahmed and M1 Krumpelt. Hydrogen from hydrocarbon fuels for fuel cells. *International journal of hydrogen energy*, 26(4):291–301, 2001.

[107] Betterenergy. Getting to half oil. http://www.better-energy-llc.com/well-tank-energy-efficiencies-gasoline-diesel/, October 2014. visited on 15-05-2016.

[108] Sheldon S Williamson and Ali Emadi. Comparative assessment of hybrid electric and fuel cell vehicles based on comprehensive well-to-wheels efficiency analysis. *Vehicular Technology, IEEE Transactions on*, 54(3):856–862, 2005.

[109] Hamilton Sundstrand Power Systems. Auxiliary and ground power systems reference guide. https://hsapps.utc.com/powersystems/2190600_web.pdf. visited on 20-05-2016.

[110] Patrick C Vratny, Philipp Forsbach, Arne Seitz, and Mirko Hornung. Investigation of universally electric propulsion for transport aircraft. September 2014.

[111] G Deboy, H Hulsken, H Mitlehner, and R Rupp. A comparison of modern power device concepts for high voltage applications: Field stop-igbt, compensation devices and sic devices. In *Bipolar/BiCMOS Circuits and Technology Meeting, 2000. Proceedings of the 2000*, pages 134–141. IEEE, 2000.

[112] Kuang Sheng, Barry W Williams, and Stephen J Finney. A review of igbt models. *Power Electronics, IEEE Transactions on*, 15(6):1250–1266, 2000.

[113] SEMIKRON. Igbt4 modules semix305. https://www.semikron.com/dl/service-support/downloads/download/semikron-datasheet-semix305gd07e4-21919520, July 2014. Datasheet SEMiX305GD07E4, visited on 23-05-2016.

[114] Ali Engineer Power Electronics Husain. Block diagram of an induction motor and inverter. http://powerelectronics.com/site-files/powerelectronics.com/files/archive/powerelectronics.com/power_management/three-phase-inverter-fig1.jpg, May 2011. visited on 2016-05-09.

[115] S Koch and H Antrekowitsch. Aluminum alloys for wire harnesses in automotive engineering. *BHM Berg-und Hüttenmännische Monatshefte*, 152(2-3):62–67, 2007.

[116] Vitaly Vysotsky, Sergey Fetisov, and Viktor Sytnikov. Research and development of bi-2223-based ac power cables in russia. *Research, Fabrication and Applications of Bi-2223 HTS Wires*, 1:289, 2016.

[117] P Castiglione and PJ Shouse. The effect of ohmic cable losses on time-domain reflectometry measurements of electrical conductivity. *Soil Science Society of America Journal*, 67(2):414–424, 2003.

[118] Ashraf W Lotfi and Fred C Lee. A high frequency model for litz wire for switch-mode magnetics. In *Industry Applications Society Annual Meeting, 1993., Conference Record of the 1993 IEEE*, pages 1169–1175. IEEE, 1993.

[119] Gerald V Brown. Weights and efficiencies of electric components of a turboelectric aircraft propulsion system. In *49th AIAA aerospace sciences meeting including the new horizons forum and aerospace exposition*, pages 3025–3042, 2011.

[120] Berica Cavi S.p.a. Current capability insulated pvc cables. http://www.bericacavi.com/site/index.php?option=com_content&view=article&id=59, 2010. visited on 2016-06-12.

[121] Axon' Cable. Maximum current of an operating wire. http://www.axon-cable.com/en/06_customerArea/03_toolbox/04_intensity/index.aspx, 2016. visited on 2016-06-11.

[122] Egbert Torenbeek. *Synthesis of subsonic airplane design: an introduction to the preliminary design of subsonic general aviation and transport aircraft, with emphasis on layout, aerodynamic design, propulsion and performance*. Springer Science & Business Media, 2013.

[123] Robert L Vogt. Future trends in turboshaft engines up to the 5000 horsepower class. In *ASME 1991 International Gas Turbine and Aeroengine Congress and Exposition*, pages V002T02A003–V002T02A003. American Society of Mechanical Engineers, 1991.

[124] Nathan Meier. Jet engine specification database. http://www.jet-engine.net/, 2005. visited on 2016-05-24.

[125] Eduardo Moreno Gallart. Design of auxiliary power unit (apu) for co-operation with a turboshaft engine. 2013.

[126] SEMIKRON. Igbt4 modules skm900. https://www.semikron.com/dl/service-support/downloads/download/semikron-datasheet-skm900ga12e4-22892130, July 2014. Datasheet SKM900GA12E4, visited on 03-04-2016.

[127] Kelly Controllers. Brushless kls-d controllers. http://kellycontroller.com/brushless-kls-controllers-c-105_107.html, 2016. visited on 2016-05-23.

[128] Unitek Industrie Elektronik. Thyristor-drive classic. http://www.unitek-online.de/en/produkte/thyristor.html, 2016. visited on 2016-05-23.

[129] emDrive mobility. Drives. http://www.emdrive-mobility.com/Drives.html, 2015. visited on 2016-05-23.

[130] Sevcon. Ac controllers. http://www.sevcon.com/ac-controllers/gen-4-size-8.aspx, 2012. visited on 2016-05-23.

[131] John Deere. Jdes power drive family of inverters. http://www.deere.com/en_US/docs/pdfs/brochures/pd-family-inverters.pdf, 2016. visited on 2016-05-23.

[132] Brusa Metric Mind Corporation. Ev ac power inverters. http://www.metricmind.com/category/ev-ac-drive-systems/ev-ac-power-inverters/, 2016. visited on 2016-05-23.

[133] TM4 Electrodynamic Systems. Co150 traction inverter. http://www.tm4.com/products/power-electronics/co150-traction-inverter/, 2016. visited on 2016-05-23.

[134] H. Polinder Technical University of Delft. Electric drives for aerospace and the energy transition. personal communication, November 2015.

[135] Stefano Campanari, Giampaolo Manzolini, and Fernando Garcia De la Iglesia. Energy analysis of electric vehicles using batteries or fuel cells through well-to-wheel driving cycle simulations. *Journal of Power Sources*, 186(2):464–477, 2009.

[136] R Edwards, JF Larivé, D Rickeard, and W Weindorf. Well-to-tank report version 4.0. *JEC Wellto-Wheels Analysis of Future Automotive Fuels and Powertrains in the European Context, Italy, doi*, 10:40526, 2013.

[137] General Motors Corp. Well-to-tank energy use and greenhouse gas emissions of transportation fuels – north american analysis. June 2001.

[138] Martin Eberhard and Marc Tarpenning. The 21st century electric car. *Tesla Motors Inc.*, July 2006.

[139] Sheble Aviation. Multi engine airplane - twin engine airplane – flying on one engine. http://www.multiengineairplane.com/flying-on-one-engine/, 2012. visited on 15-04-2016.

[140] Dieter SCHOLZ. Aircraft design. hamburg university of applied sciences, department of automotive and aeronautical engineering. *Aircraft Design and Systems Group (Aero), Short Course Notes*, June 2008.

[141] Priyanka Barua, Tahir Sousa, and Dieter Scholz. Empennage statistics and sizing methods for dorsal fins. April 2013.

[142] Mohammad Sadraey. *Aircraft Performance: Analysis*. VDM Verlag Publishing, 2009. Chapter 3.

[143] Dimitri Simos and LLOYD R JENKINSON. Optimization of the conceptual design and mission profiles of short-haul aircraft. *Journal of Aircraft*, 25(7):618–624, 1988.

[144] GasTurb12. Power generation. http://www.gasturb.de/power-generation.html. visited on 06-03-2016.

[145] O Majeed. Parametric specific fuel consumption analysis of the pw120a turboprop engine. In *17th Canadian Aeronautics and Space Institute Propulsion Symposium*, pages 5–7, 2009.

[146] David W Riggins, Christopher D Wilson, Bryce Alexander Roth, and Robert Alan McDonald. Performance characterization of turboshaft engines via availability and second law analysis. 2002.

[147] Energy Saving Products BU IOR Rectifier. Igbt operating frequency. www.irf.com/product-info/igbt/operatingfrequency.pdf, July 2013. visited on 2016-06-16.